Binary Neutron Star Mergers in the QCD Phase Diagram

TALK AT THE NIKHEF INSTITUTE IN AMSTERDAM

AMSTERDAM, NETHERLAND, 04. JULY 2018

MATTHIAS HANAUSKE, KENTARO TAKAMI, LUKE BOVARD, JOSE FONT, FILIPPO GALEAZZI, JENS PAPENFORT, LUKAS WEIH, ELIAS MOST, FEDERICO GUERCILENA, ZEKIYE SIMAY YILMAZ, CHRISTINA MITROPOULOS, JAN STEINHEIMER, STEFAN SCHRAMM, VERONICA DEXHEIMER, DAVID BLASCHKE, MARK ALFORD, KAI SCHWENZER, ANDREAS ZACCHI, JÜRGEN SCHAFFNER-BIELICH, LAURA TOLOS, GLORIA MONTAÑA, MICHAEL RATTAY, HORST STÖCKER AND LUCIANO REZZOLLA

FRANKFURT INSTITUTE FOR ADVANCED STUDIES
JOHANN WOLFGANG GOETHE UNIVERSITÄT
INSTITUT FÜR THEORETISCHE PHYSIK
ARBEITSGRUPPE RELATIVISTISCHE ASTROPHYSIK
D-60438 FRANKFURT AM MAIN

Content

- GW170817 - The long-awaited event
  - Constraining the EOS using data from GW170817
- Hypermassive neutron stars and the QCD phase diagram
  - Neutron star mergers and the EOS of elementary matter
  - The hadron-quark phase transition and the neutron star merger product
- Detecting the hadron-quark phase transition with gravitational waves
  - The twin star collapse
  - Rotational behavior of deconfined quark matter
- Summary and Outlook

Erste Gravitationswelle im Jahr 2015 gefunden!!

Kollision zweier Schwarzer Löcher GW150914

Massen: 36 & 29 Sonnenmassen

Abstand zur Erde 410 Mpc (1.34 Milliarden Lichtjahre)

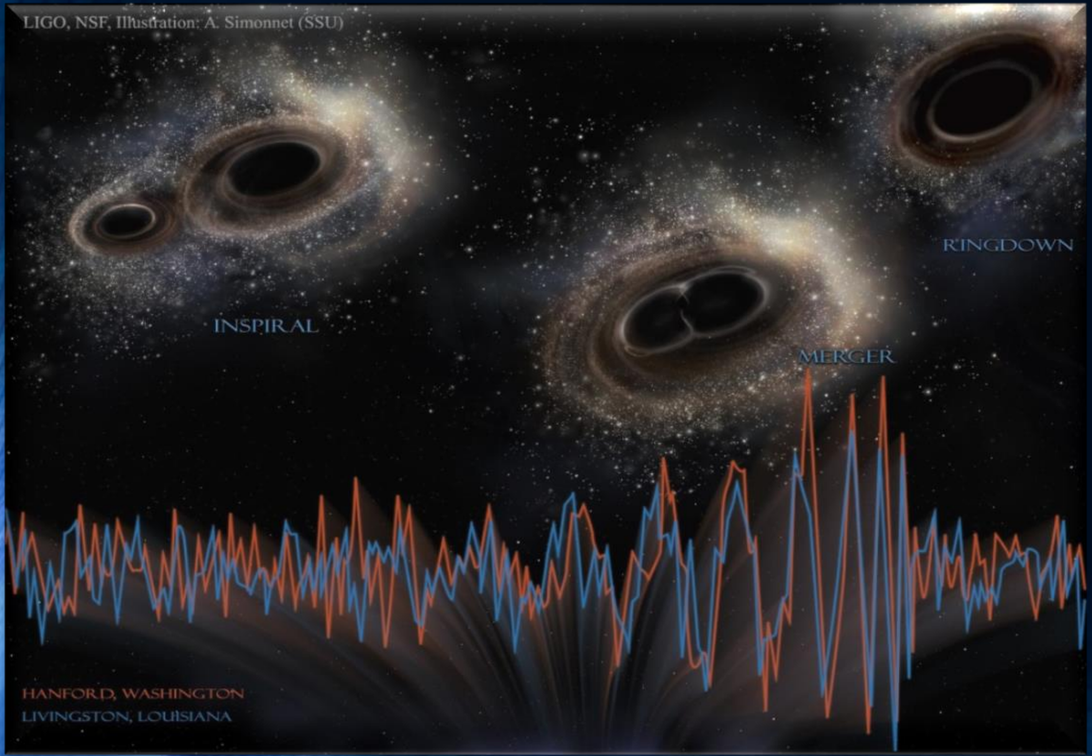

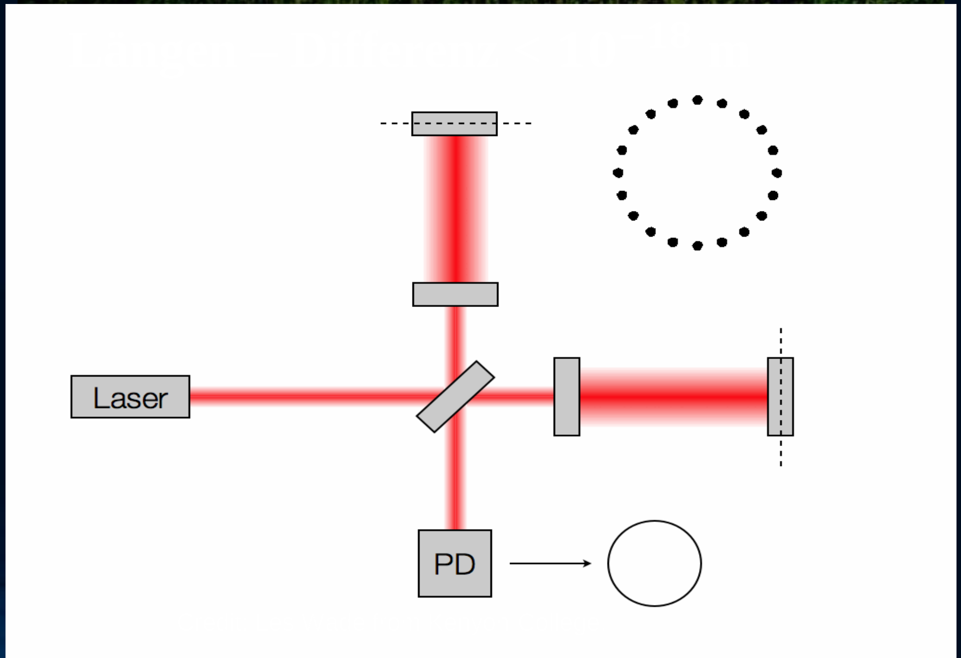

The long-awaited event GW170817

	Low-spin priors ($\|\chi\| \leq 0.05$)	High-spin priors ($\|\chi\| \leq 0.89$)
Primary mass m_1	1.36–1.60 $M_\odot$	1.36–2.26 $M_\odot$
Secondary mass m_2	1.17–1.36 $M_\odot$	0.86–1.36 $M_\odot$
Chirp mass $\mathcal{M}$	$1.188^{+0.004}_{-0.002} M_\odot$	$1.188^{+0.004}_{-0.002} M_\odot$
Mass ratio m_2/m_1	0.7–1.0	0.4–1.0
Total mass m_{tot}	$2.74^{+0.04}_{-0.01} M_\odot$	$2.82^{+0.47}_{-0.09} M_\odot$
Radiated energy E_{rad}	$> 0.025 M_\odot c^2$	$> 0.025 M_\odot c^2$
Luminosity distance D_L	40^{+8}_{-14} Mpc	40^{+8}_{-14} Mpc
Viewing angle Θ	$\leq 55°$	$\leq 56°$
Using NGC 4993 location	$\leq 28°$	$\leq 28°$
Combined dimensionless tidal deformability $\tilde{\Lambda}$	≤ 800	≤ 700
Dimensionless tidal deformability $\Lambda(1.4 M_\odot)$	≤ 800	≤ 1400

Die gemessene Gravitationswelle und der darauf folgende hochenergetische Lichtblitz

Der von dem Gammastrahlen Detektor FERMI gemessene Gammastrahlen Ausbruch
(1.7 Sekunden später)

Die von dem Gravitationswellen Detektor LIGO detektierte Frequenz der Gravitationswelle

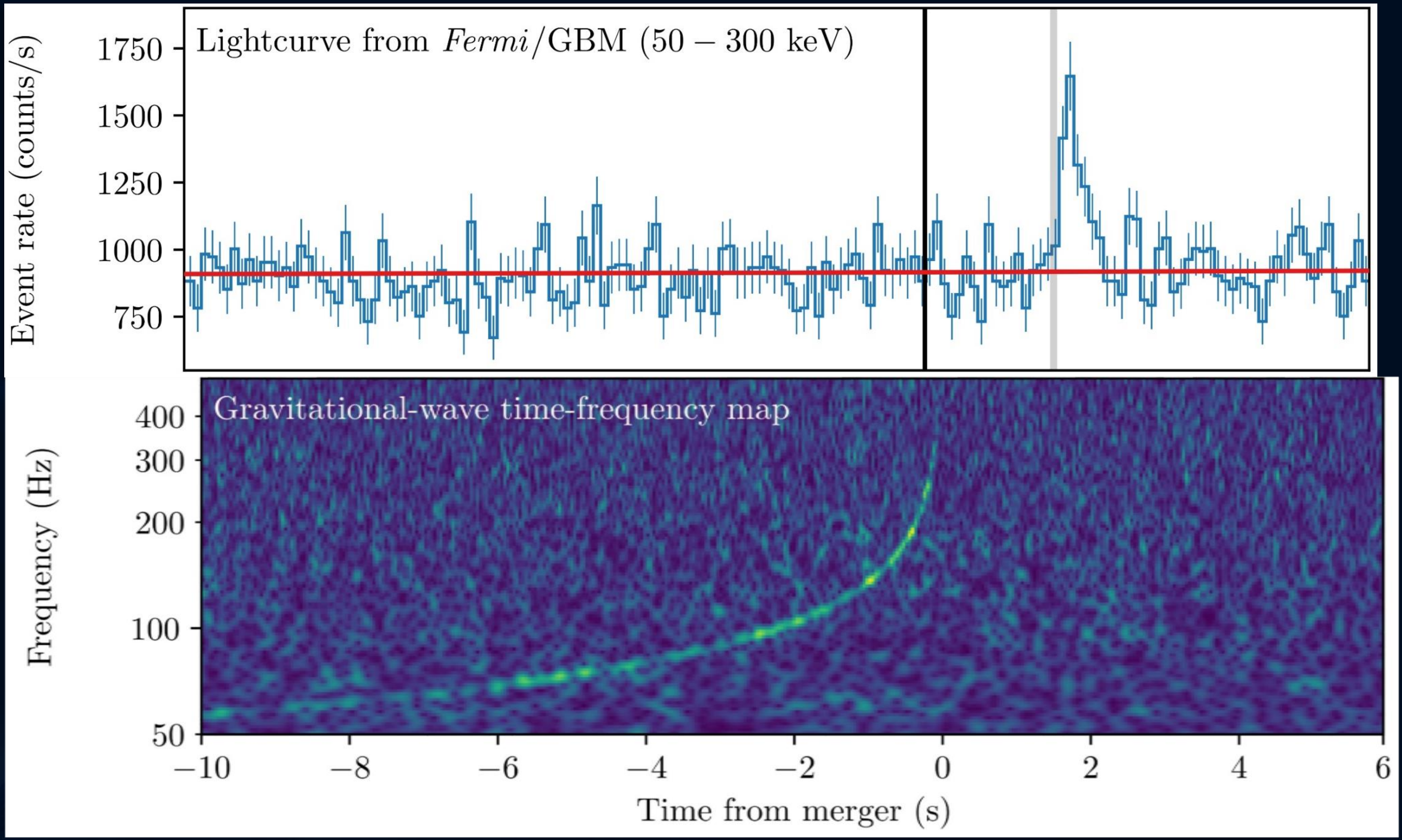

GW170817: Observation of Gravitational Waves from a Binary Neutron Star Inspiral, LIGO Scientific Collaboration and Virgo Collaboration, Phys. Rev. Lett. 119, 161101 (2017), Gravitational Waves and Gamma-Rays from a Binary Neutron Star Merger: GW170817 and GRB170817A, LIGO, Virgo, Fermi GBM, and INTEGRAL Collaborations, Astrophys. J. Lett. 848, L13 (2017)

GW170817

Tage, Wochen und Monate später detektierten weltweit unterschiedliche Teleskope (radio, infrarot, optische,…) eine Nachstrahlung dieser Neutronenstern Kollision

Multi-Messenger Observations of a Binary Neutron Star Merger, LIGO and Virgo Collaborations together with 50 teams of electromagnetic and neutrino astronomers, Astrophys. J. Lett. 848, L12 (2017)

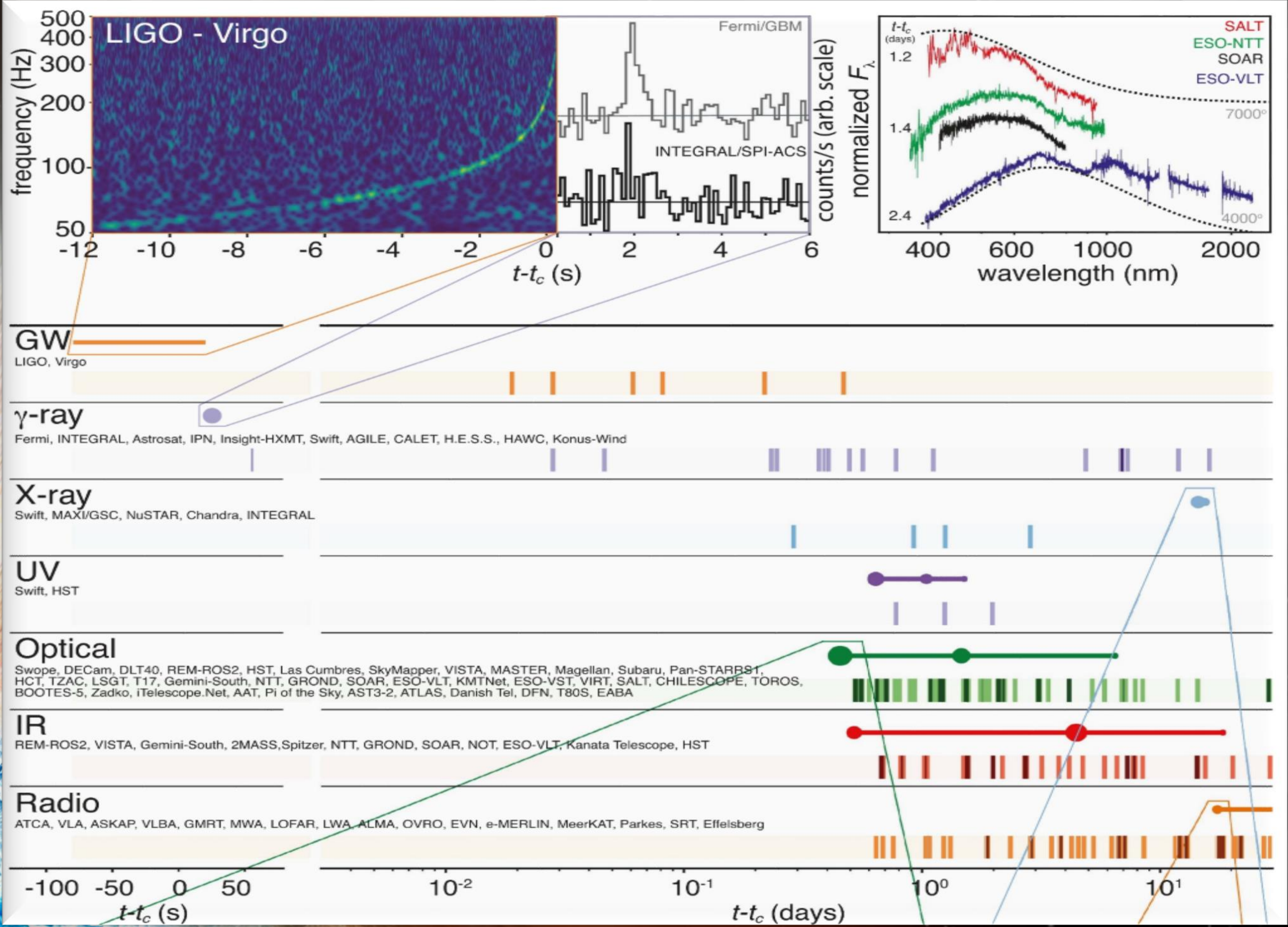

GW170817: Constraining the Neutron Star Radius and EOS

Talk by Bangalore Sathyaprakash and James Lattimer

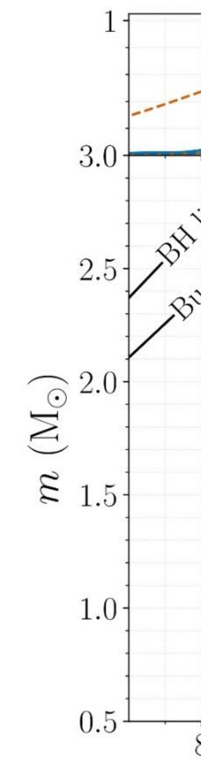

FIG. 3. Margin
and a parametr
posterior corre
the top left der
used for the po
of the 90% cre

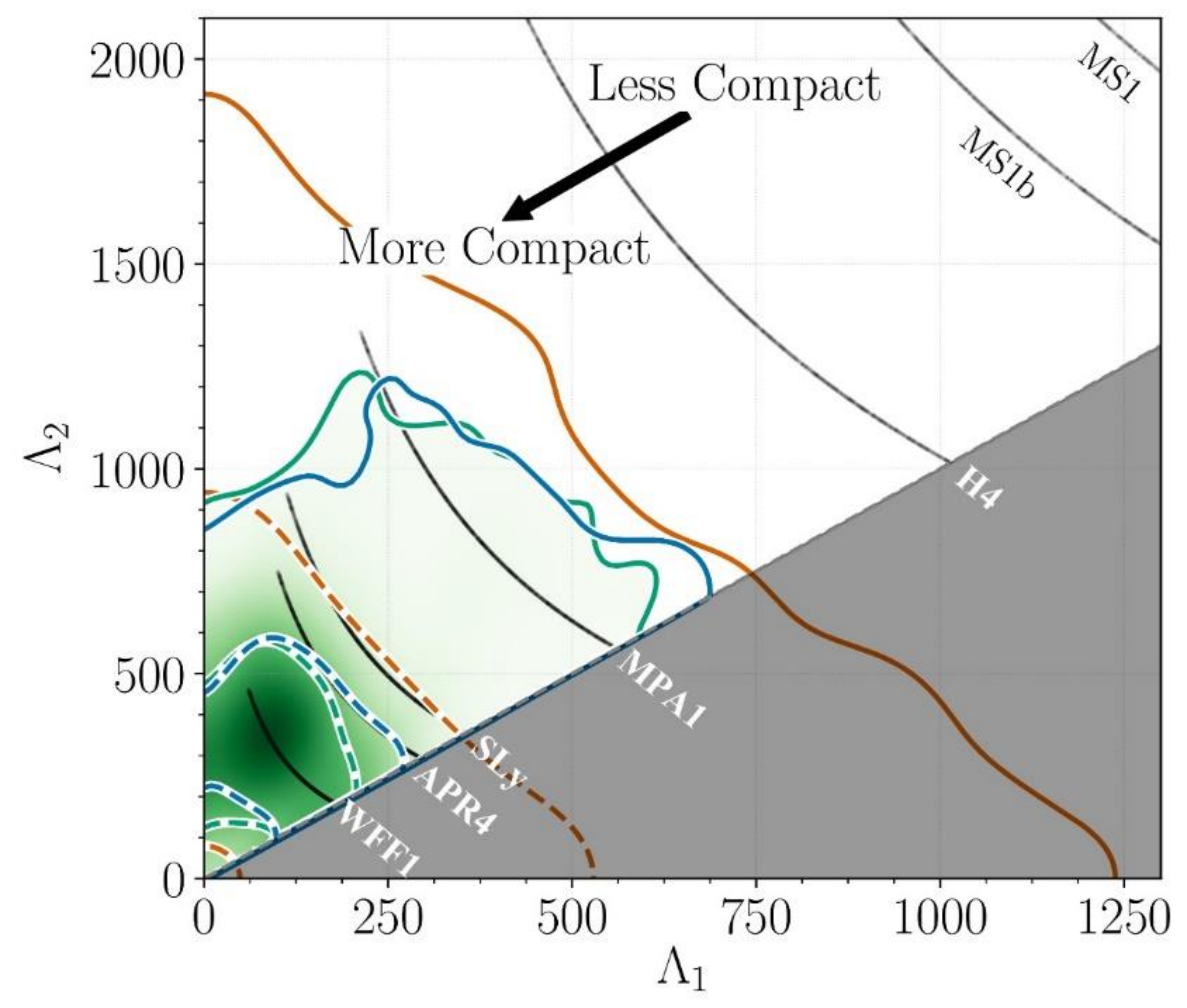

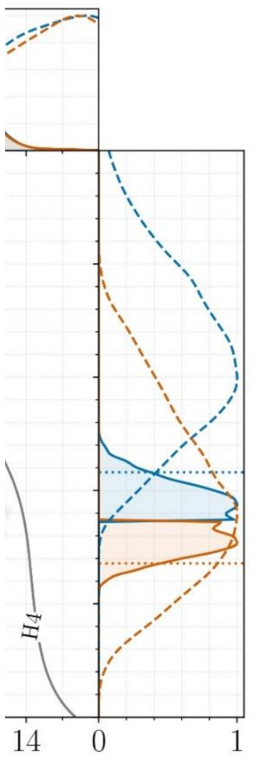

relations (left panel)
lue (bottom orange)
n grey. The lines in
plots, solid lines are
used for the bounds

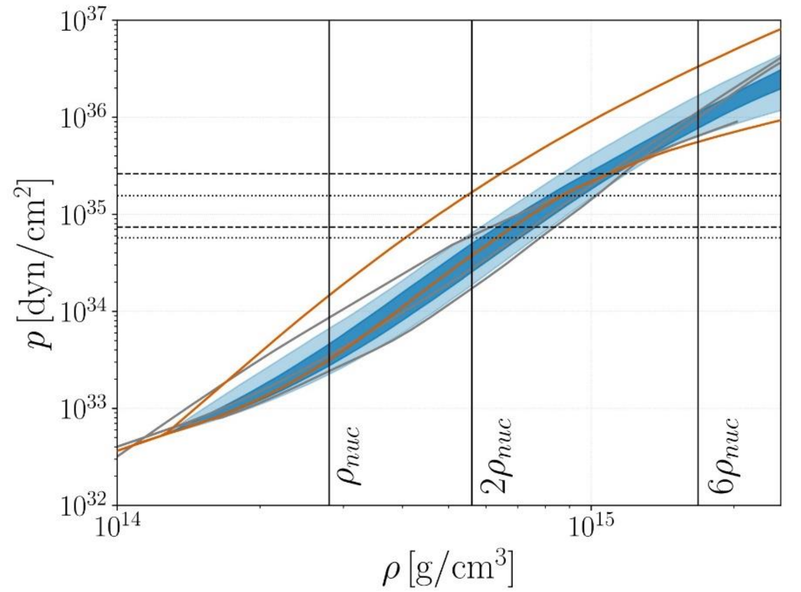

FIG. 2. Marginalized posterior (blue) and prior (orange) for the pressure p as a function of the rest-mass density ρ of the NS interior using the spectral EOS parametrization and imposing a lower limit on the maximum NS mass supported by the EOS of $1.97\,M_\odot$. The dark (light) blue shaded region corresponds to the 50% (90%) posterior credible level and the orange lines show the 90% prior credible interval. Horizontal lines denote the 90% credible interval for the central pressure of the heavier (dashed) and the lighter (dotted) binary components. Vertical lines correspond to once, twice, and six times the nuclear saturation density. Overplotted in grey are representative EOS models [121, 122, 124], using data taken from [19]; from top to bottom at $2\rho_{nuc}$ we show H4, APR4, and WFF1.

GW170817: Measurements of neutron star radii and equation of state, *The LIGO /Virgo Collaboration*, arXiv:1805.11581v1

GW170817: Constraining the Neutron Star Radius

Impact of Phase Transitions

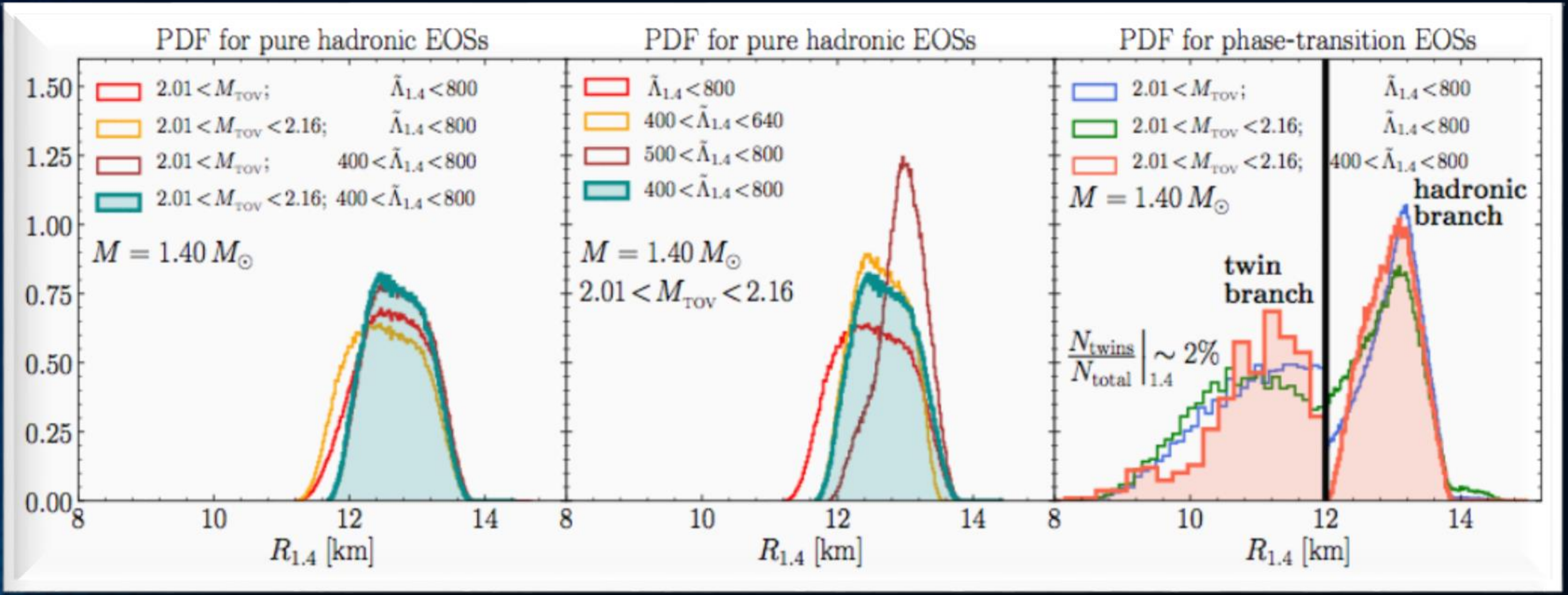

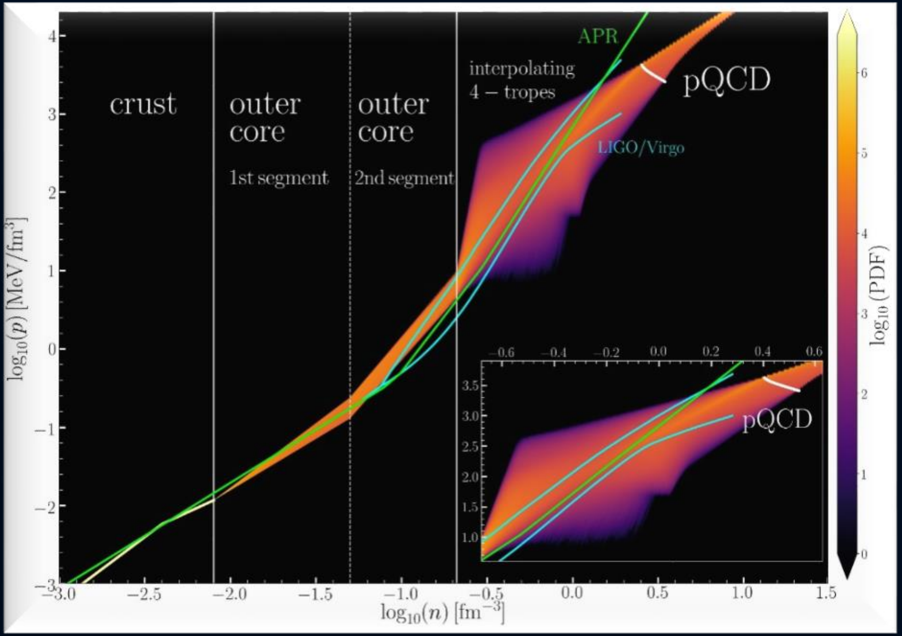

$$12.00 < R_{1.4}/\mathrm{km} < 13.45 \qquad \bar{R}_{1.4} = 12.45\,\mathrm{km}$$ EOSs without phase transitions

$$8.53 < R_{1.4}/\mathrm{km} < 13.74 \qquad \bar{R}_{1.4} = 13.06\,\mathrm{km}$$ EOSs with phase transitions

E.Most, L.Weih, L.Rezzolla, J. Schaffner-Bielich "New constraints on radii and tidal deformabilities of neutron stars from GW170817", arXiv:1803.00549, (accepted in PRL)

See also: De, Finstad, Lattimer, Brown, Berger, Biwer, (2018), arXiv:1804.08583 ; Bauswein, Just, Janka, N. Stergioulas, APJL 850, L34 (2017) ; Fattoyev, Piekarewicz, Horowitz, PRL 120, 172702 (2018) ; Nandi & Char, Astrophys. J. 857, 12 (2018) ; Paschalidis, Yagi, Alvarez-Castillo, Blaschke, Sedrakian, PRD 97, 084038 ; Ruiz, Shapiro, Tsokaros, PRD 97, 021501 (2018) ; Annala, Gorda, Kurkela, Vuorinen, PRL 120, 172703 (2018) ; Raithel, Özel, Psaltis, (2018) arXiv:1803.07687

GW170817: Constraining the maximum mass of Neutron Stars

Talk by Cole Miller

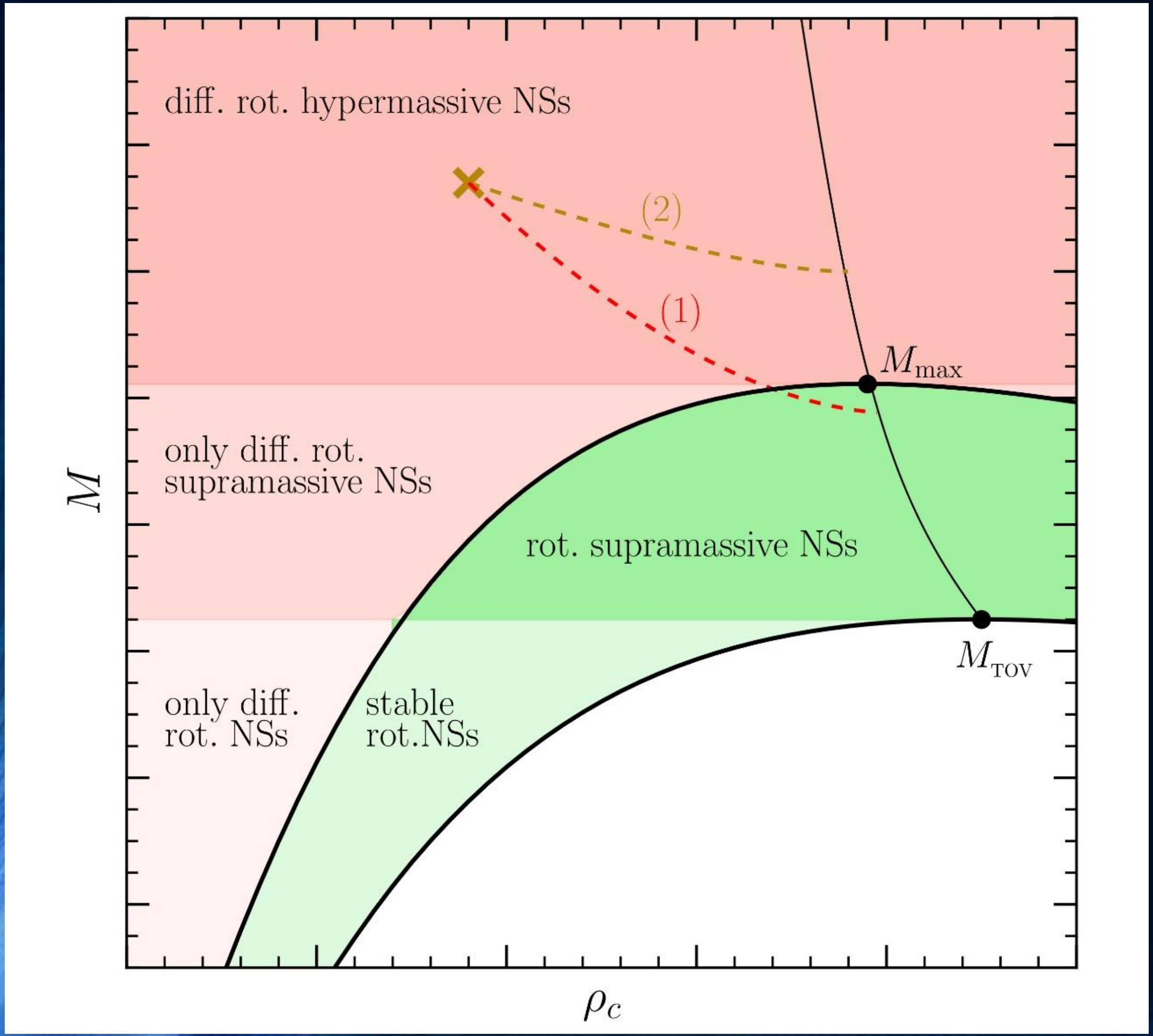

The highly differentially rotating hypermassive/supramassive neutron star will spin down and redistribute its angular momentum (e.g. due to viscosity effects, magnetic braking). After ~1 second it will cross the stability line as a uniformly rotating supramassive neutron star (close to M_{max}) and collapse to a black hole. Parts of the ejected matter will fall back into the black hole producing the gamma-ray burst.

L.Rezzolla, E.Most, L.Weih, "Using Gravitational Wave Observations and Quasi-Universal Relations to constrain the maximum Mass of Neutron Stars",The Astrophysical Journal Letters 852, L25 (2018):
2.01 +/-0.04 < M_{TOV} < 2.16 +/-0.17

See also: S.Lawrence et al. ,APJ808,186, 2015
Margalit & Metzger, The Astrophysical Journal Letters 850, L19 (2017): M_{TOV} < 2.17 (90%)
Zhou, Zhou, Li, PRD 97, 083015 (2018)
Ruiz, Shapiro, Tsokaros, PRD 97,021501 (2018)

Numerical Relativity and Relativistic Hydrodynamics of Binary Neutron Star Mergers

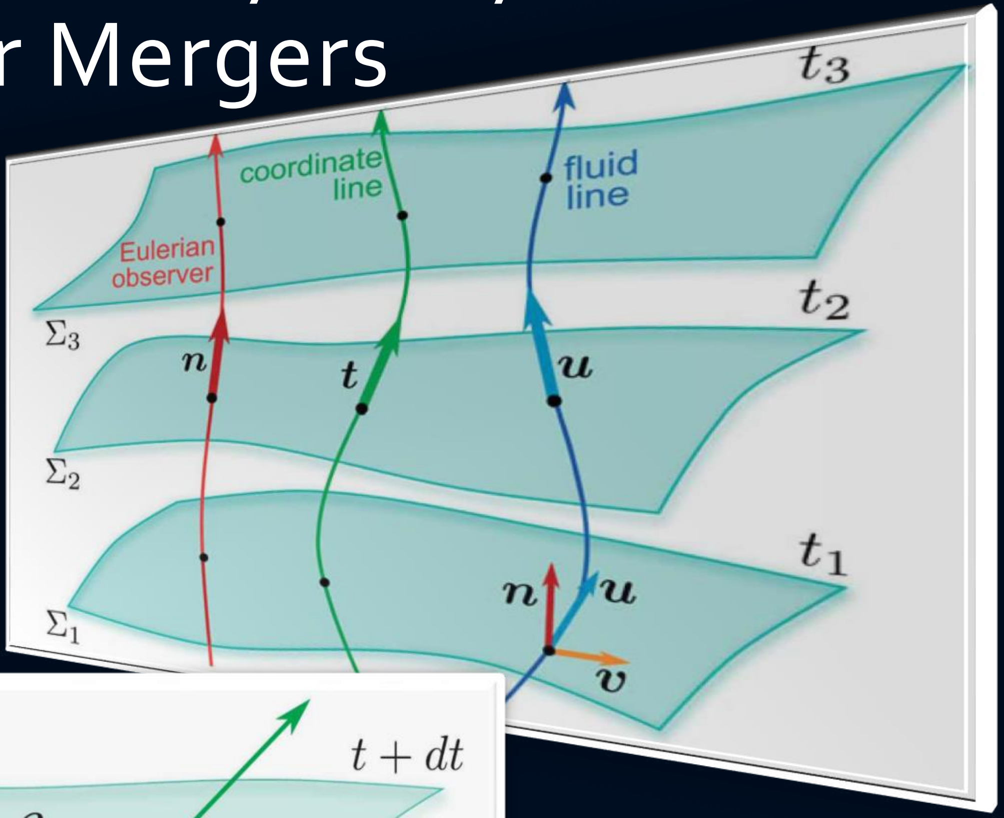

Numerical simulations of a merger of two compact stars are based on a (3+1) decomposition of spacetime of the Einstein and hydrodynamic equations.

$$R_{\mu\nu} - \frac{1}{2} g_{\mu\nu} R = 8\pi T_{\mu\nu}$$

$$\nabla_\mu (\rho u^\mu) = 0\,, \qquad \nabla_\nu T^{\mu\nu} = 0\,.$$

(3+1) decomposition of spacetime

$$g_{\mu\nu} = \begin{pmatrix} -\alpha^2 + \beta_i \beta^i & \beta_i \\ \beta_i & \gamma_{ij} \end{pmatrix}$$

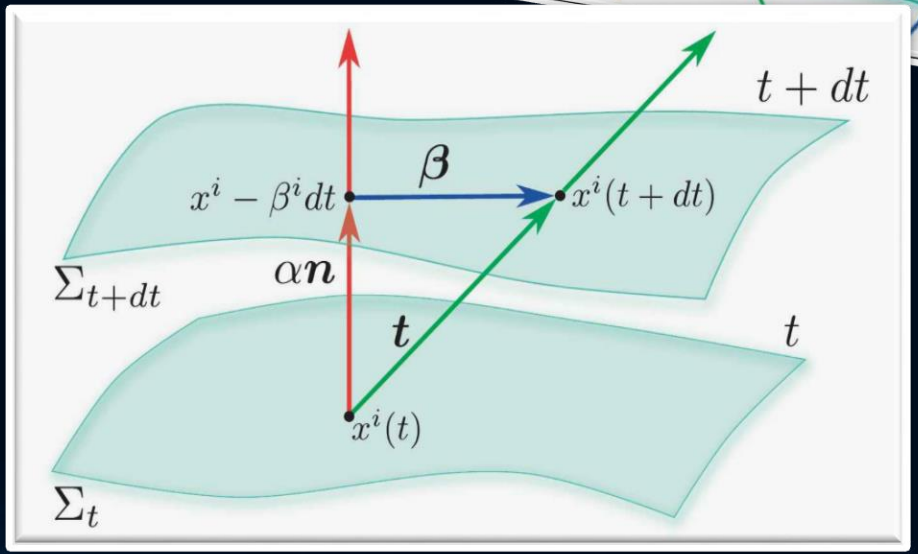

$$d\tau^2 = \alpha^2(t, x^j) dt^2 \qquad x^i_{t+dt} = x^i_t - \beta^i(t, x^j) dt$$

All figures and equations from: Luciano Rezzolla, Olindo Zanotti: Relativistic Hydrodynamics, Oxford Univ. Press, Oxford (2013)

Gravitational Waves from Neutron Star Mergers

Neutron Star Collision (Simulation)

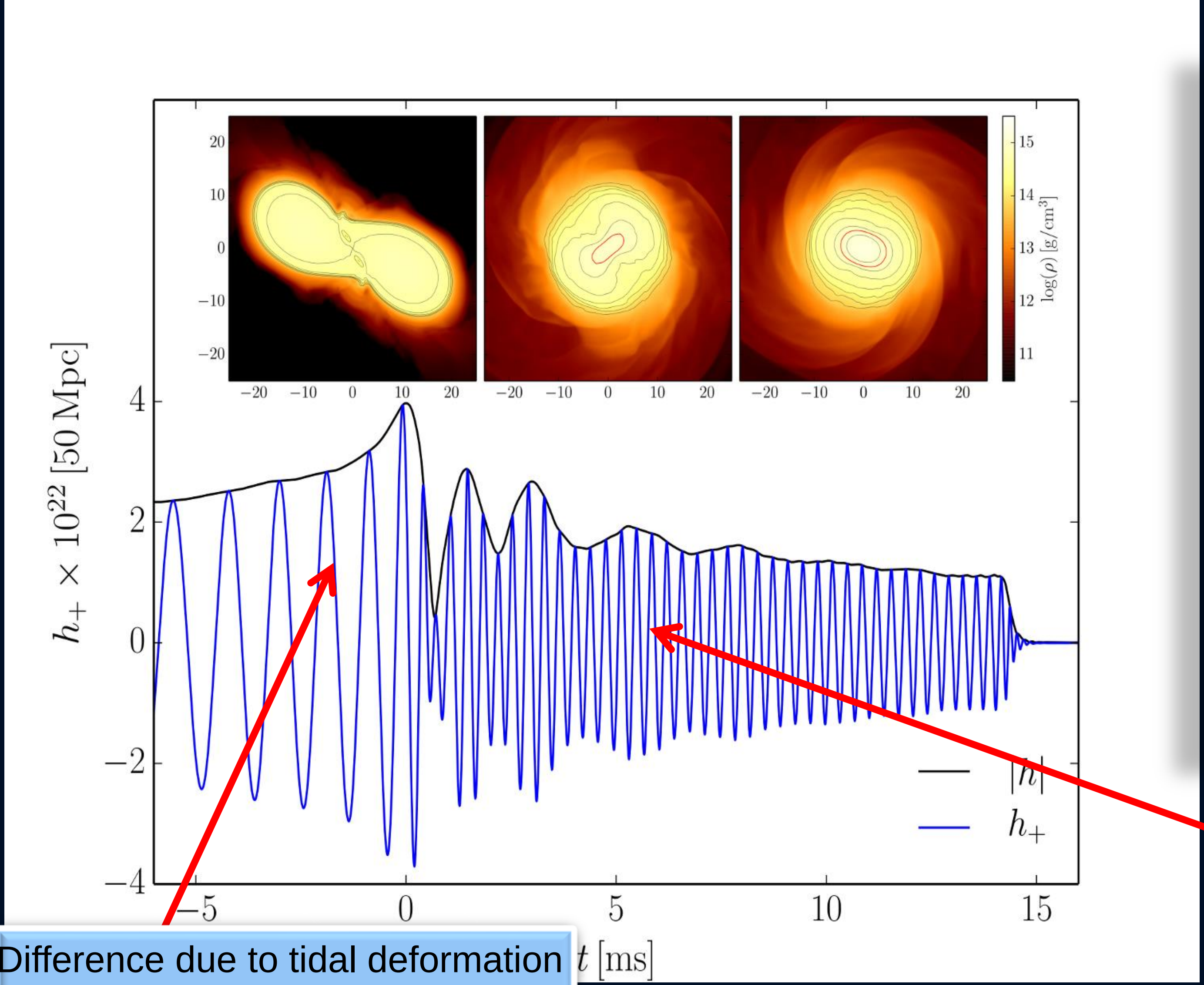

Difference due to tidal deformation in the late inspiral phase

Collision of two Black Holes
GW150914

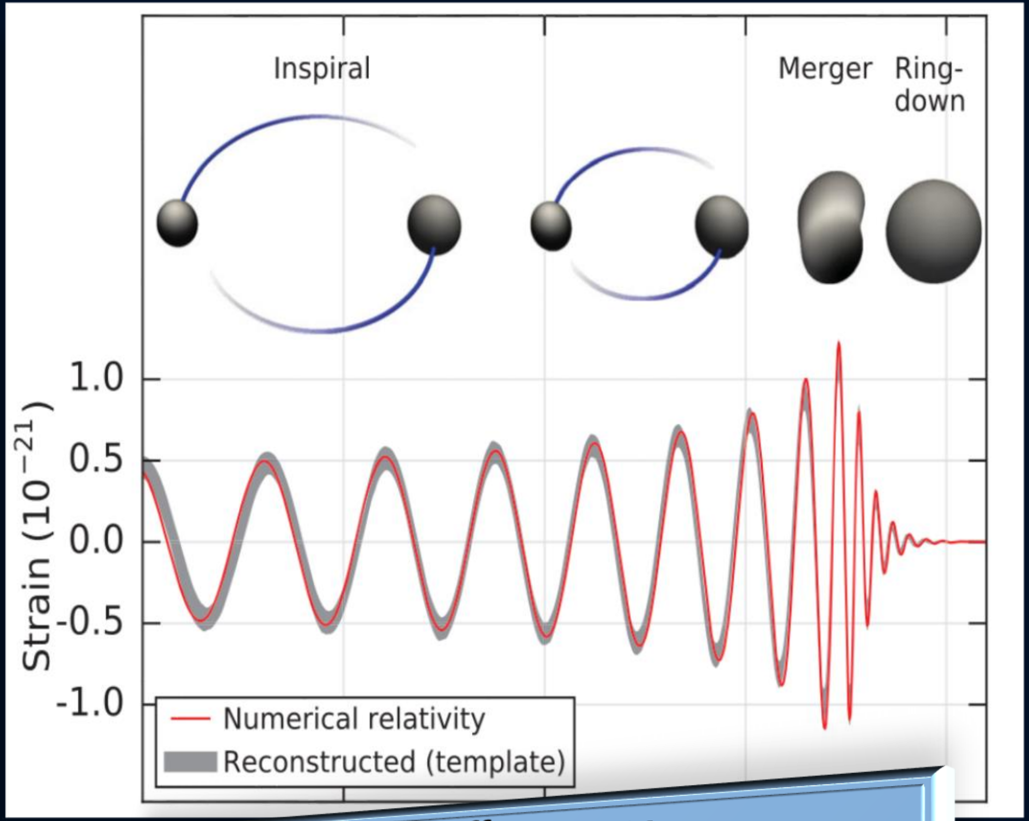

Main difference:
In binary neutron star mergers a **Post-Merger Phase** often exists

GW-Spectrum for different EOSs

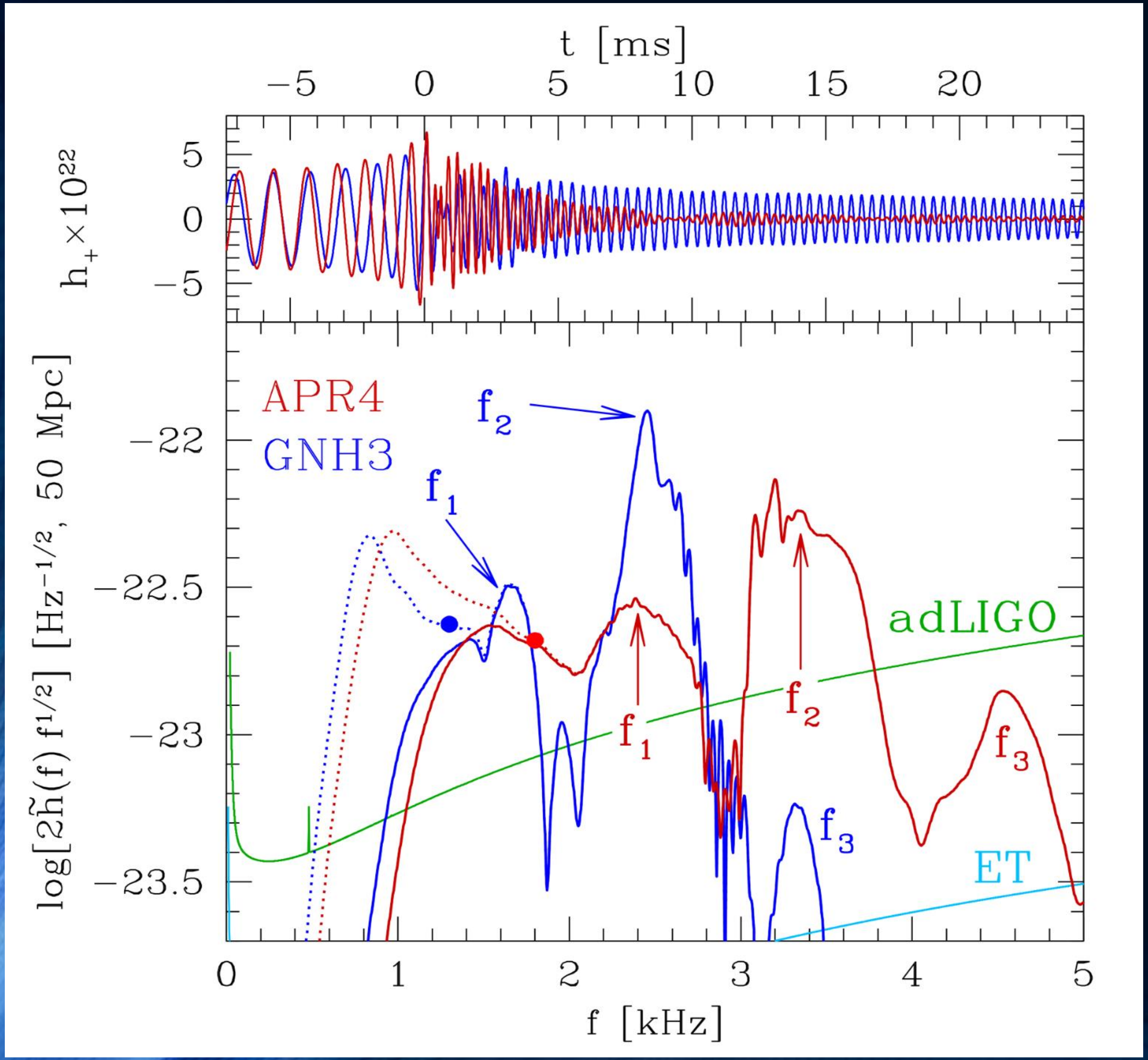

See:

Oechslin+2007, Baiotti+2008, Bauswein+ 2011, 2012, Stergioulas+ 2011, Hotokezaka+ 2013, Takami 2014, 2015, Bernuzzi 2014, 2015, Bauswein+ 2015, Clark+ 2016, Rezzolla+2016, de Pietri+ 2016, Feo+ 2017, Bose+ 2017

Kentaro Takami, Luciano Rezzolla, and Luca Baiotti, Physical Review D 91, 064001 (2015)

Hotokezaka, K., Kiuchi, K., Kyutoku, K., Muranushi, T., Sekiguchi, Y. I., Shibata, M., & Taniguchi, K. (2013). Physical Review D, 88(4), 044026.

Bauswein, A., & Janka, H. T. (2012). Physical review letters, 108(1), 011101.

Clark, J. A., Bauswein, A., Stergioulas, N., & Shoemaker, D. (2015). arXiv:1509.08522.

Bernuzzi, S., Dietrich, T., & Nagar, A. (2015). Physical review letters, 115(9), 091101.

Time Evolution of the GW-Spectrum

The power spectral density profile of the post-merger emission is characterized by several distinct frequencies. After approximately 5 ms after merger, the only remaining dominant frequency is the f_2-frequency (See e.g. L.Rezzolla and K.Takami, PRD, 93(12), 124051 (2016))

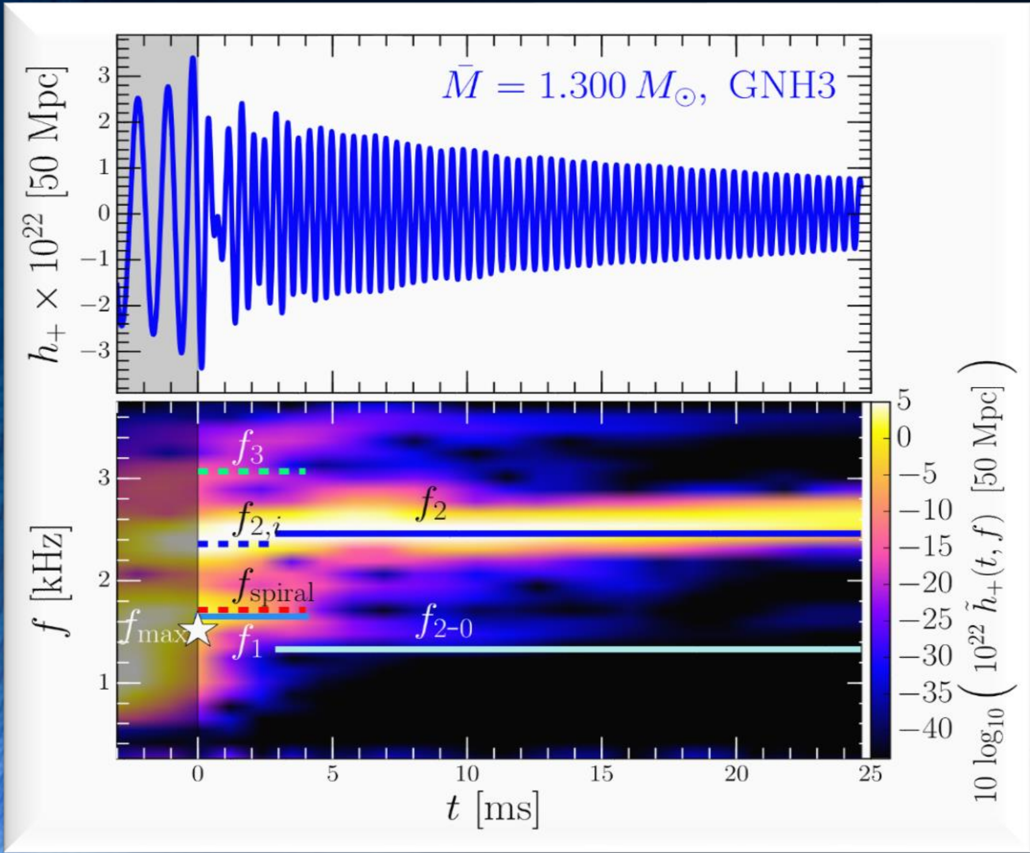

Stiff EOS

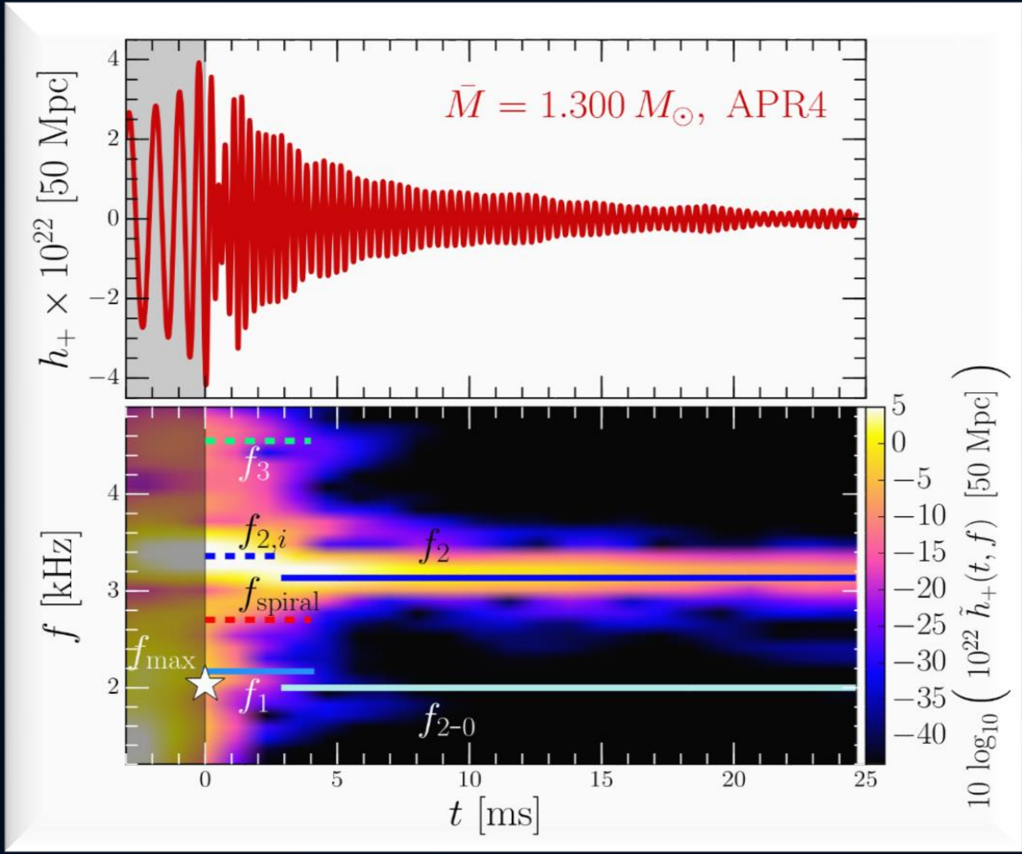

Soft EOS

Unfortunately, due to the low sensitivity at high gravitational wave frequencies, no post-merger signal has been found in GW170817.

But advanced detectors / next-generation detectors might be able to detect!!?

Evolution of the frequency spectrum of the emitted gravitational waves for the stiff GNH3 (left) and soft APR4 (right) EOS.

Binary Merger of two Neutron Stars for different EoSs

High mass simulations
(M=1.35 Msolar)

Central value of the lapse function α_c (upper panel) and maximum of the rest mass density ρ_{max} in units of ρ_0 (lower panel) versus time for the high mass simulations.

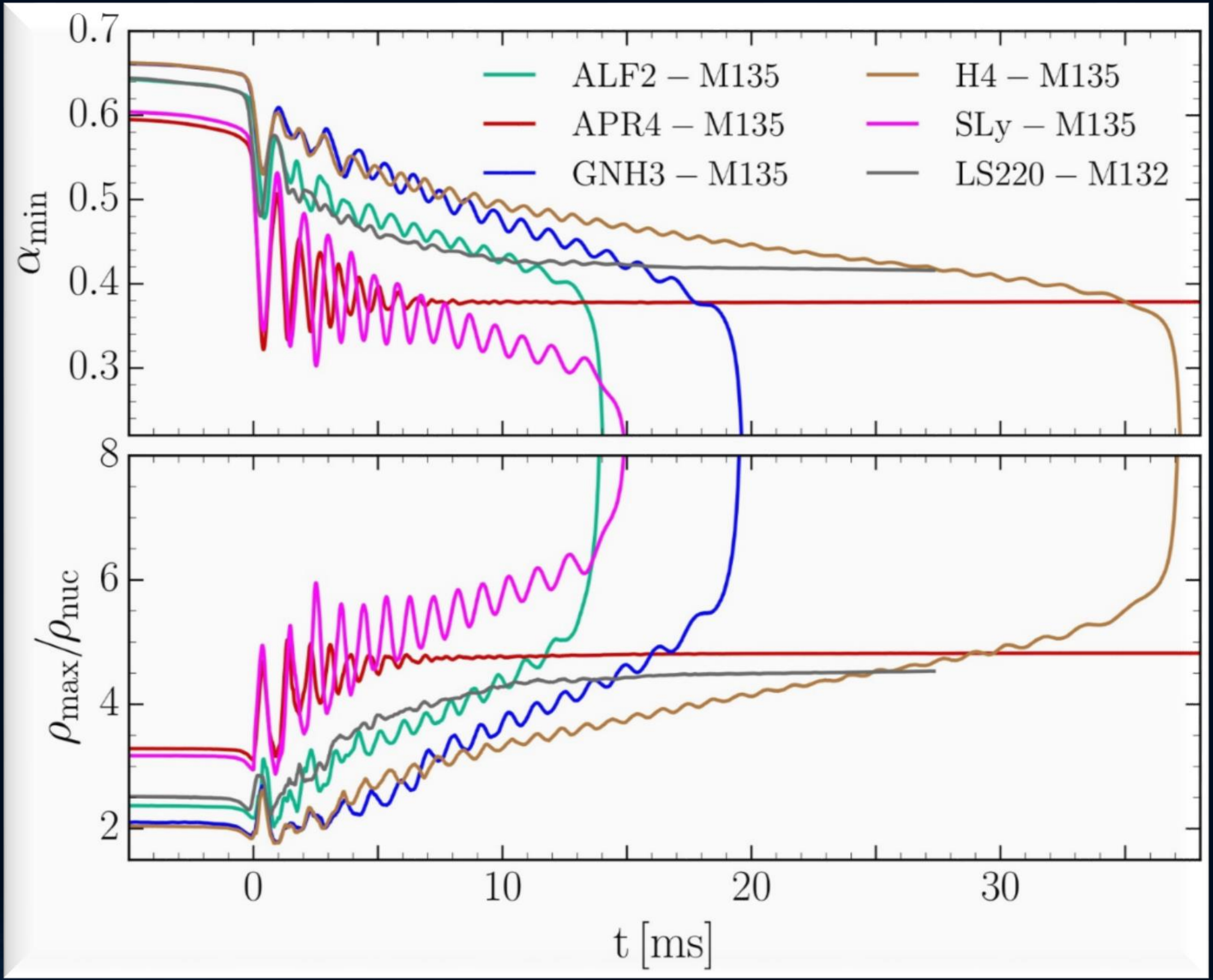

Hanauske, et.al. PRD, 96(4), 043004 (2017)

The QCD – Phase Transition and the Interior of a Hybrid Star

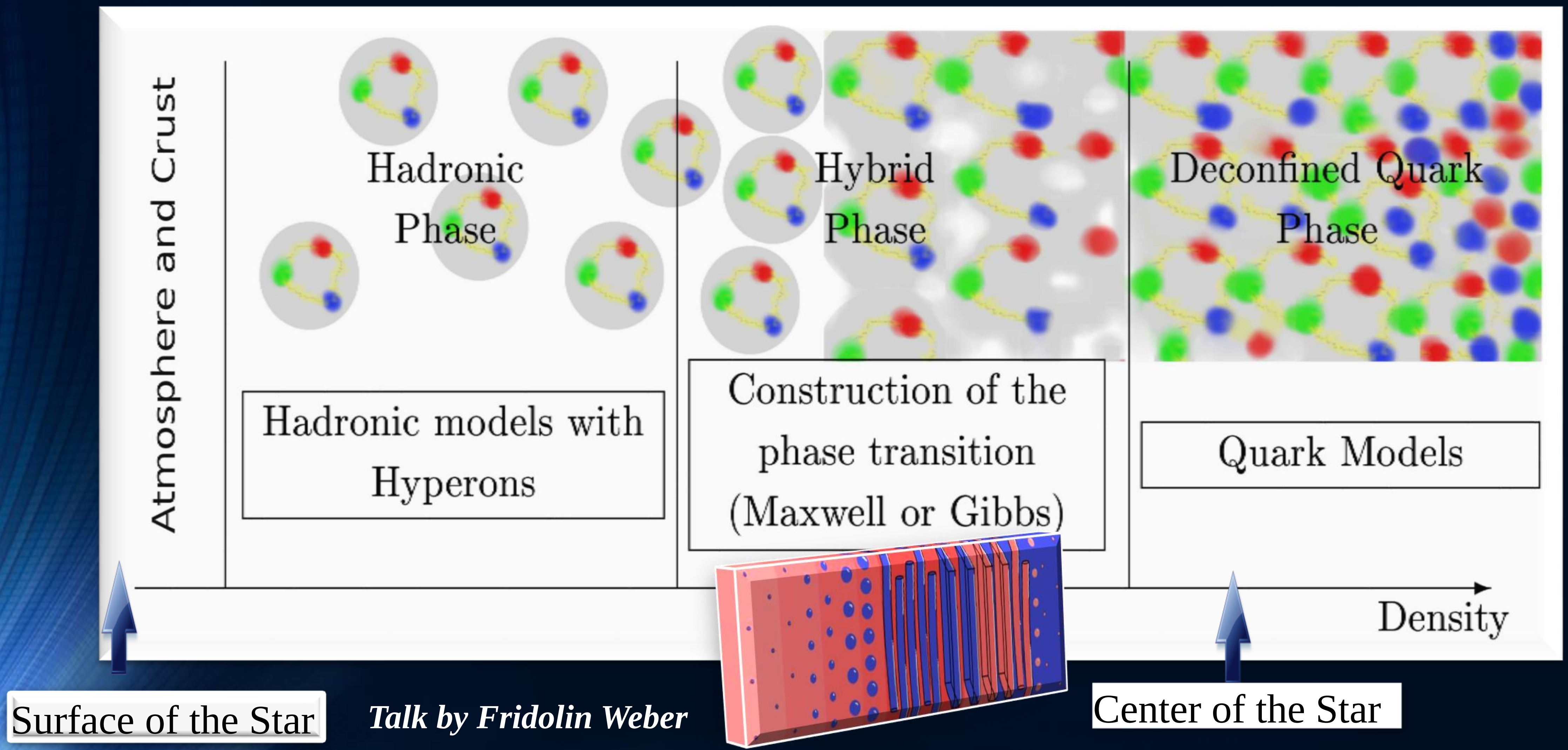

Talk by Fridolin Weber

Matthias Hanauske; Doctoral Thesis:
Properties of Compact Stars within QCD-motivated Models; University Library Publication Frankfurt (2004)

Evolution of the density in the post merger phase

ALF2-EOS: Mixed phase region starts at $3\rho_0$ (see red curve), initial NS mass: 1.35 M_{solar}

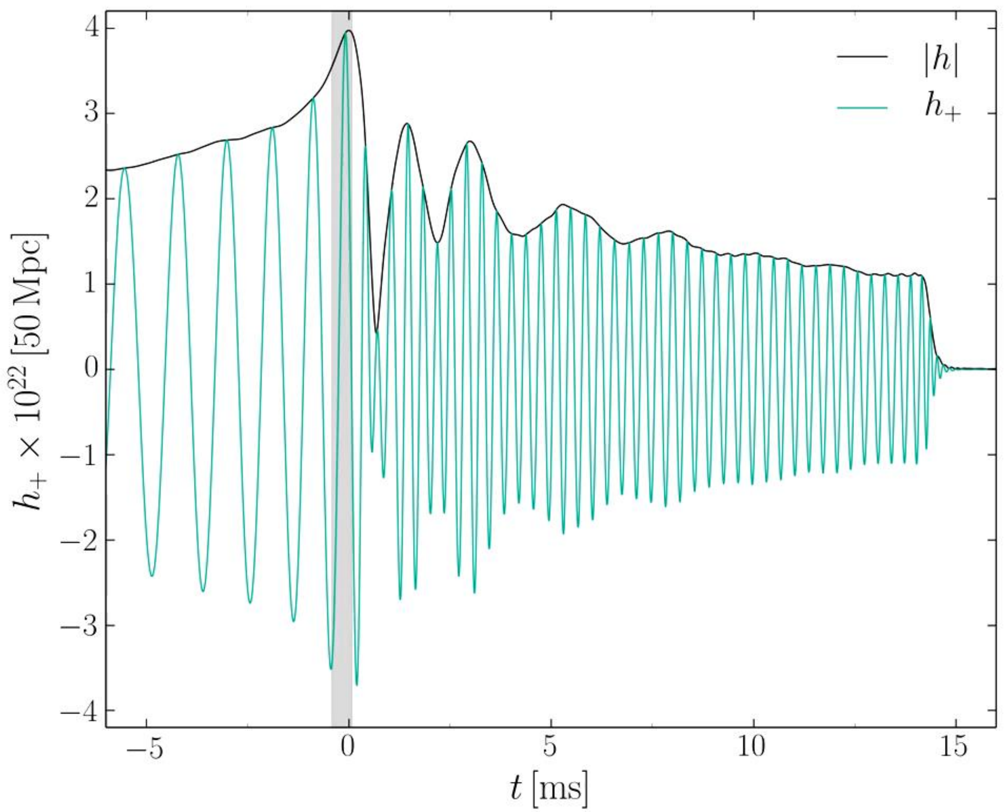

Gravitational wave amplitude
at a distance of 50 Mpc

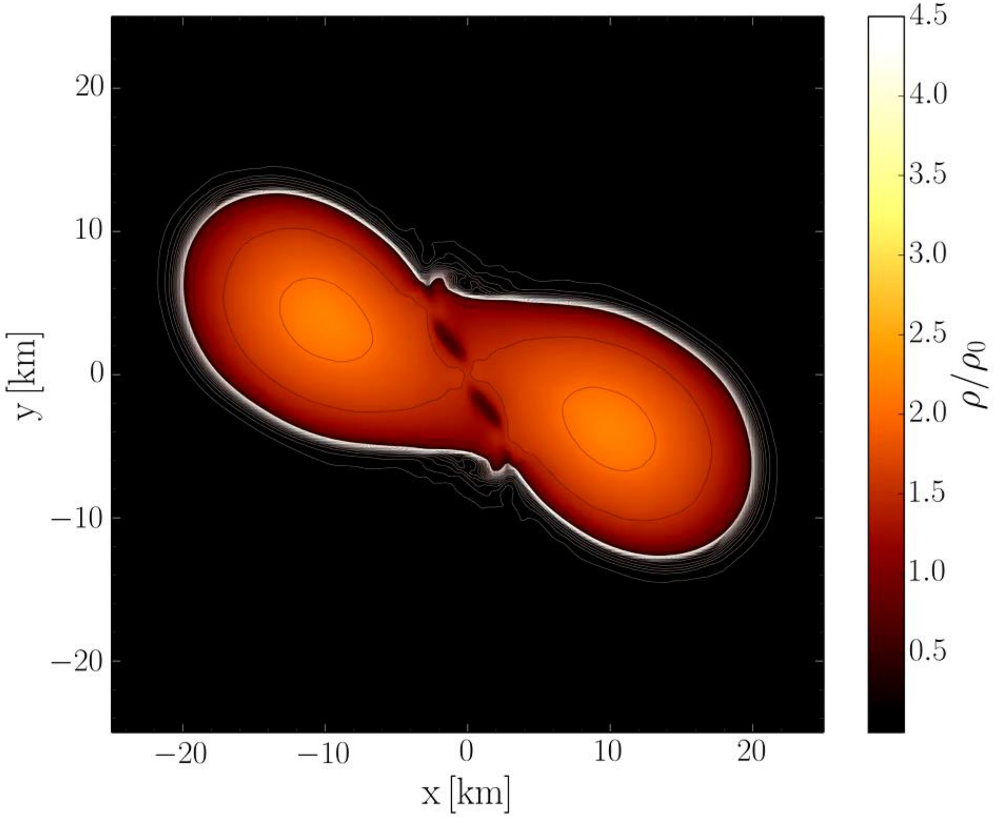

Rest mass density distribution $\rho(x,y)$
in the equatorial plane

in units of the nuclear matter density ρ_0

The QCD Phae Diagram

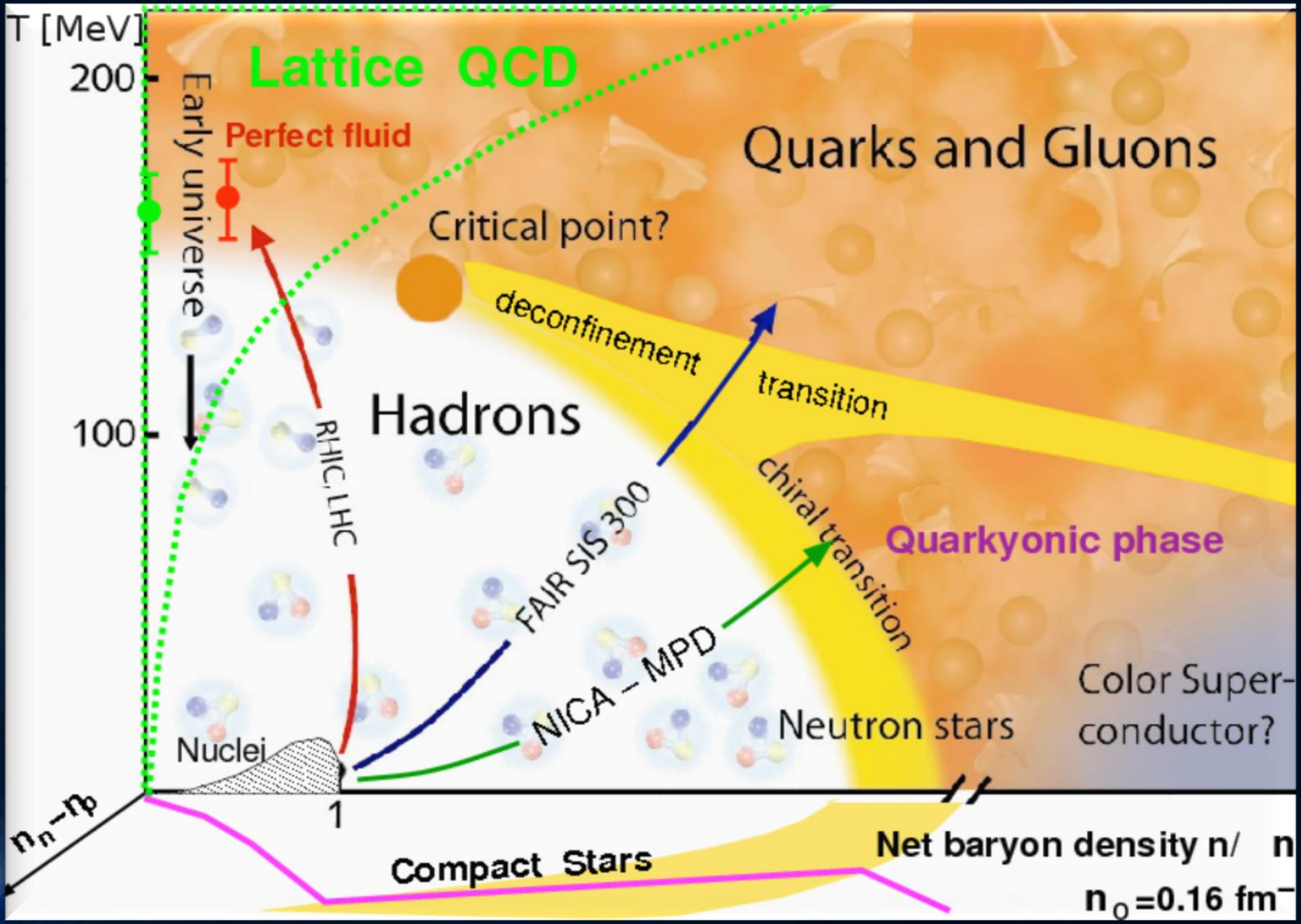

Credits to http://inspirehep.net/record/823172/files/phd_qgp3D_quarkyonic2.png

The Gibbs Construction

Hadronic and quark surface:

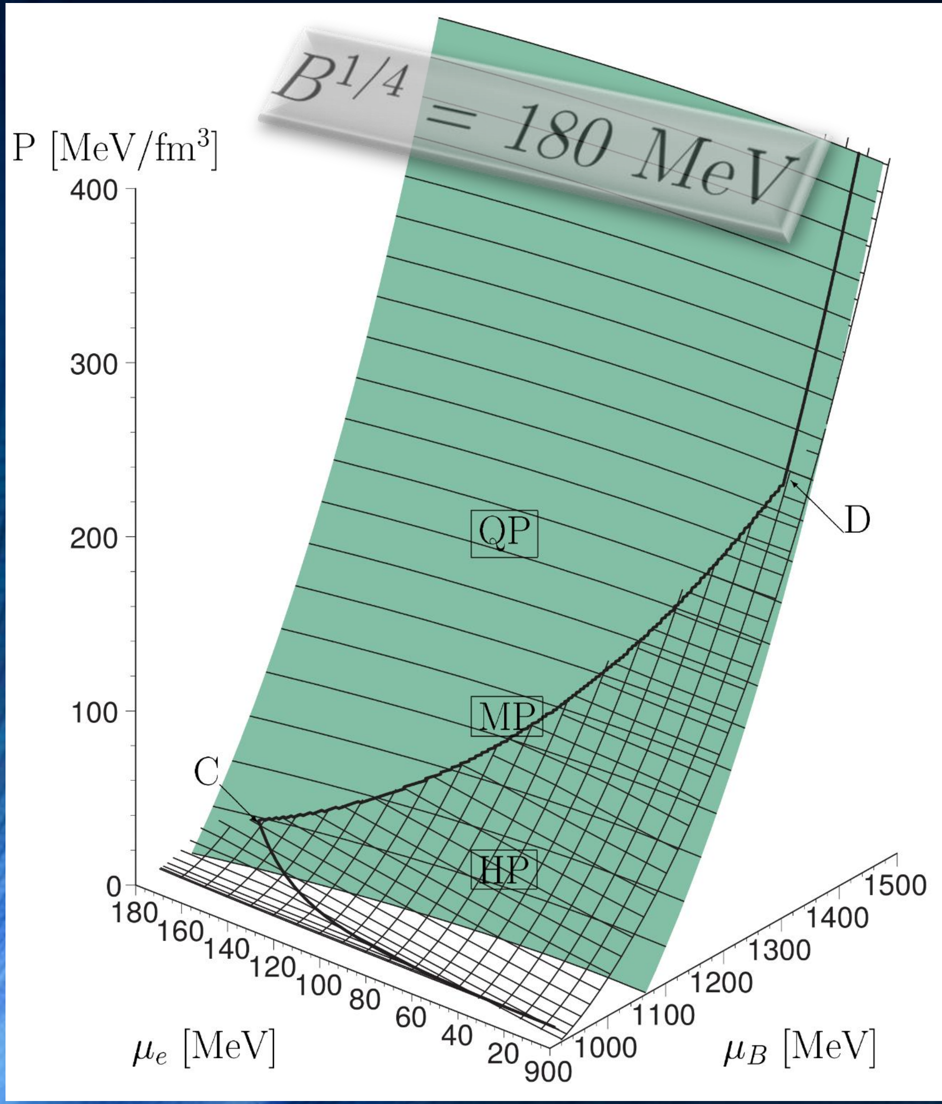

Charge neutrality condition is only globally realized

$$\rho_e := (1-\chi)\,\rho_e^H(\mu_B,\mu_e) + \chi\,\rho_e^Q(\mu_B,\mu_e) = 0\,.$$

The pressure in the mixed phase depends on two independent chemical potentials

$$\begin{aligned} P^H(\mu_B,\mu_e) &= P^Q(\mu_B,\mu_e)\,, \\ \mu_B = \mu_B^H &= \mu_B^Q\,, \\ \mu_e = \mu_e^H &= \mu_e^Q \end{aligned}$$

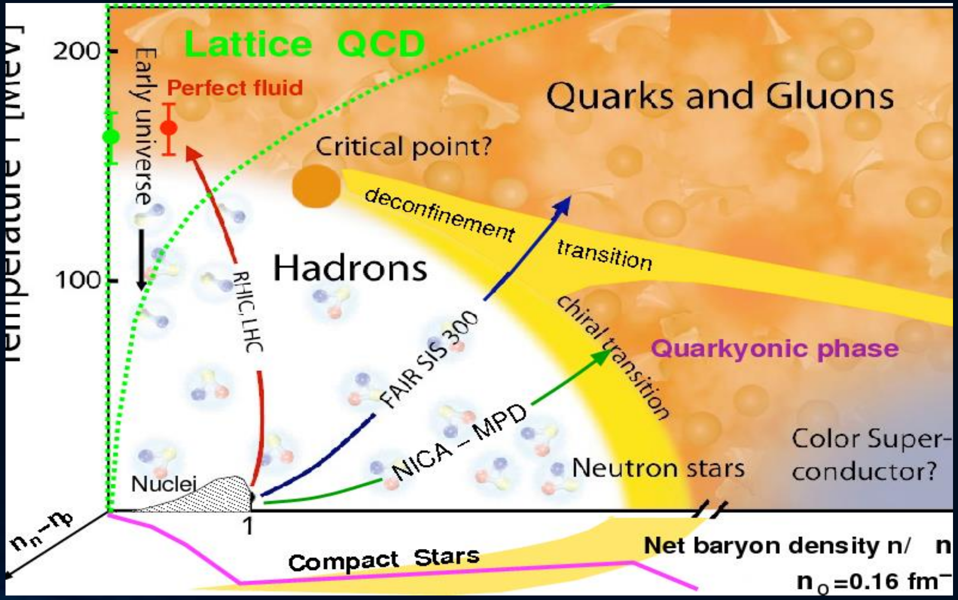

The Gibbs Construction

Hadronic and quark surface:

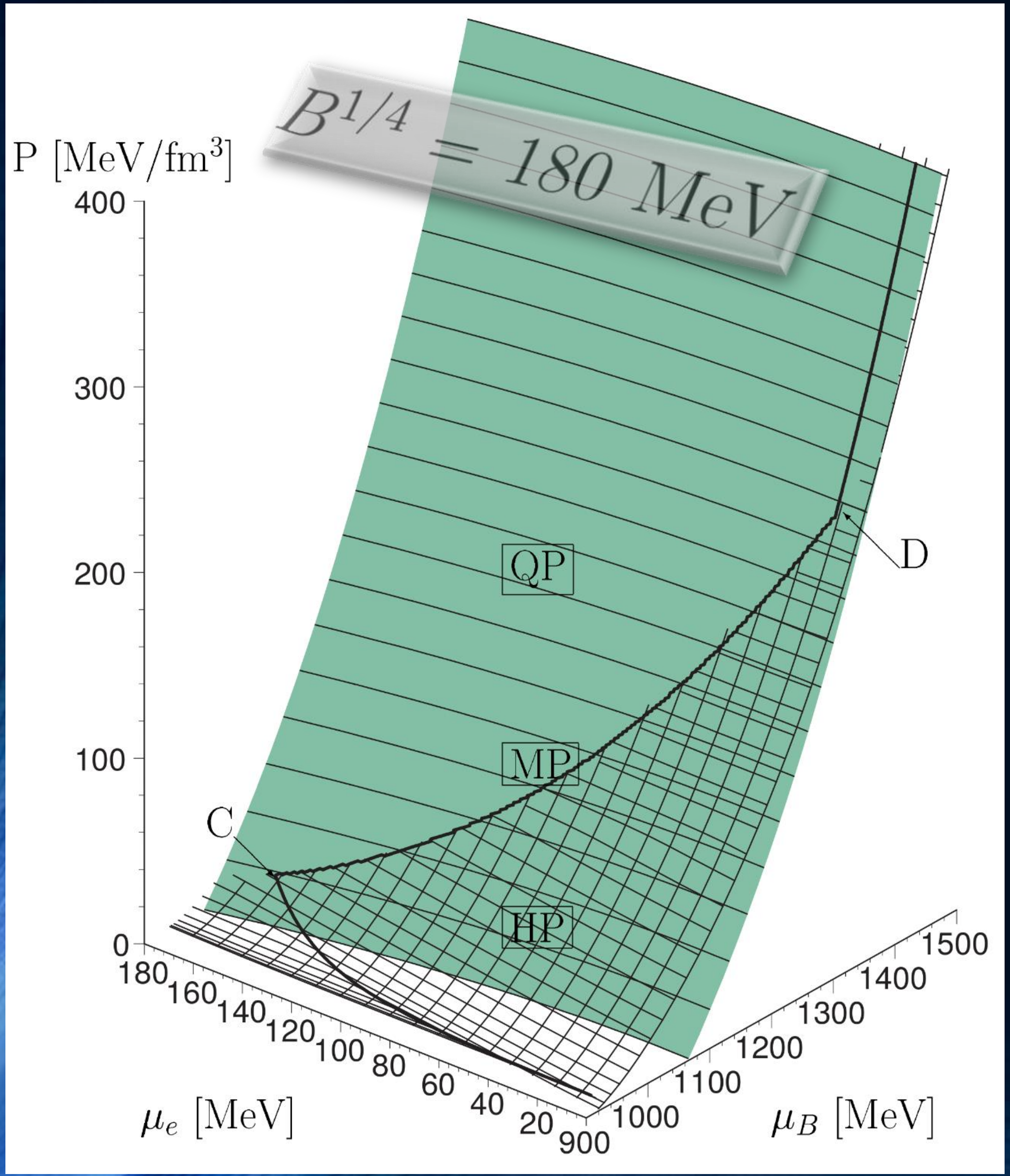

Charge neutrality condition is only globally realized

$$\rho_e := (1-\chi)\,\rho_e^H(\mu_B,\mu_e) + \chi\,\rho_e^Q(\mu_B,\mu_e) = 0\,.$$

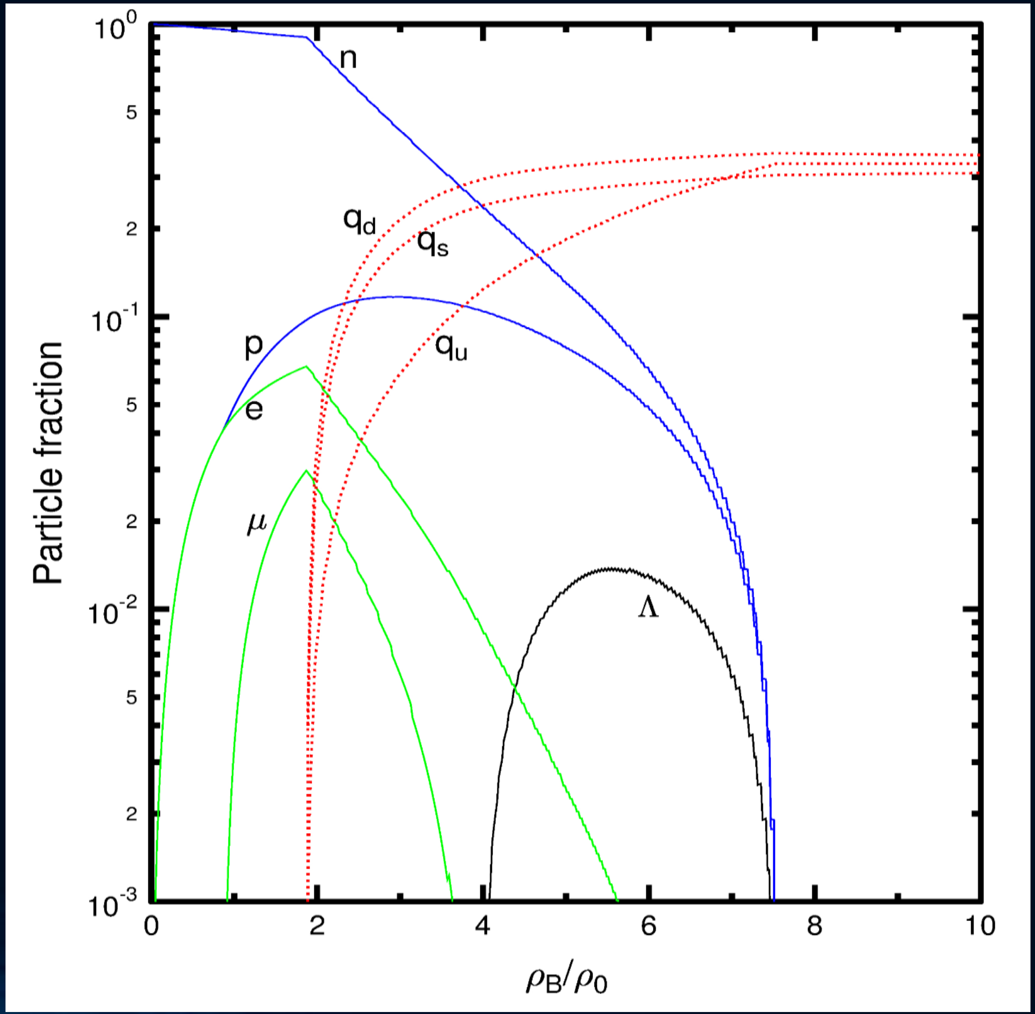

The Gibbs Construction

Hadronic and quark surface:

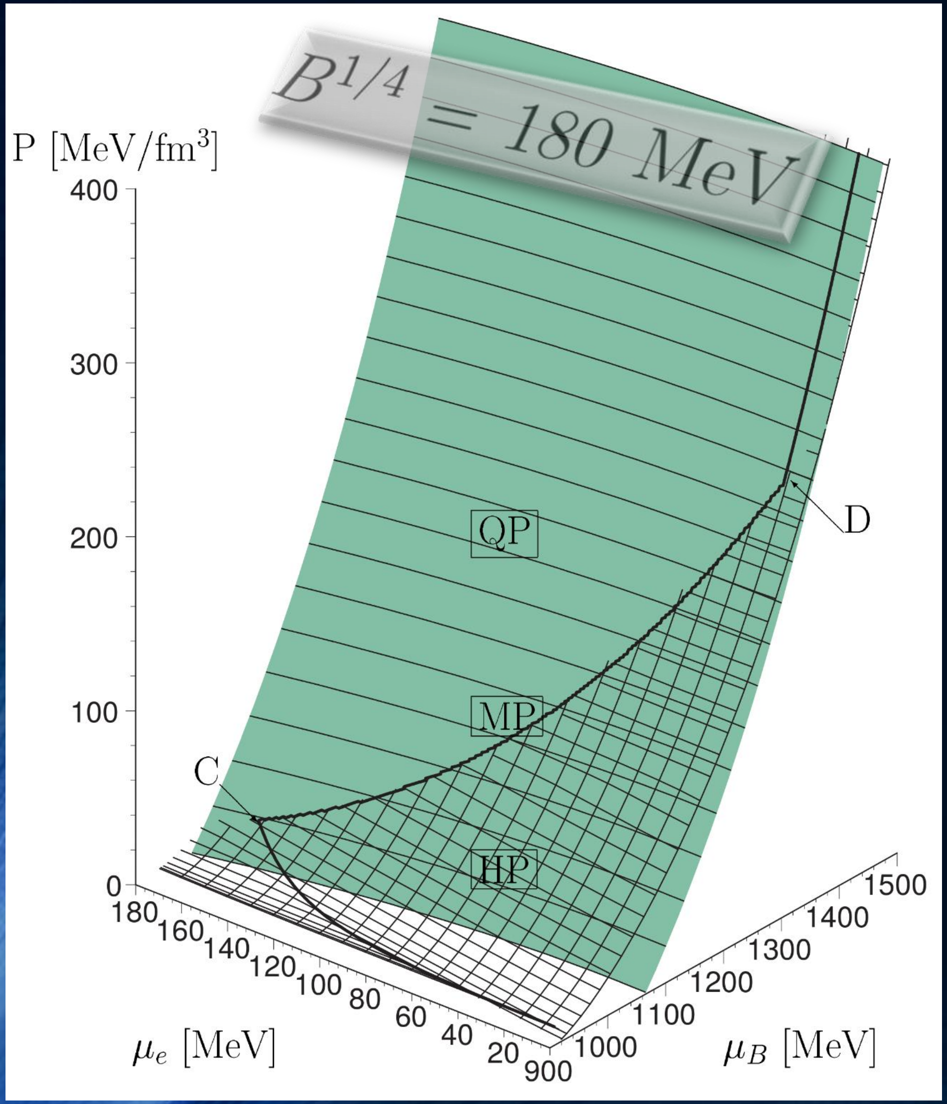

Particle composition:

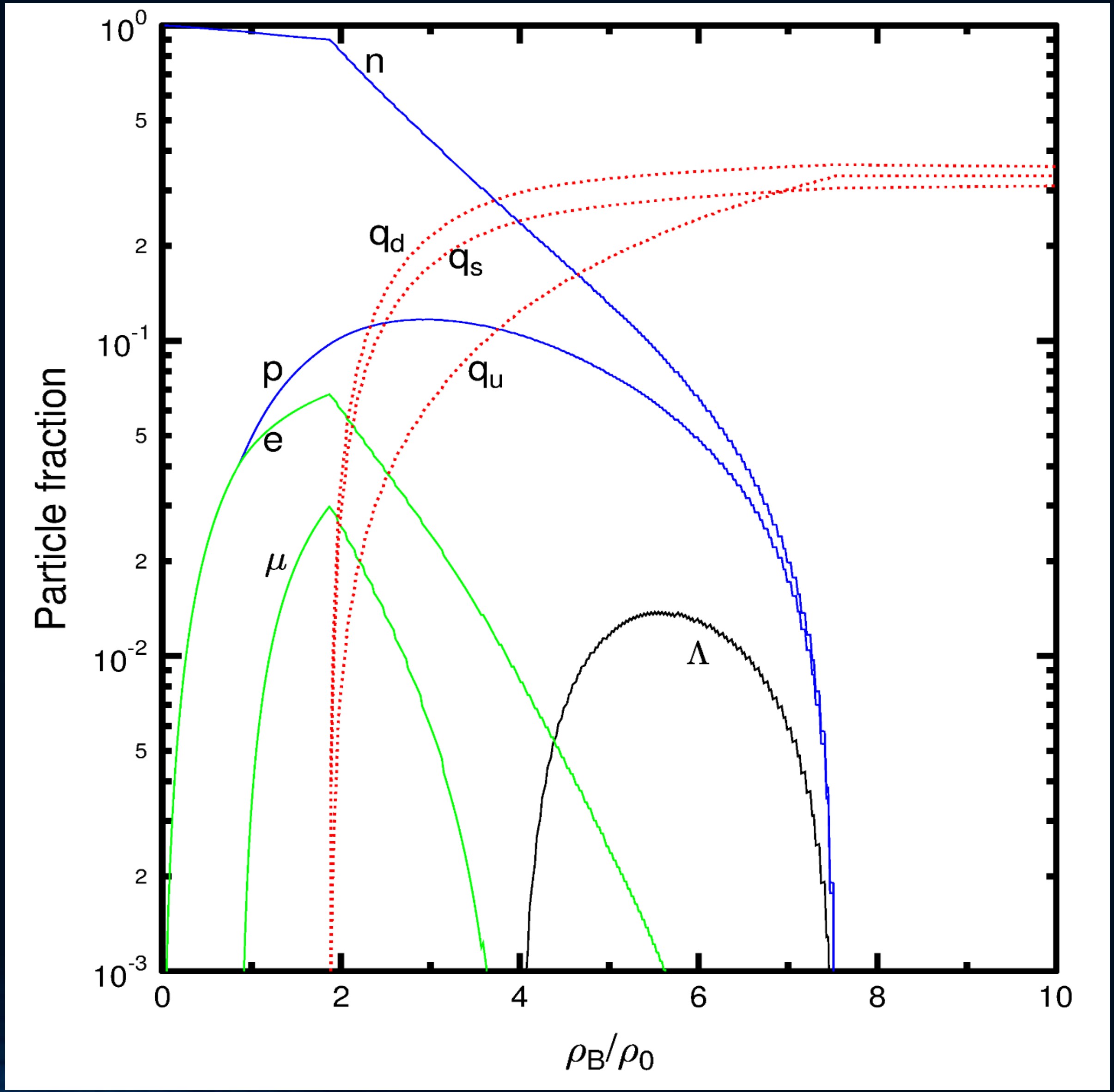

The Gibbs Construction

Hadronic and quark surface:

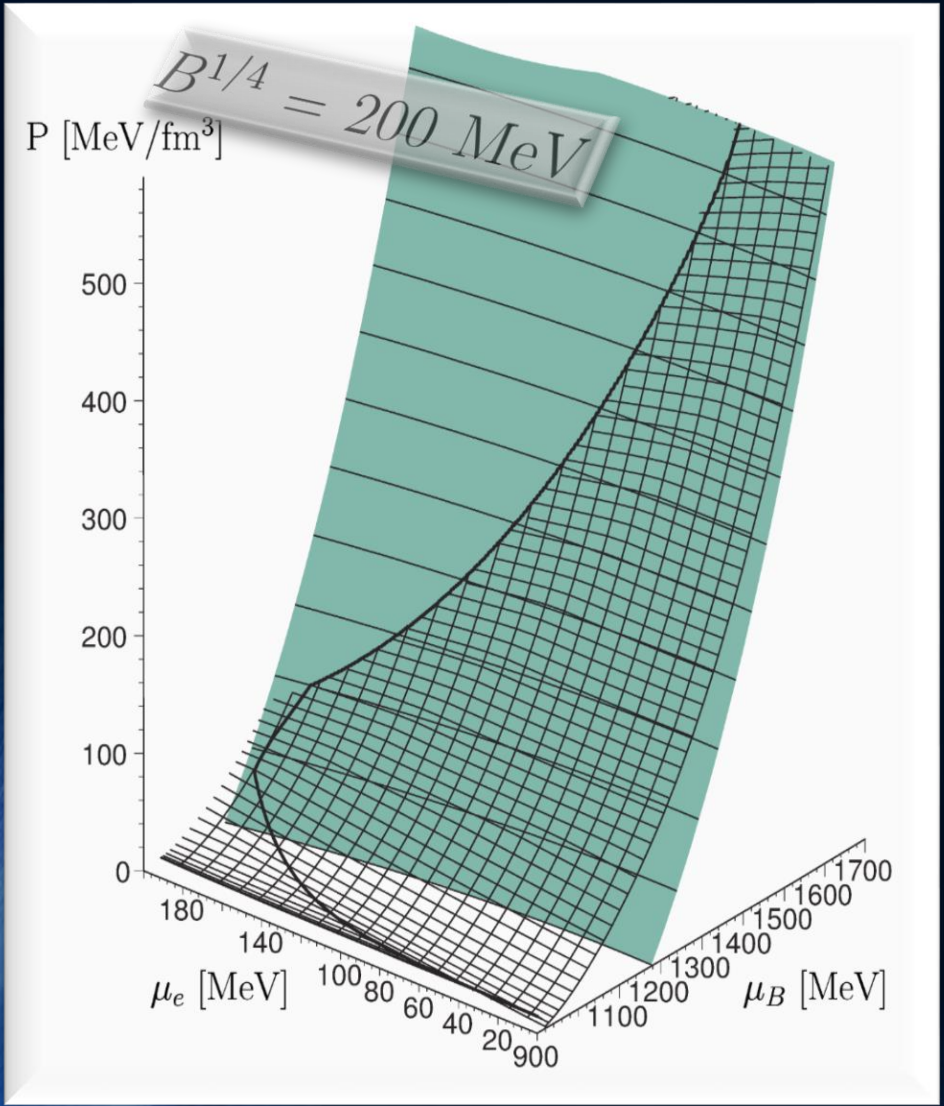

Particle composition:

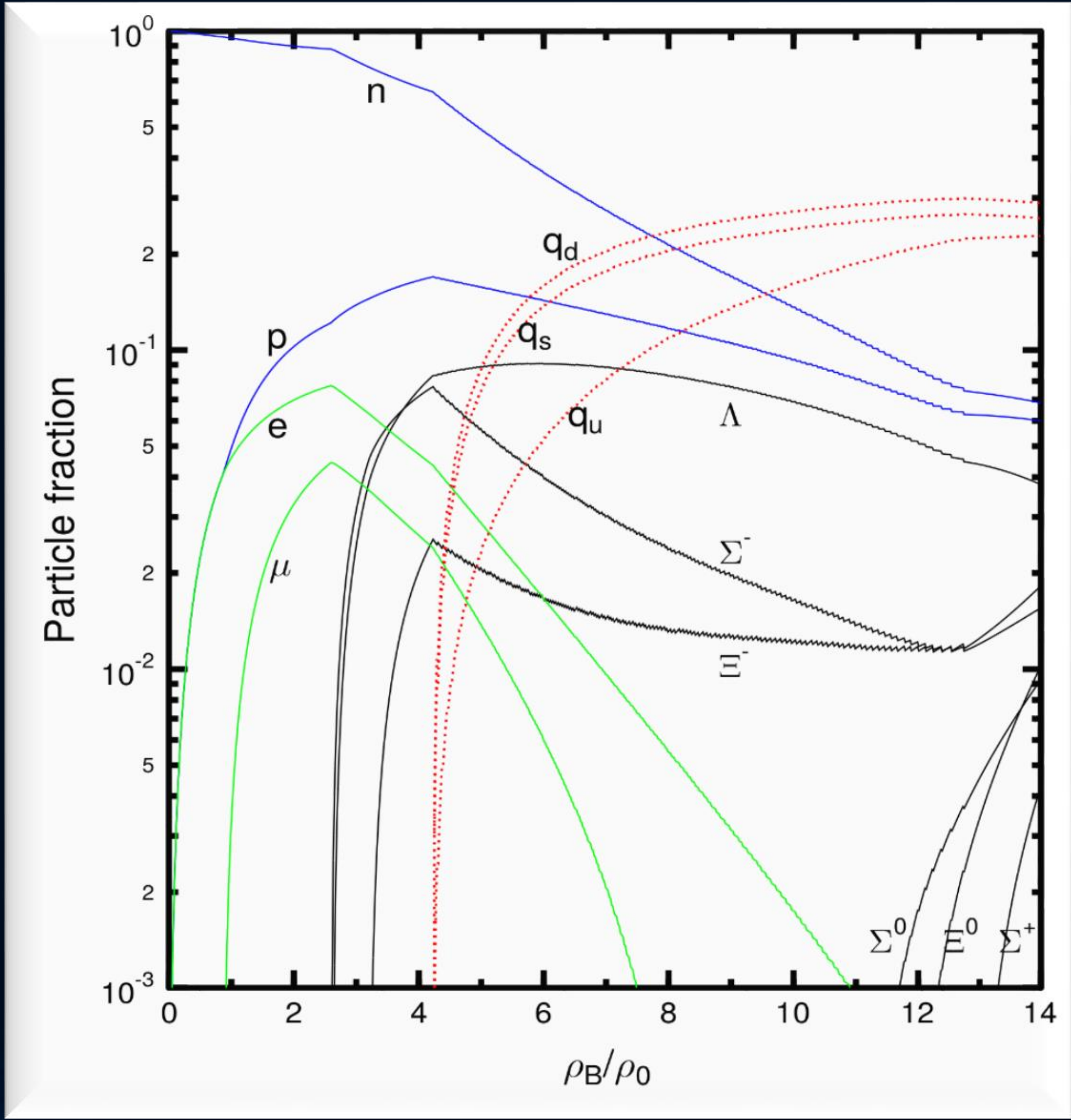

M. Hanauske, Dissertation, "Properties of Compact Stars within QCD-motivated Models"

The Maxwell Construction

If the surface tension between the hadron and quark phase is relatively large, the mixed phase could completely disappear, so that a sharp boundary between the two phase exists. The Hadron-quark phase transition is then described using a Maxwell construction.

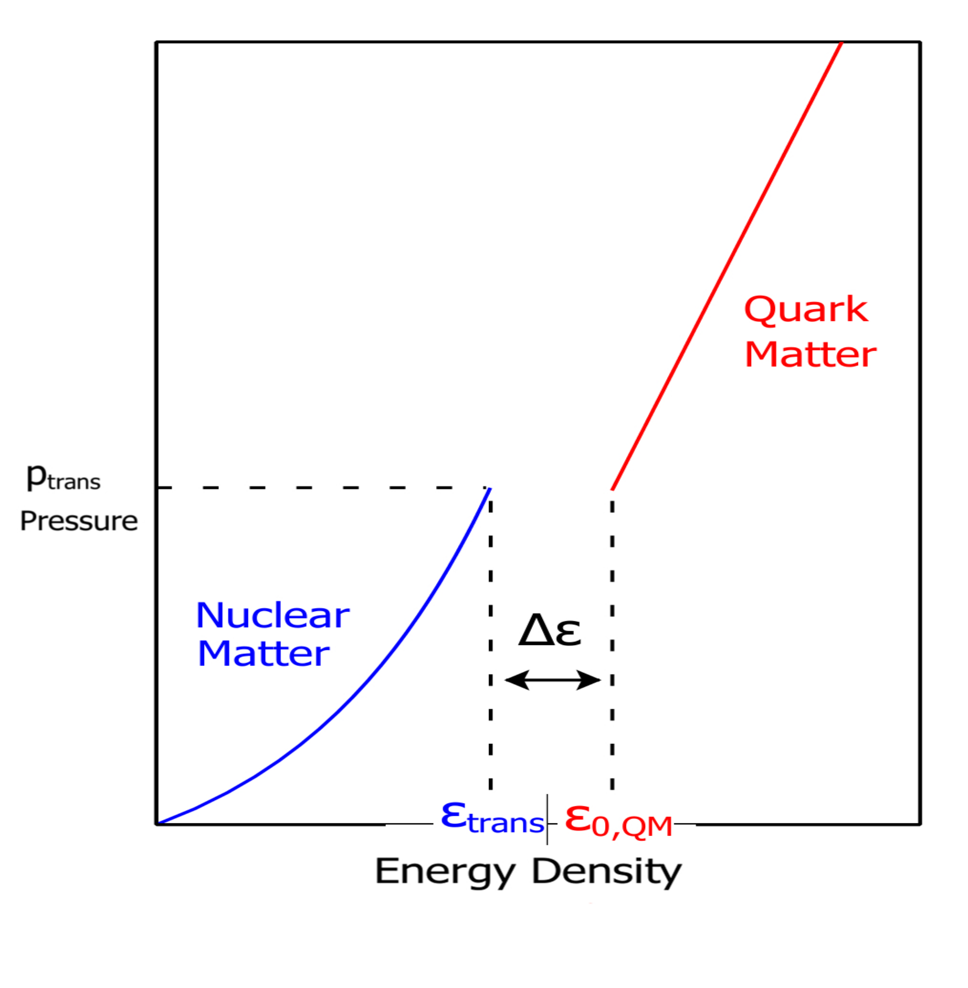

Pressure and baryon chemical potential stays constant, while the density and the charge chemical potential jump discontinuously during the phase transition.

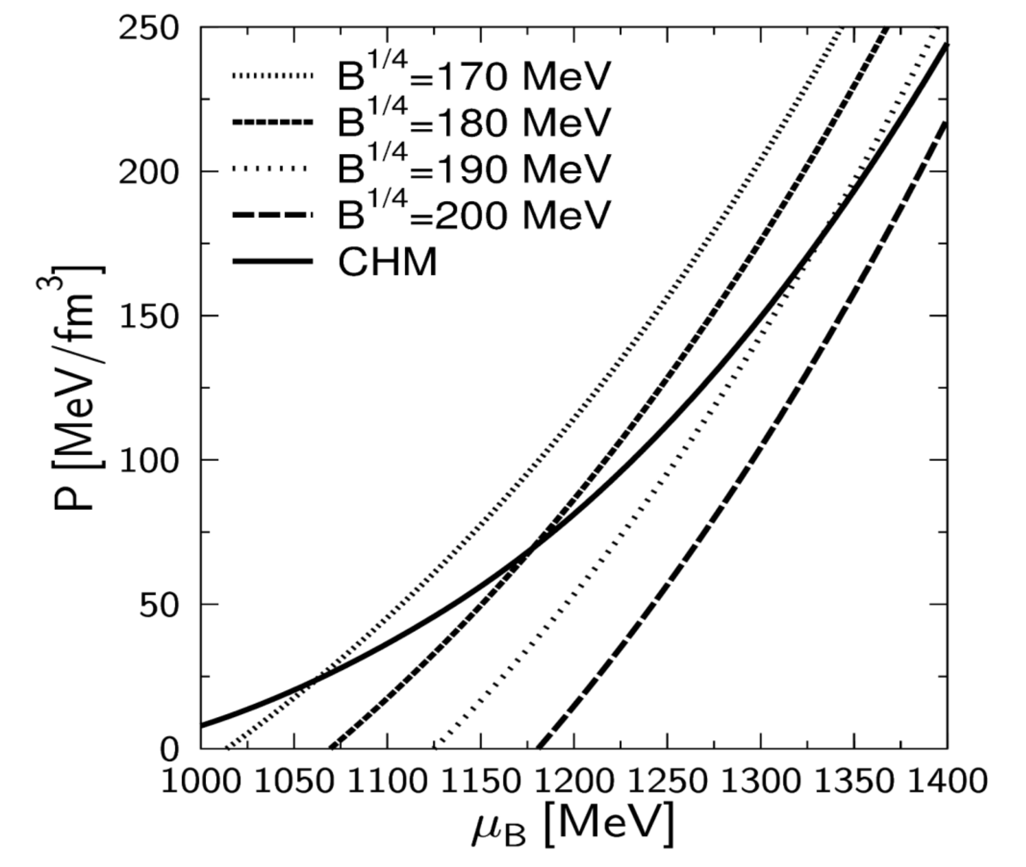

Image from M.G. Alford, S. Han, and M. Prakash, Phys. Rev. D 88, 083013 (2013)

Hybrid Star Properties

In contrast to the Gibbs construction, the star's density profile within the Maxwell construction (see right figure) will have a huge density jump at the phase transition boundary. Twin star properties can be found more easily when using a Maxwell construction.

Mass-Density relation

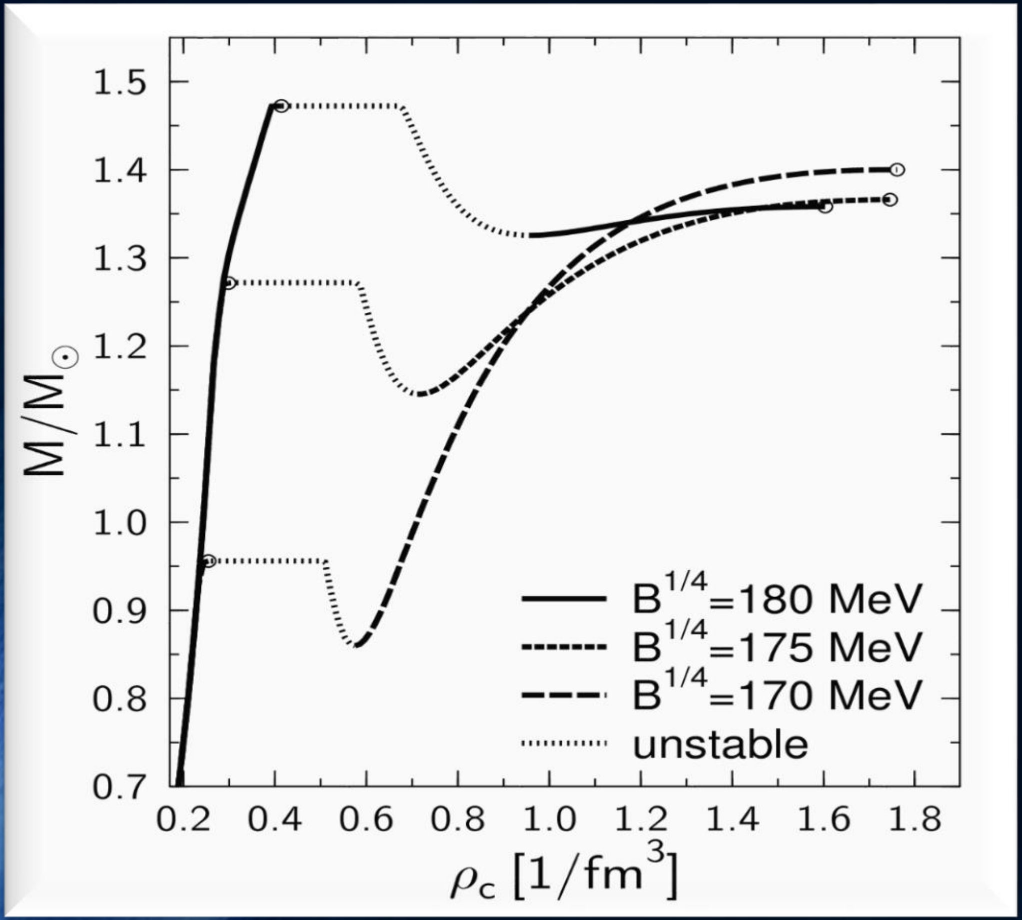

Energy-density profiles

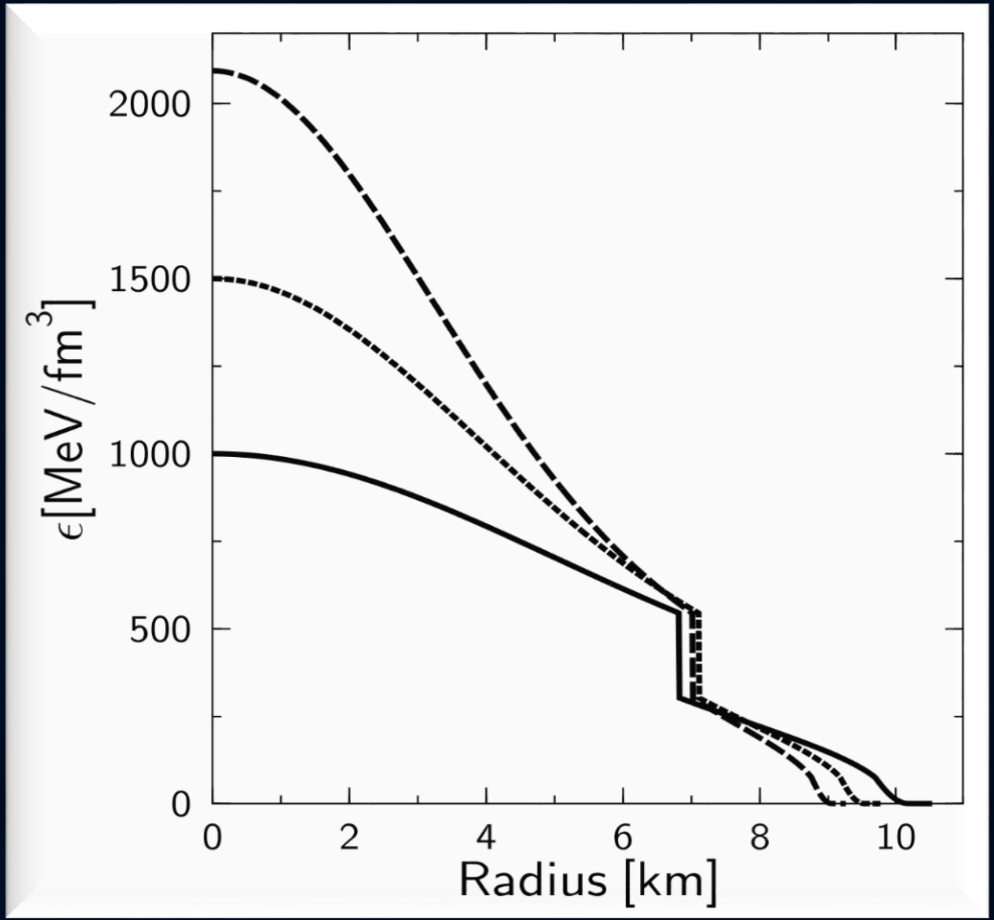

Matthias Hanauske: "How to detect the QGP with telescopes", GSI Annual Report 2003, p.96

Hypermassive Neutron Stars in the QCD Phase Diagram

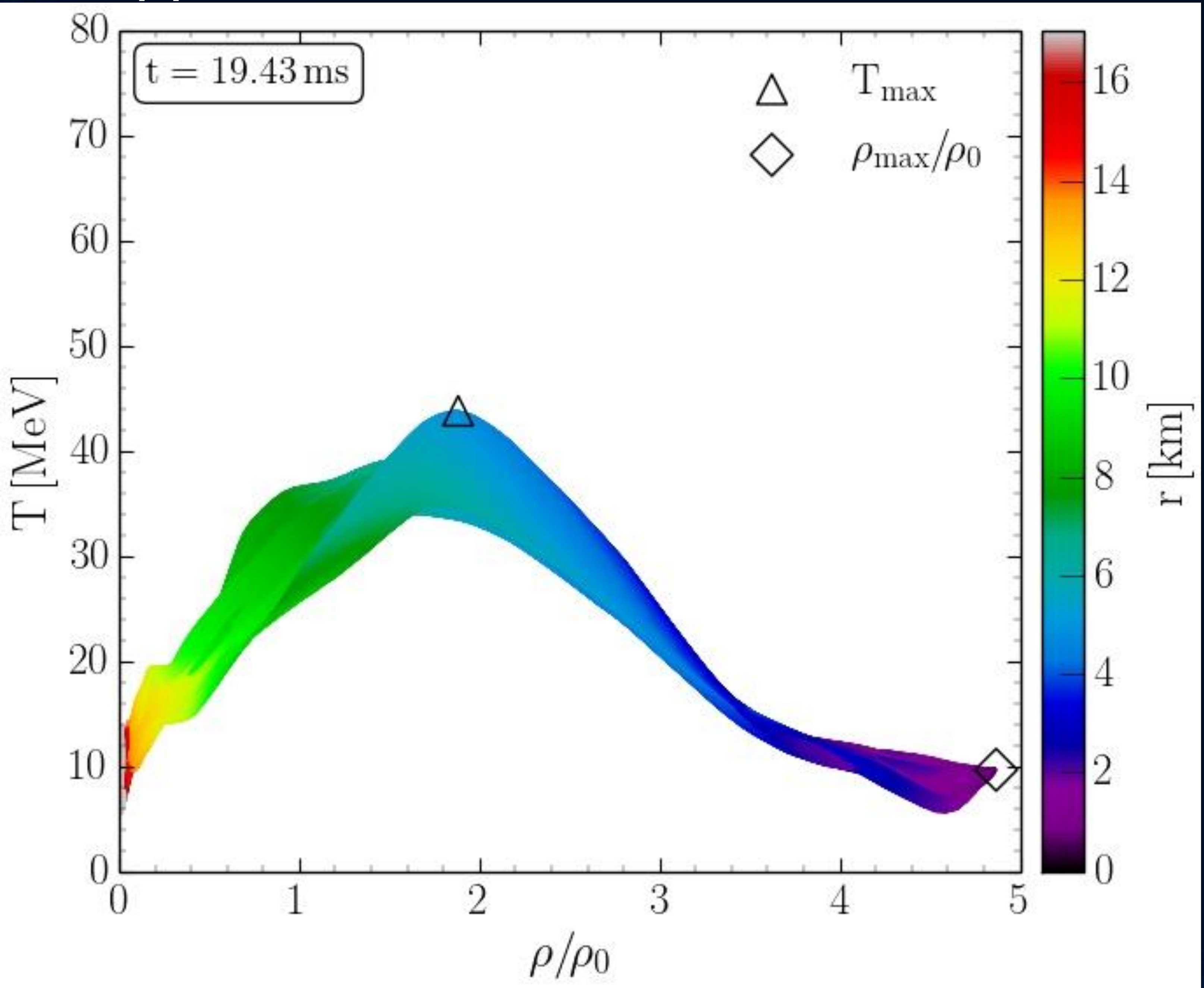

Density-temperature profiles inside the inner area of a hypermassive neutron star simulated within the LS220 EOS (☹ see talk by J.Lattimer) with a total mass of M_{total}=2.7 M_{solar} in the style of a (T- ρ) QCD phase diagram plot at t=19.43 ms after the merger.

The color-coding indicate the radial position r of the corresponding (T- ρ) fluid element measured from the origin of the simulation (x , y) = (0 , 0) on the equatorial plane at z = 0.

The open triangle marks the maximum value of the temperature while the open diamond indicates the maximum of the density.

QCD Phase Diagram: The Late Inspiral Phase

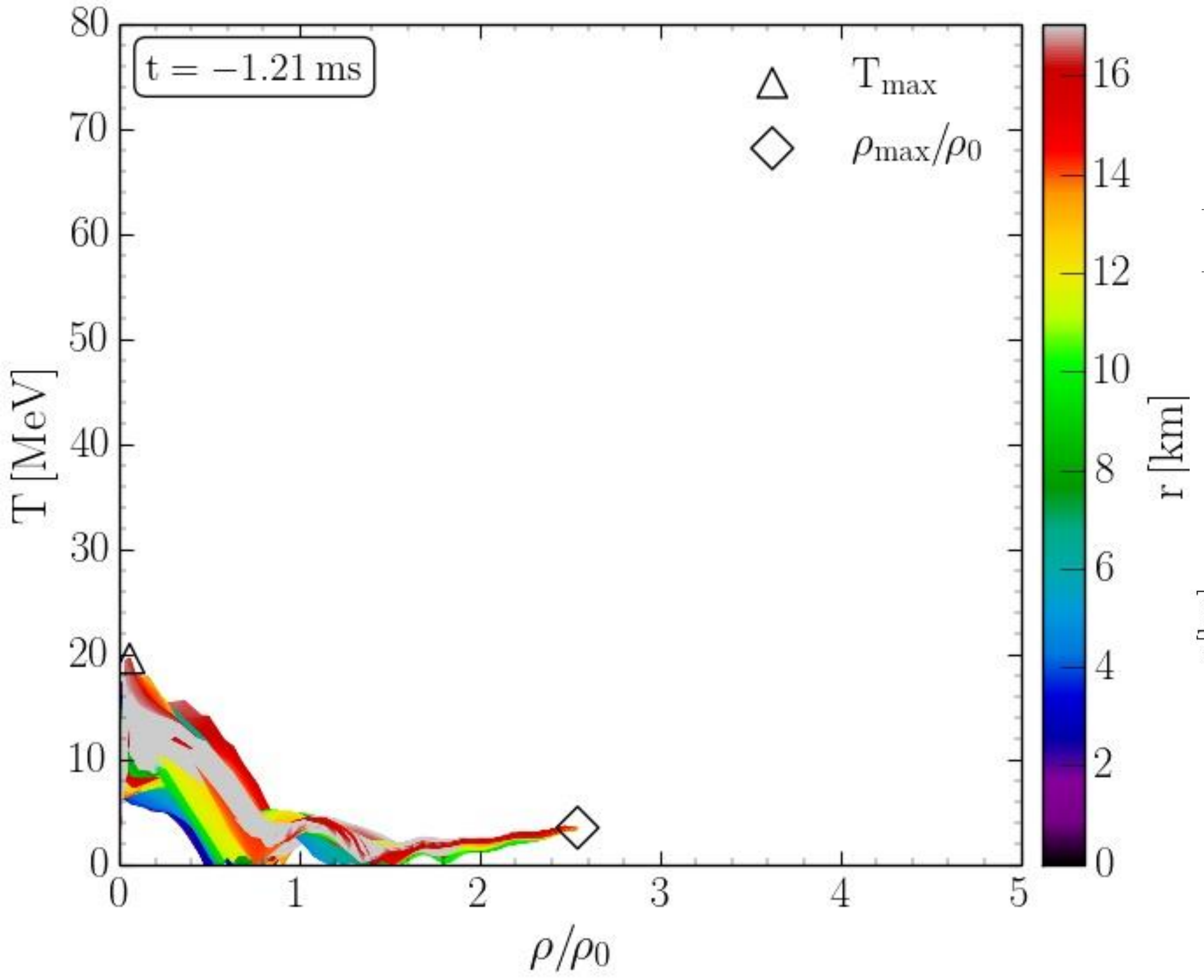

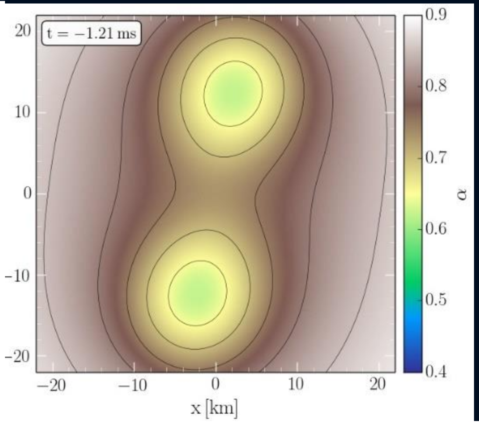

Lapse function α (left)

rest mass density ρ

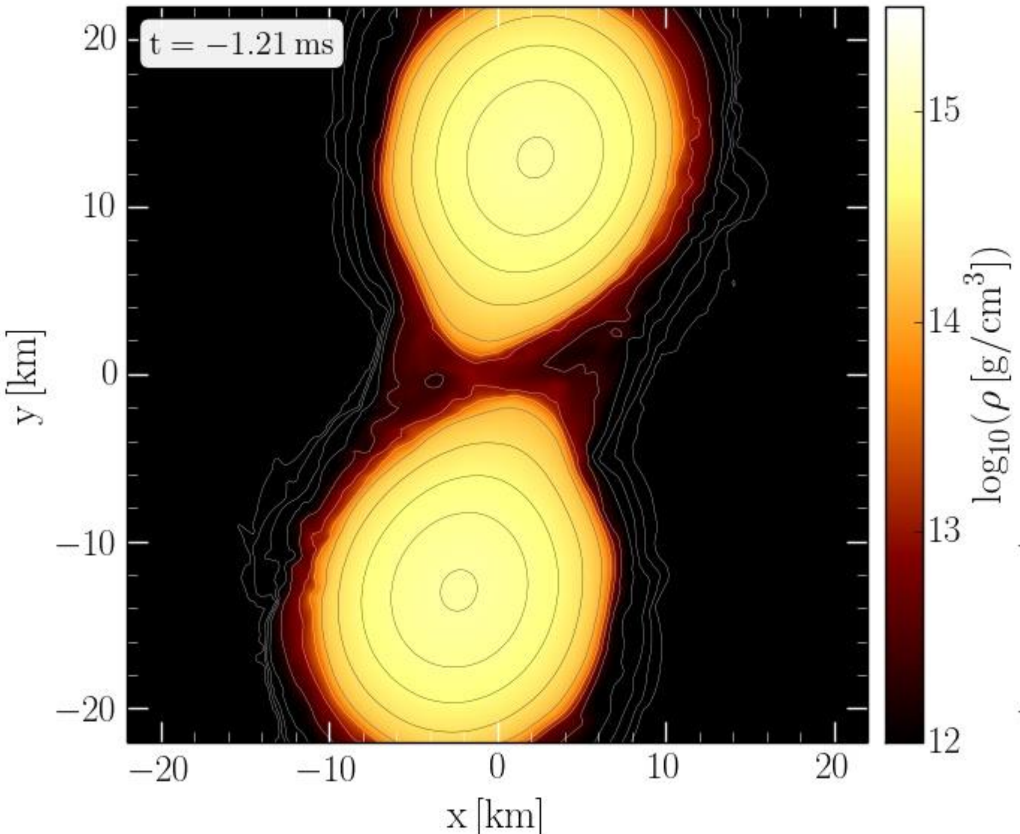

QCD Phase Diagram: The Late Inspiral Phase

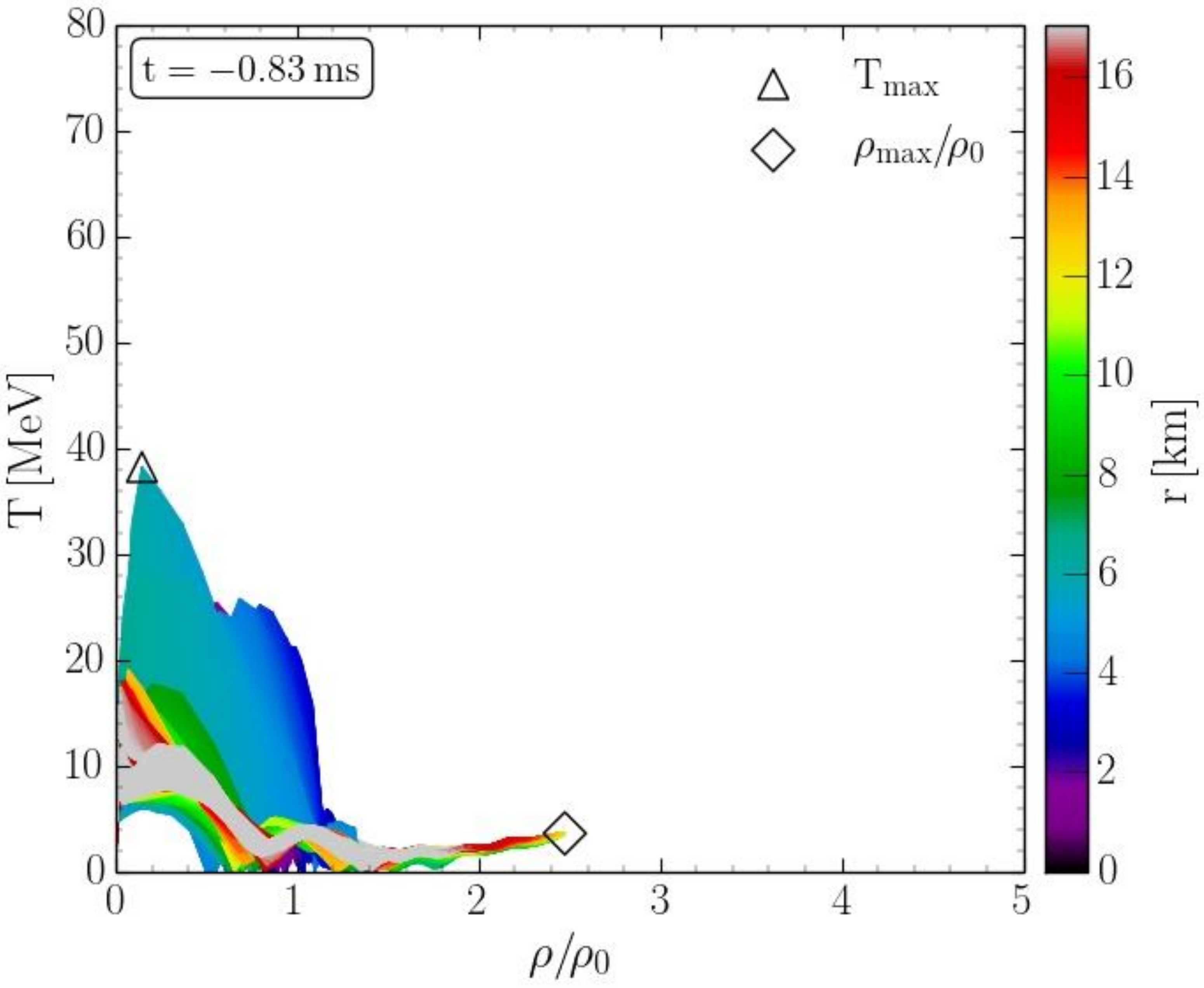

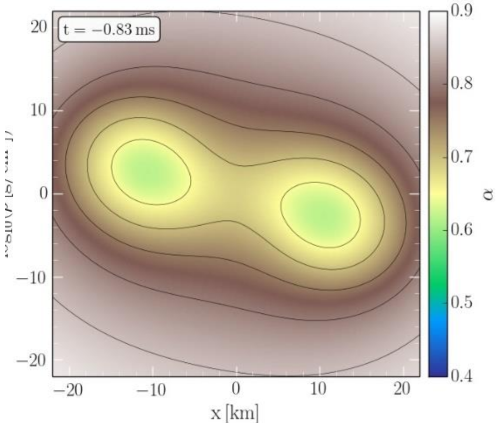

Lapse function α (left)

rest mass density ρ

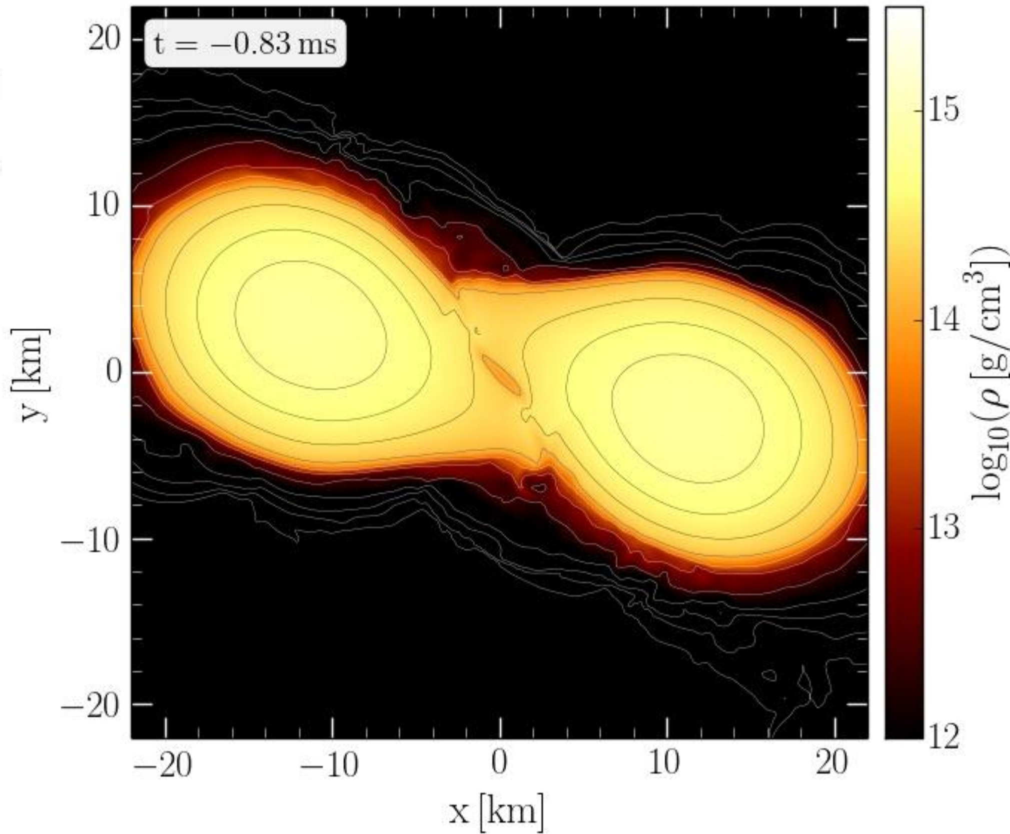

QCD Phase Diagram: The Late Inspiral Phase

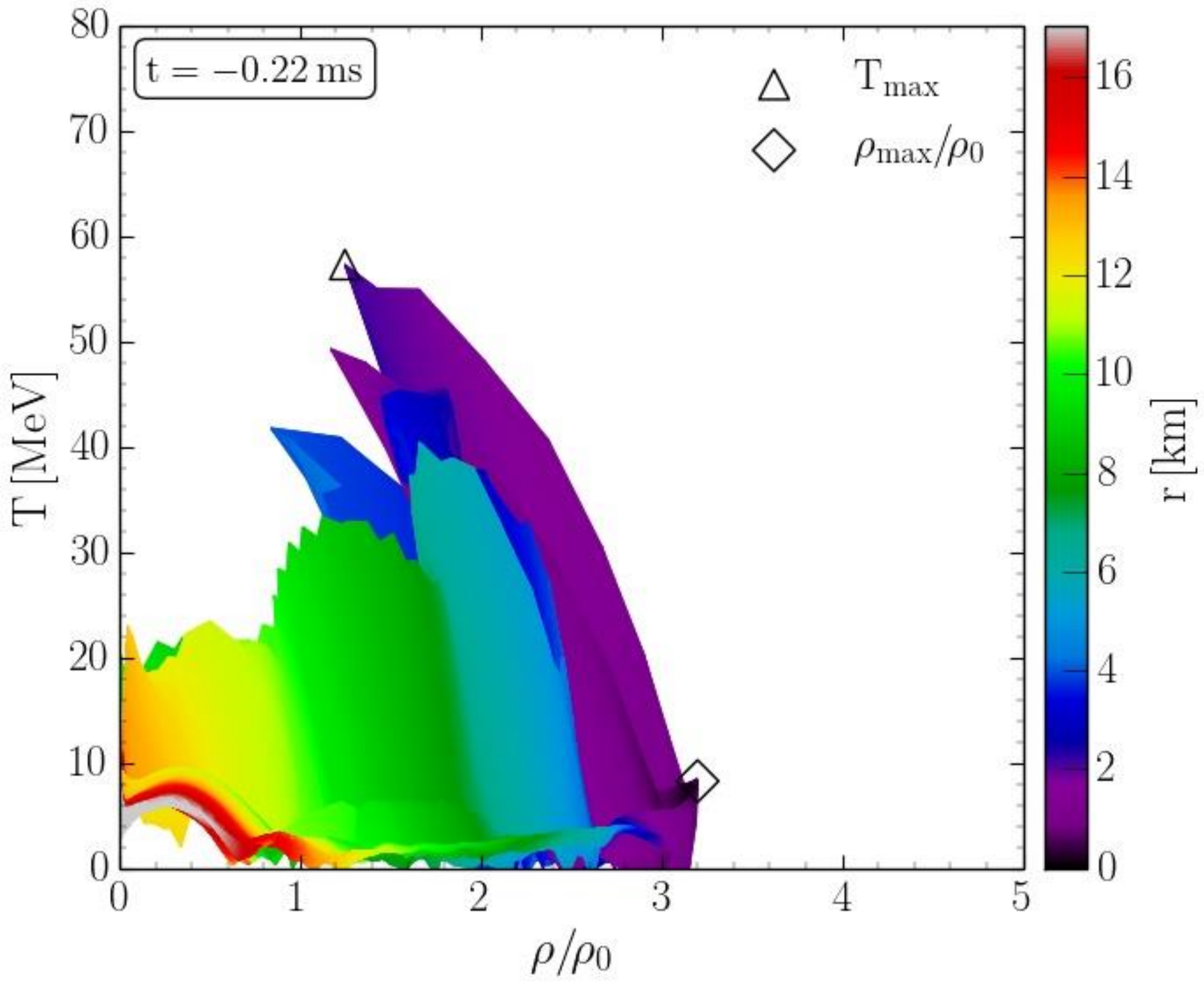

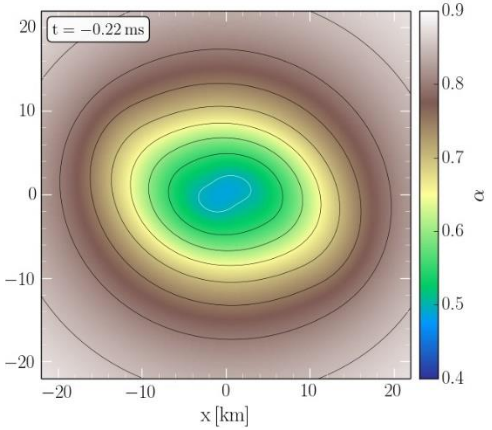

Lapse function α (left)

rest mass density ρ

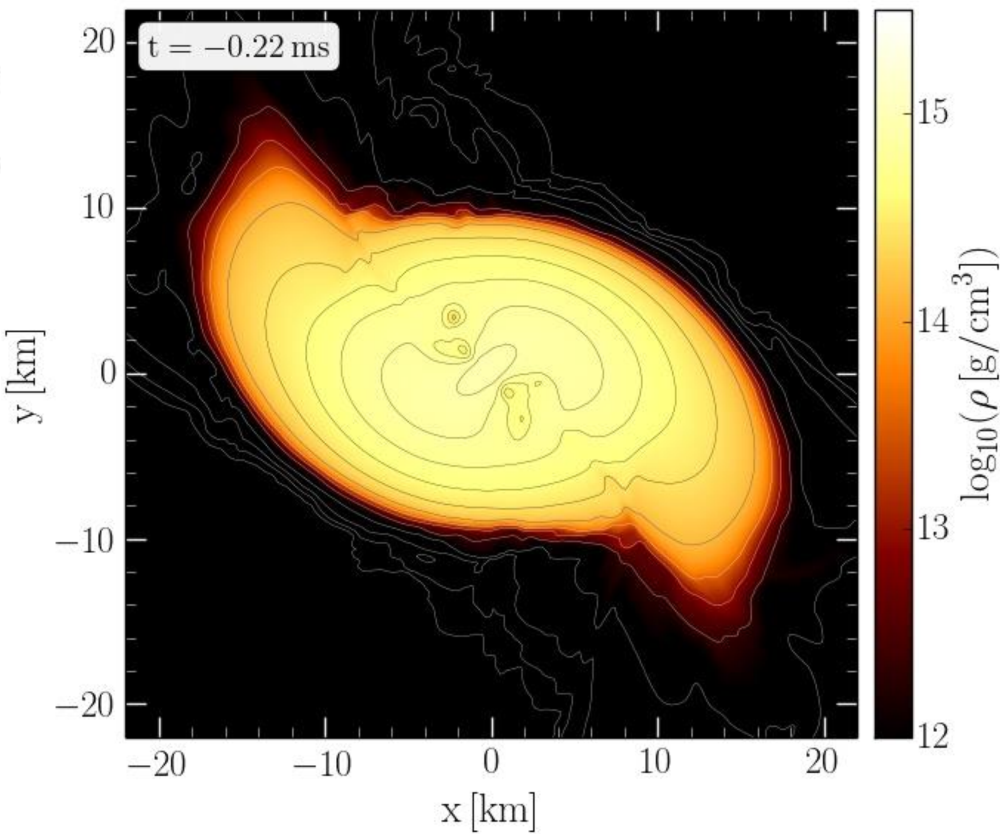

Binary Neutron Star Mergers in the QCD Phase Diagram

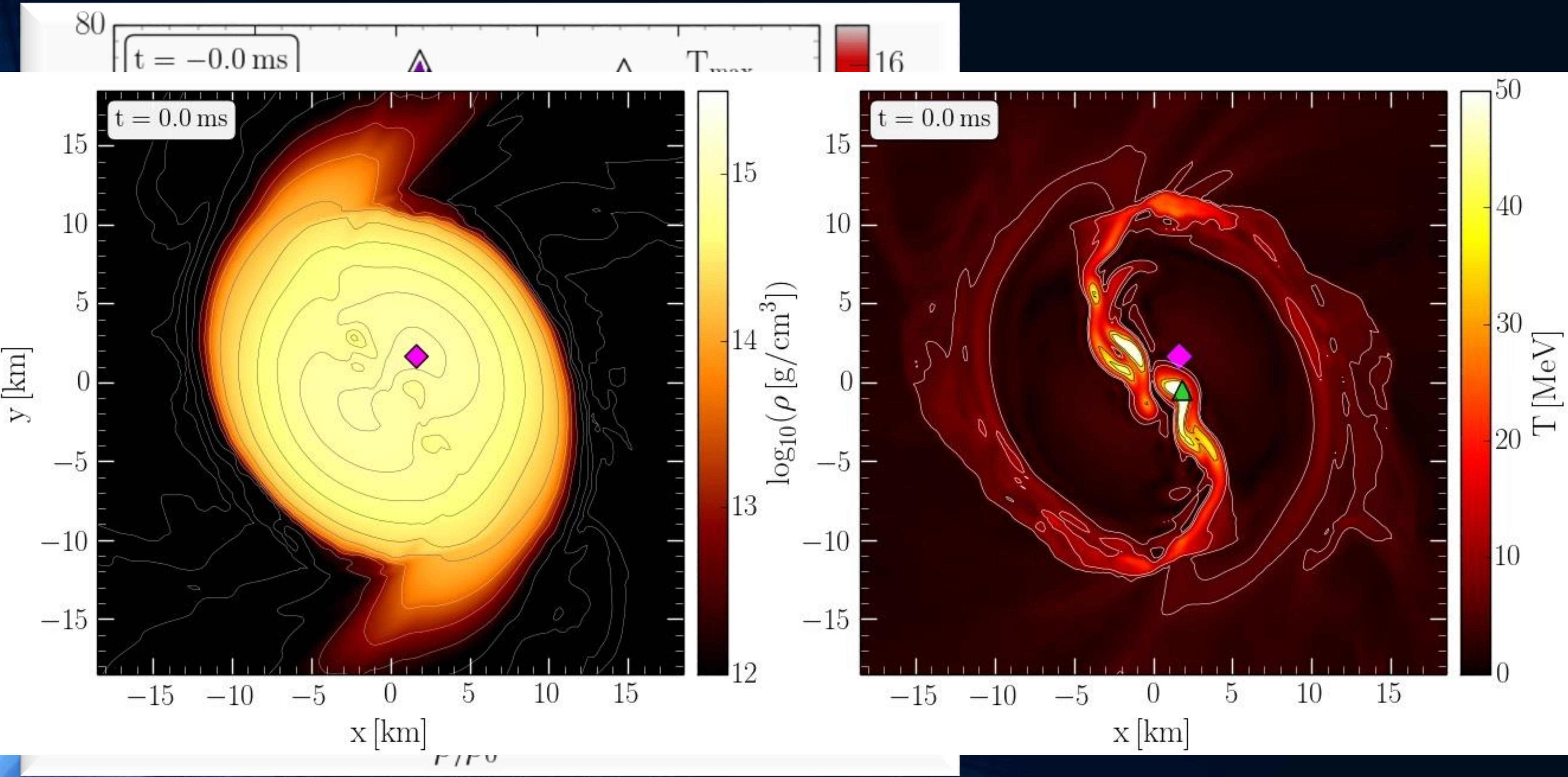

Binary Neutron Star Mergers in the QCD Phase Diagram

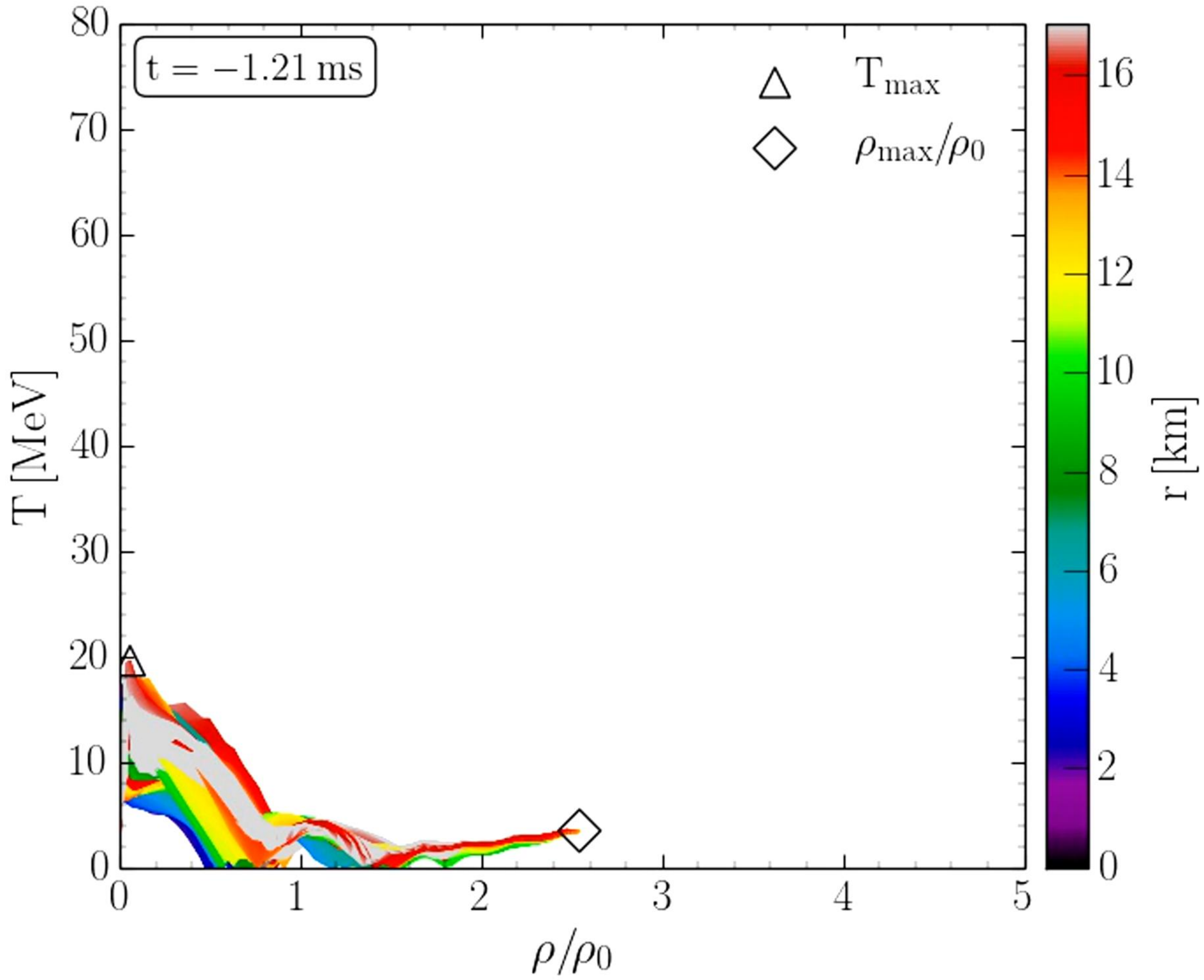

Evolution of hot and dense matter inside the inner area of a hypermassive neutron star simulated within the LS220 EOS with a total mass of $M_{total}=2.7\ M_{solar}$ in the style of a (T- ρ) QCD phase diagram plot

The color-coding indicate the radial position r of the corresponding (T- ρ) fluid element measured from the origin of the simulation (x , y) = (0 , 0) on the equatorial plane at z = 0.

The open triangle marks the maximum value of the temperature while the open diamond indicates the maximum of the density.

The Co-Rotating Frame

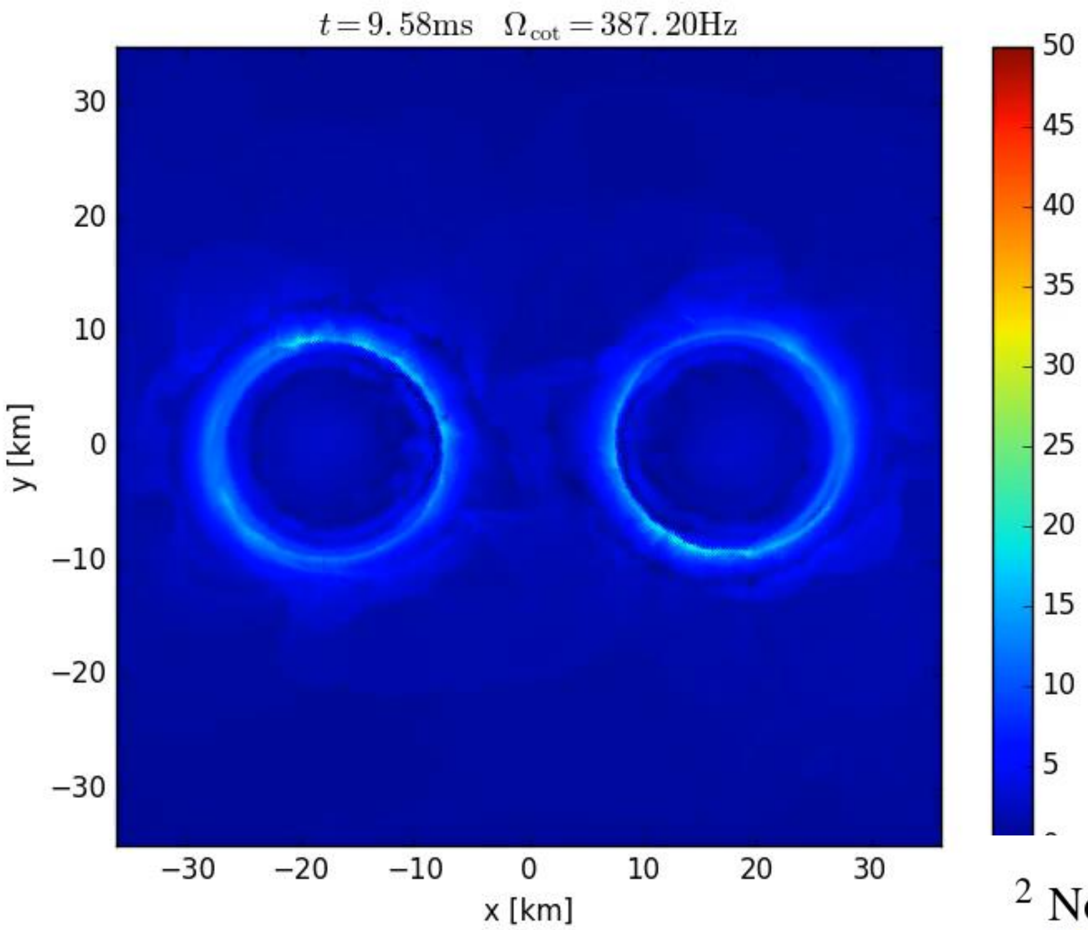

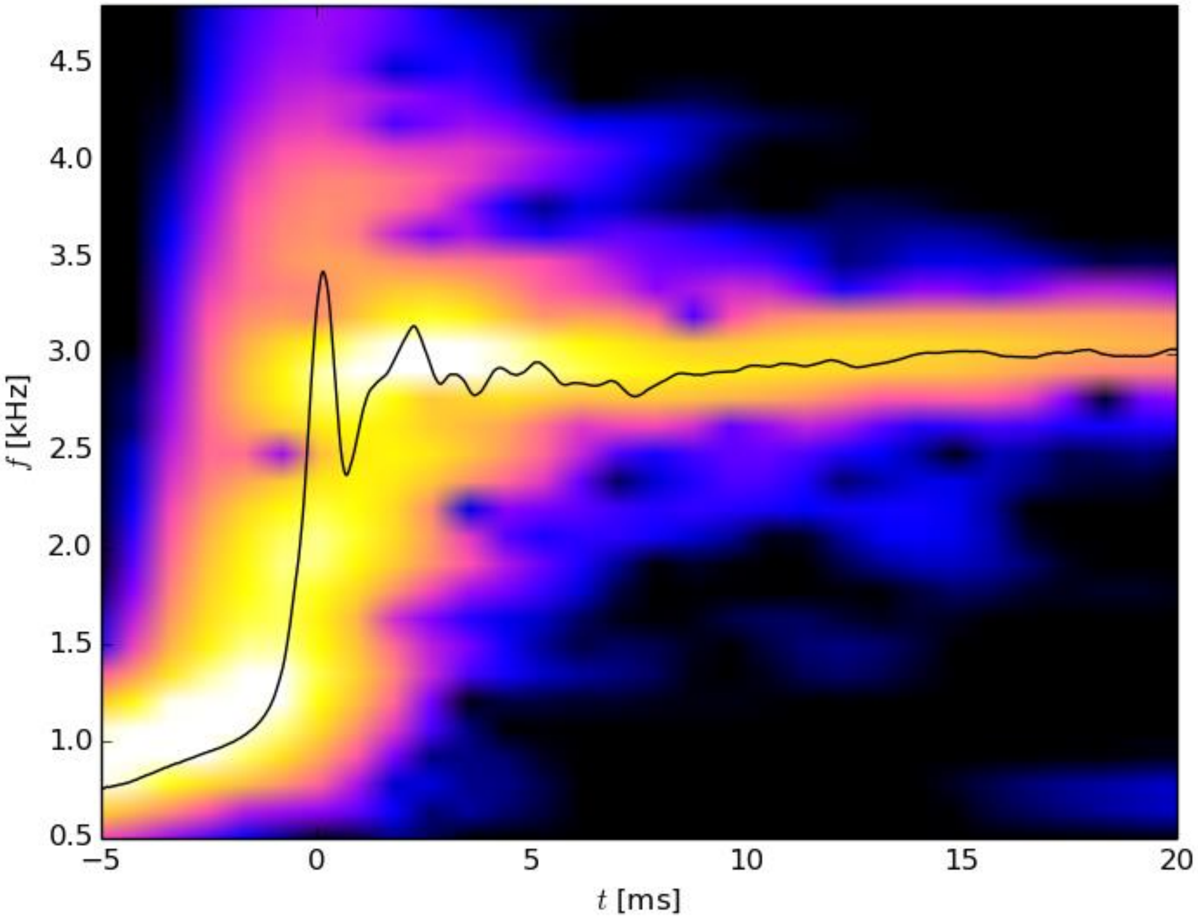

[2] Note that the angular-velocity distribution in the lower central panel of Fig. 10 refers to the corotating frame and that this frame is rotating at half the angular frequency of the emitted gravitational waves, Ω_{GW}. Because the maximum of the angular velocity Ω_{max} is of the order of $\Omega_{GW}/2$ (cf. left panel of Fig. 12), the ring structure in this panel is approximately at zero angular velocity.

Simulation and movie has been produced by Luke Bovard

Density and Temperature Evolution inside the HMNS

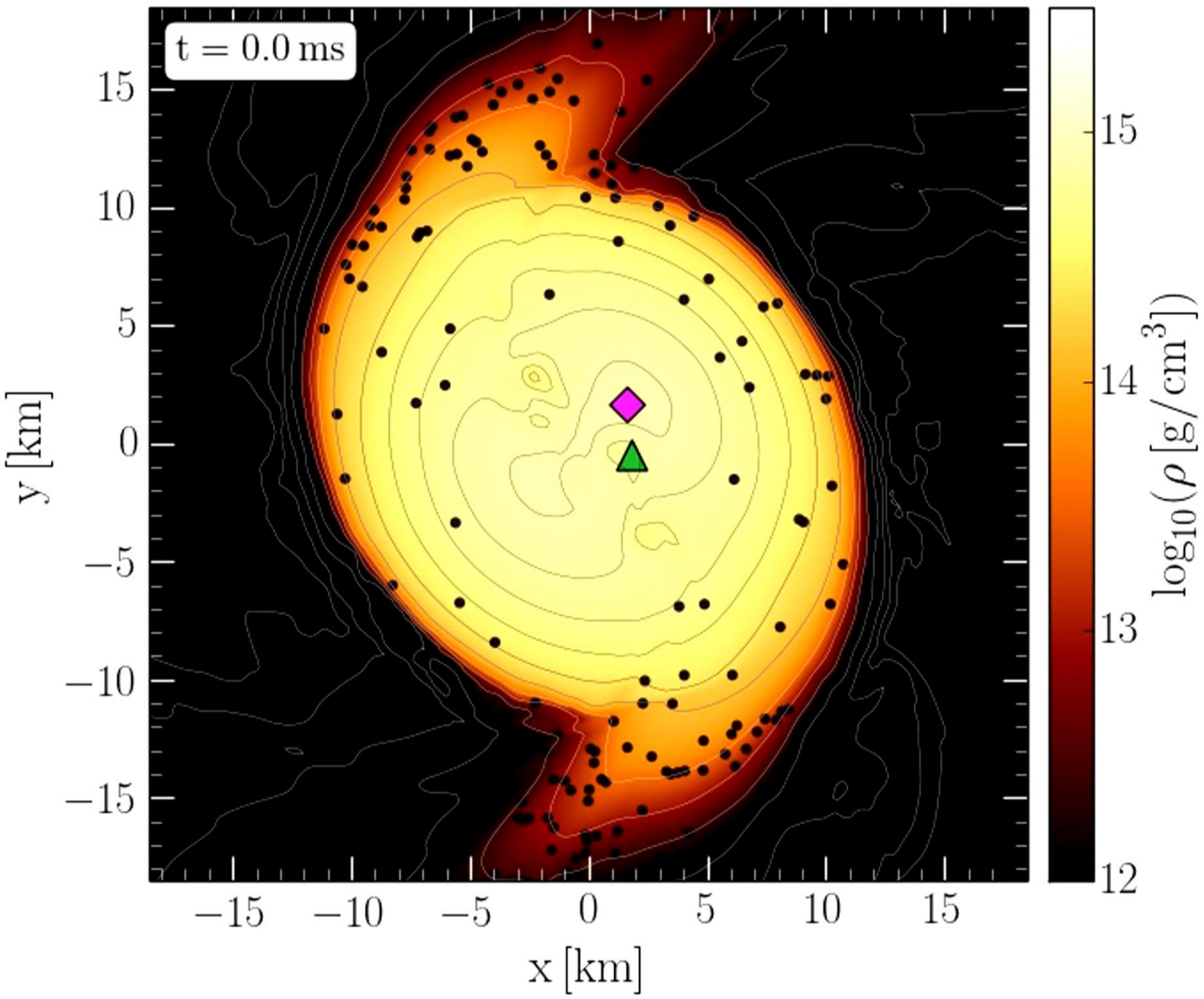

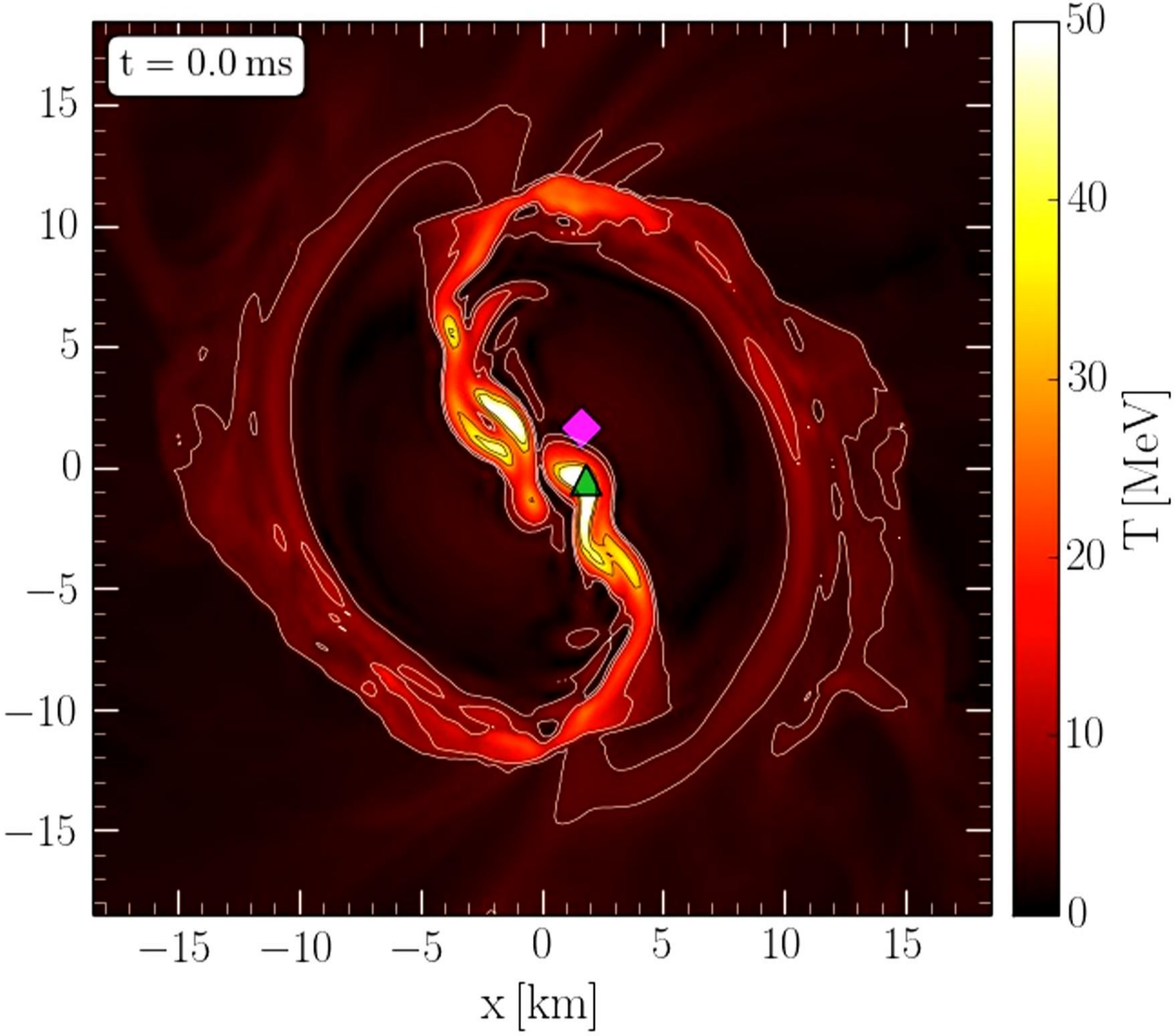

Rest mass density on the equatorial plane

Temperature on the equatorial plane

Binary Neutron Star Mergers in the QCD Phase Diagram

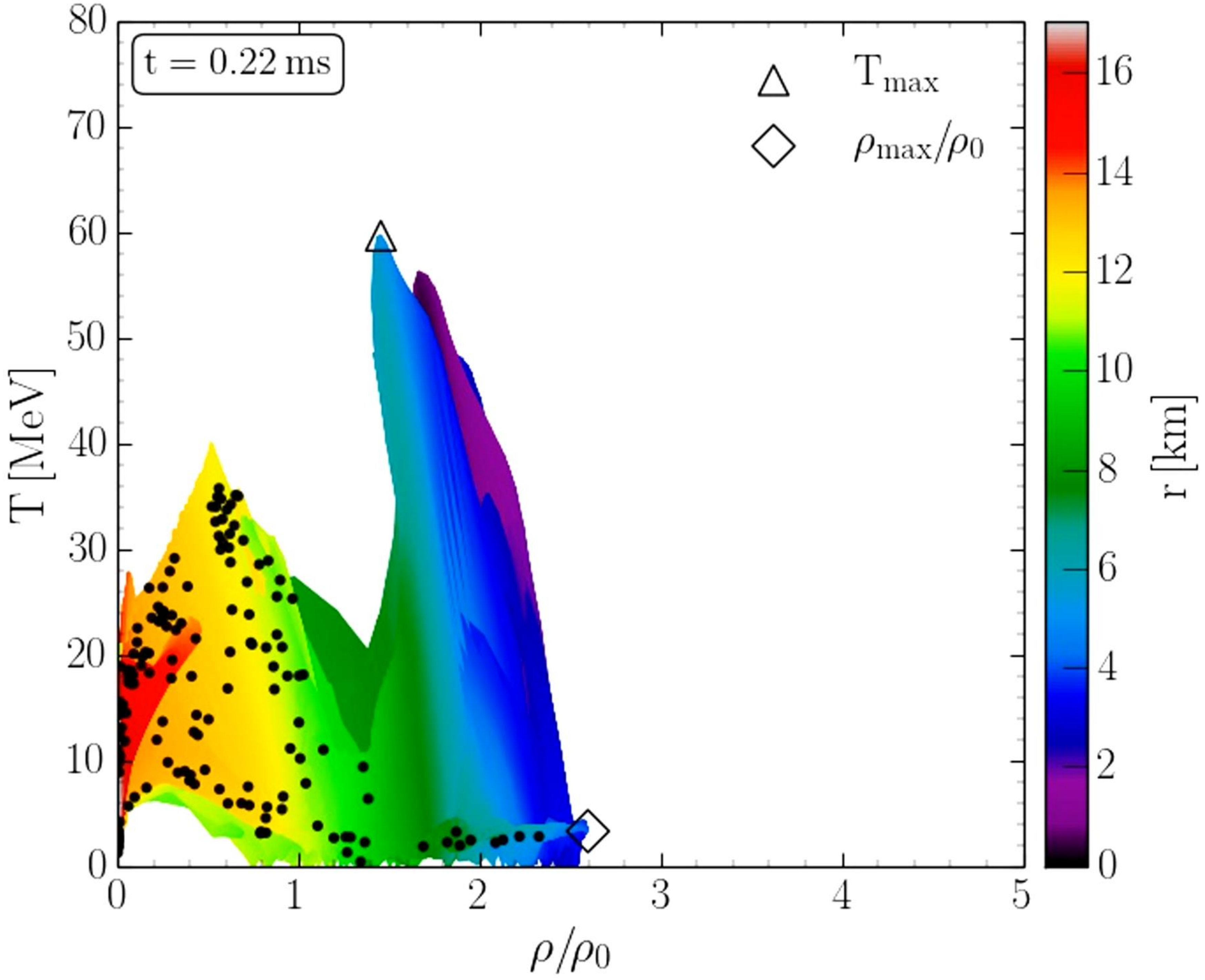

Evolution of hot and dense matter inside the inner area of a hypermassive neutron star simulated within the LS220 EOS with a total mass of M_{total}=2.7 M_{solar} in the style of a (T- ρ) QCD phase diagram plot

The color-coding indicate the radial position r of the corresponding (T- ρ) fluid element measured from the origin of the simulation (x , y) = (0 , 0) on the equatorial plane at z = 0.

The open triangle marks the maximum value of the temperature while the open diamond indicates the maximum of the density.

The Angular Velocity in the (3+1)-Split

The angular velocity Ω in the (3+1)-Split is a combination of the lapse function α , the ϕ-component of the shift vector β^{ϕ} and the 3-velocity v^{ϕ} of the fluid (spatial projection of the 4-velocity **u**):

$$\Omega(x, y, z, t) = \frac{u^{\phi}}{u^{t}} = \alpha\, v^{\phi} - \beta^{\phi}$$

Angular velocity Ω

Lapse function α

Φ-component of 3-velocity v^{φ}

Frame-dragging β^{φ}

(3+1)-decomposition of spacetime:

$$g_{\mu\nu} = \begin{pmatrix} -\alpha^2 + \beta_i \beta^i & \beta_i \\ \beta_i & \gamma_{ij} \end{pmatrix}$$

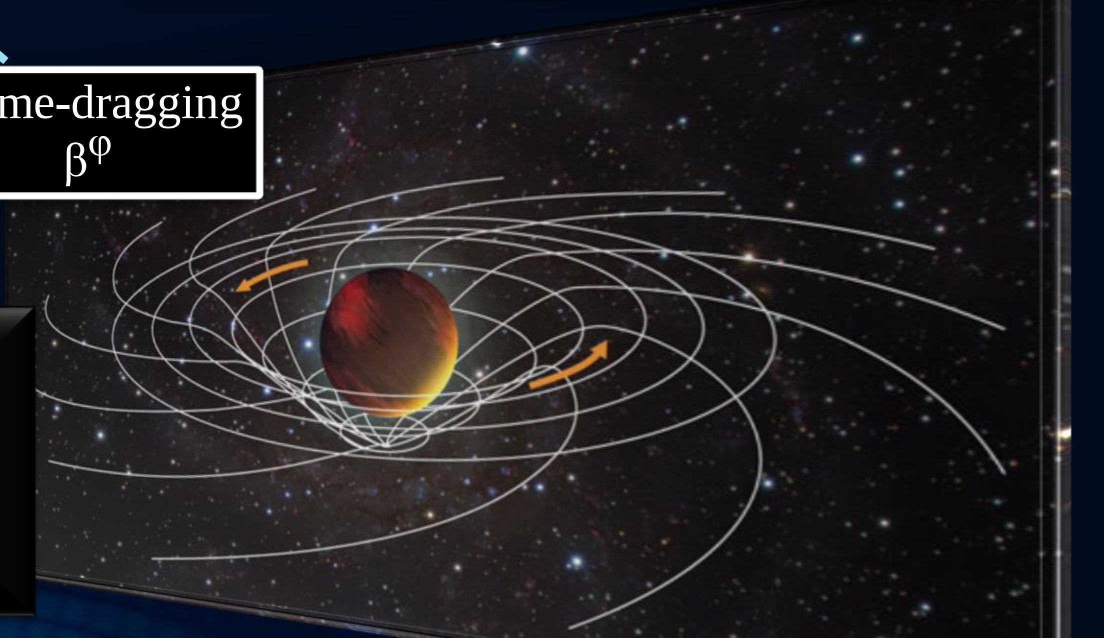

Focus: Inner core of the differentially rotating HMNS

M. Shibata, K. Taniguchi, and K. Uryu, Phys. Rev. D 71, 084021 (2005)
M. Shibata and K. Taniguchi, Phys. Rev. D 73, 064027 (2006)
F. Galeazzi, S. Yoshida and Y. Eriguchi, A&A 541, p. A156 (2012)
W. Kastaun and F. Galeazzi, Phys. Rev. D 91, p. 064027 (2015)

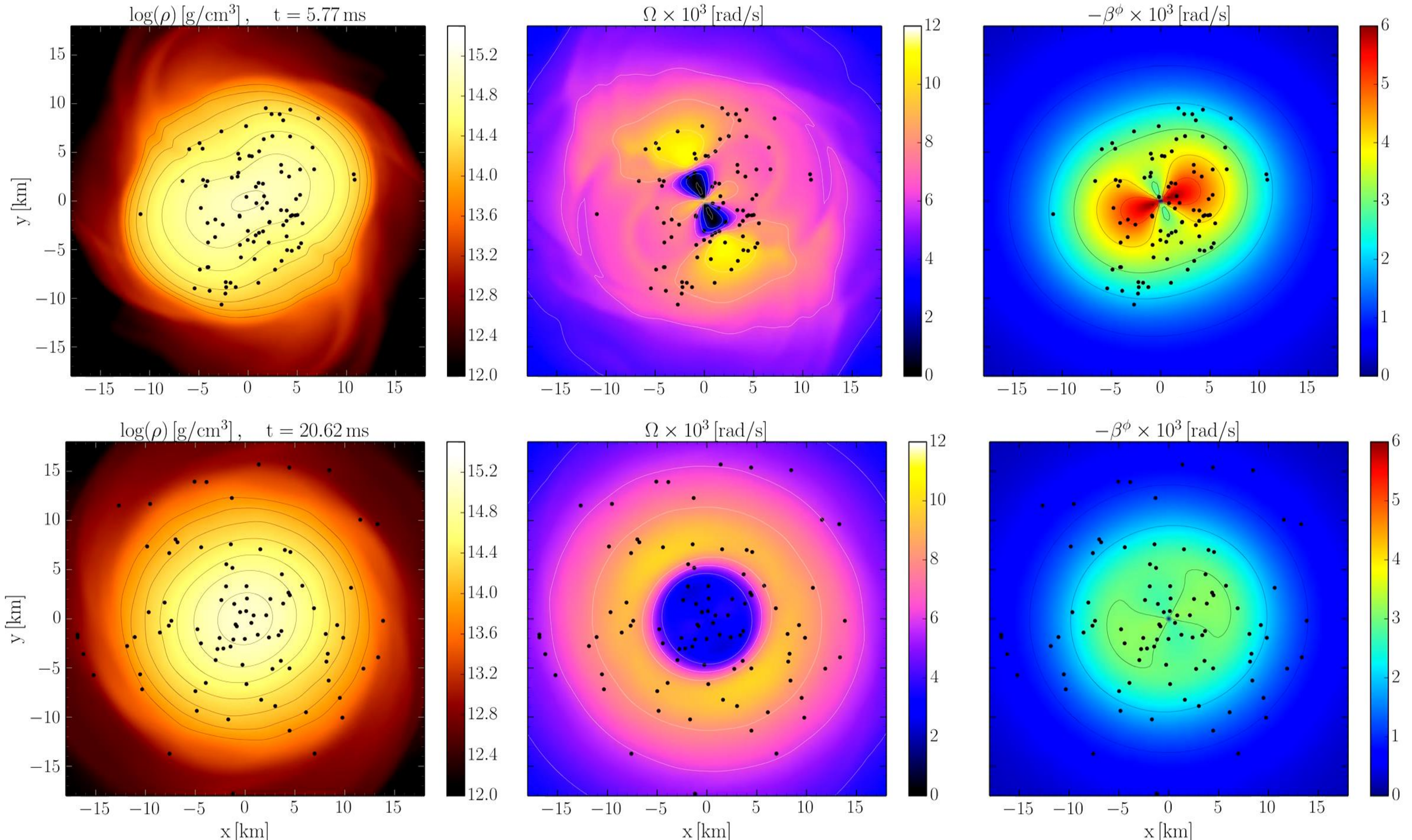

log(ρ) [g/cm³], t = 5.77 ms
Ω × 10³ [rad/s]
−β^φ × 10³ [rad/s]
log(ρ) [g/cm³], t = 20.62 ms
Ω × 10³ [rad/s]
−β^φ × 10³ [rad/s]
y [km]
x [km]

Time-averaged Rotation Profiles of the HMNSs

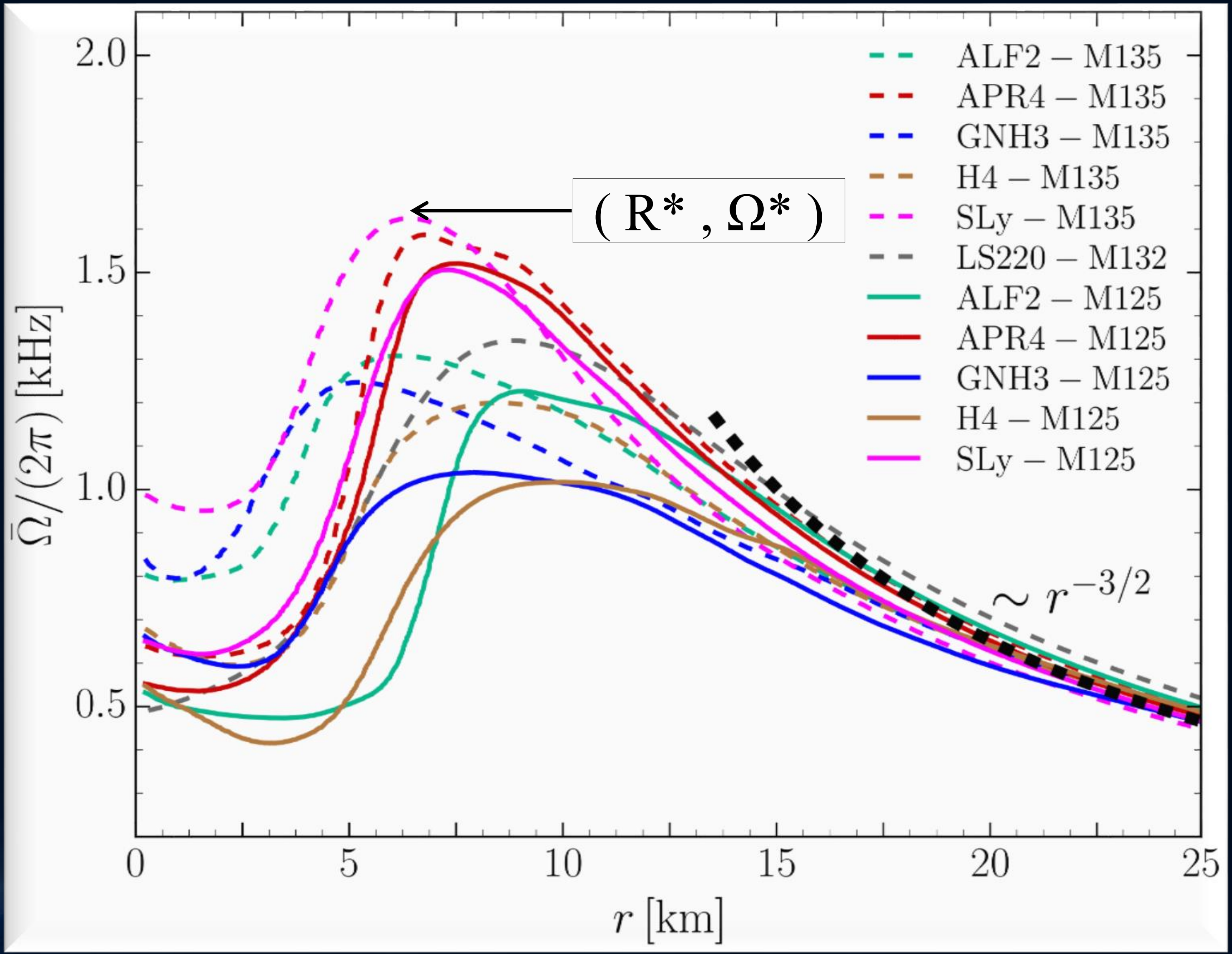

Time-averaged rotation profiles for different EoS
Low mass runs (solid curves), high mass runs (dashed curves).

Soft EoSs:
Sly
APR4

Stiff EoSs:
GNH3
H4

Temperature   Angular Velocity

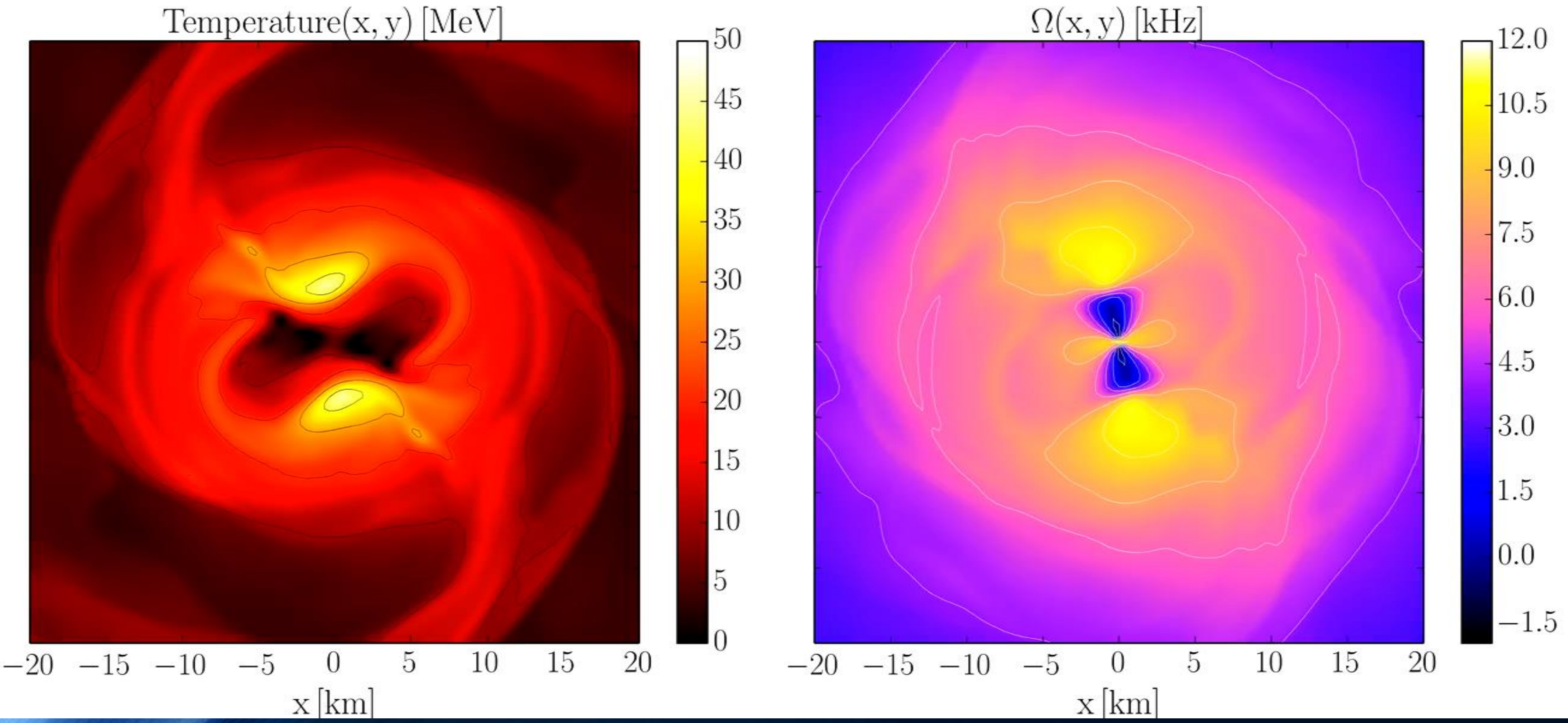

EOS: LS200 , Mass: 1.32 M_{solar} , simulation with Pi-symmetry

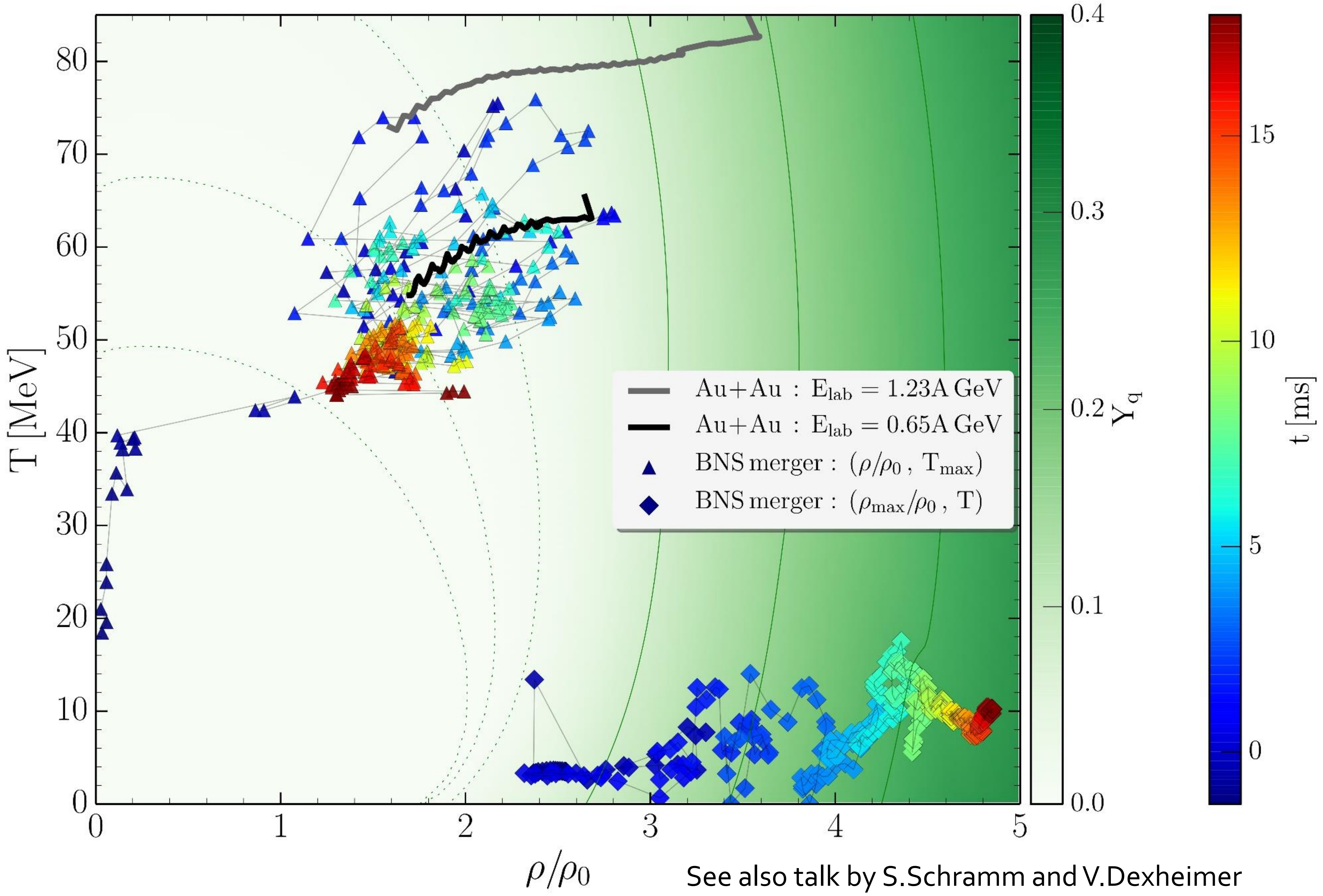

See also talk by S.Schramm and V.Dexheimer

Evolution of the maximum value of the temperature (triangles) and rest mass density (diamonds) at the equatorial plane in the interior of a HMNS using the simulation results of the LS220-M135 run
Color coding of triangles/diamonds: time of the simulation after merger in milliseconds

Grey and black curve: two heavy ion collision simulations within the quark-hadron chiral parity-doublet model

Y_q = Quark fraction

The Hadron-Quark Phase Transition and the Third Family of Compact Stars (Twin Stars)

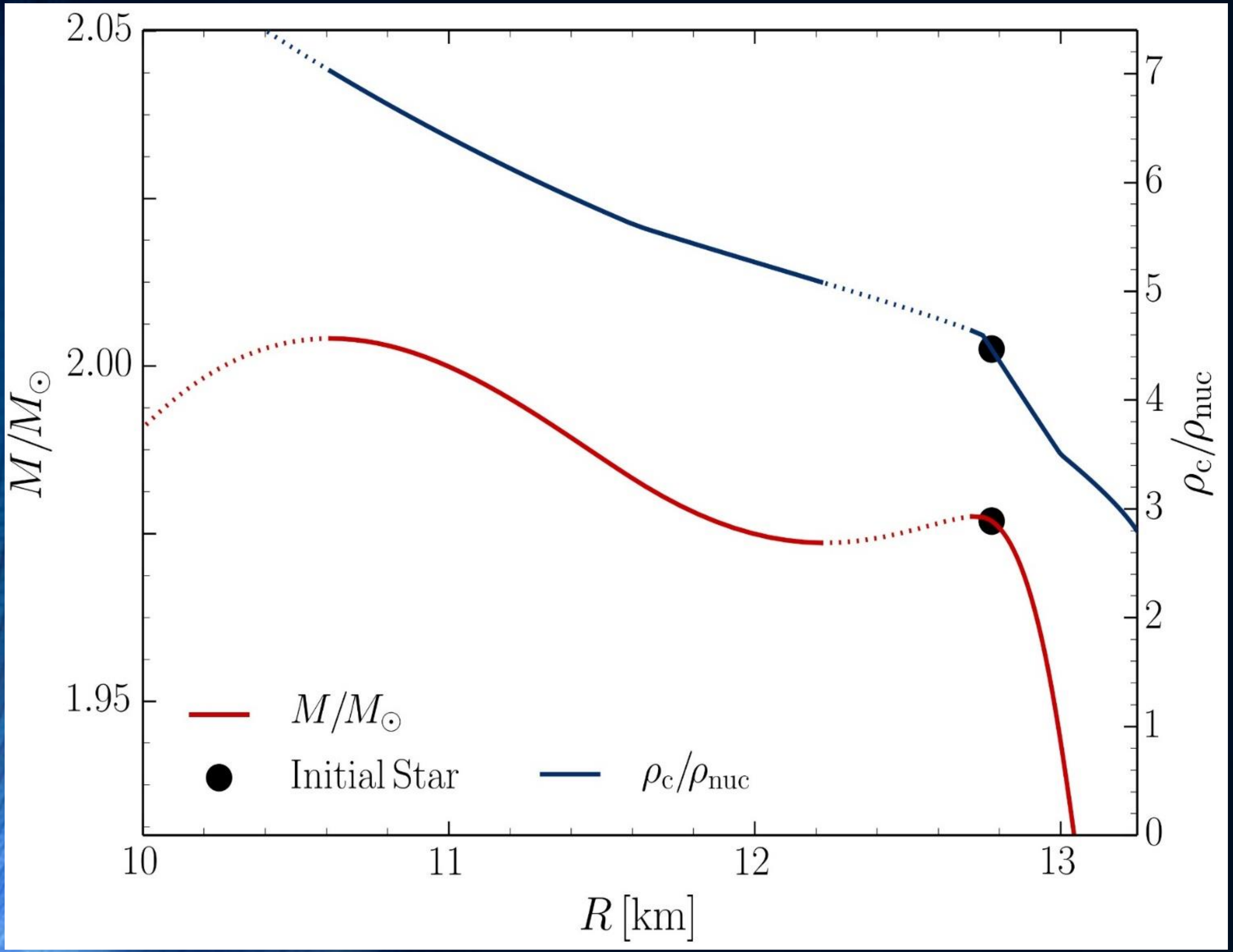

Gerlach (1968), Glendenning, N. K., & Kettner, C. (1998). Nonidentical neutron star twins. Astron. Astrophys., 353(LBL-42080), L9.

Sarmistha Banik, Matthias Hanauske, Debades Bandyopadhyay and Walter Greiner, Rotating compact stars with exotic matter, Phys.Rev.D 70 (2004) p.12304

I.N. Mishustin, M. Hanauske, A. Bhattacharyya, L.M. Satarov, H. Stöcker, and W. Greiner, Catastrophic rearrangement of a compact star due to quark core formation, Physics Letters B 552 (2003) p.1-8

M.Alford and A. Sedrakian, Compact stars with sequential QCD phase transitions. Physical review letters, 119(16), 161104 (2017)..

D.Alvarez-Castillo and D.Blaschke, High-mass twin stars with a multipolytrope equation of state. Physical Review C, 96(4), 045809 (2017) .

A. Ayriyan, N.-U. Bastian, D. Blaschke, H. Grigorian, K. Maslov, D. N. Voskresensky, How robust is a third family of compact stars against pasta phase effects?, arXiv:1711.03926 [nucl-th]

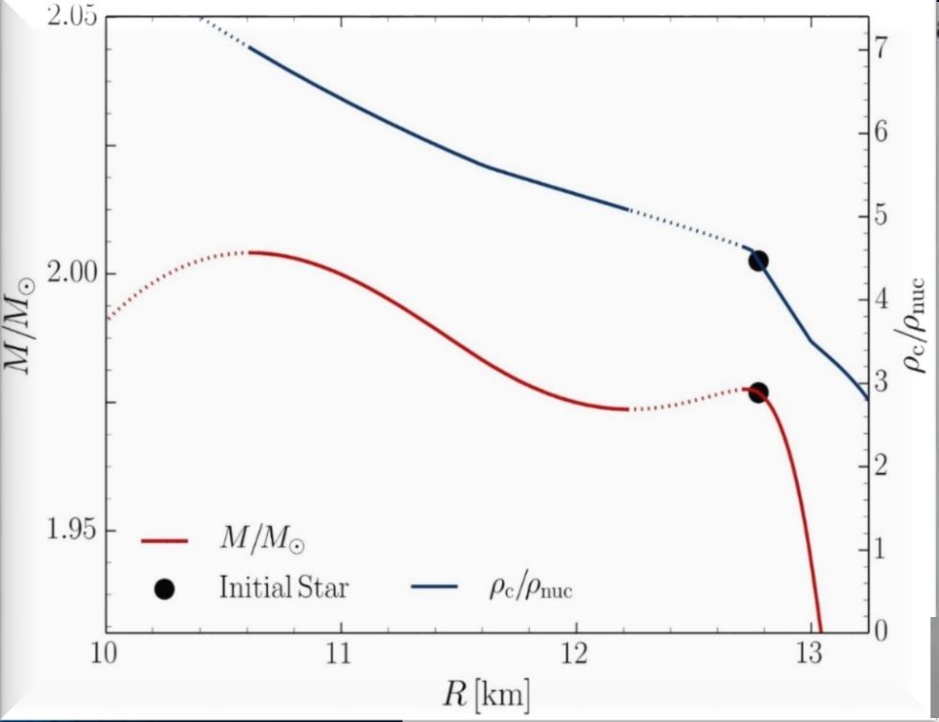

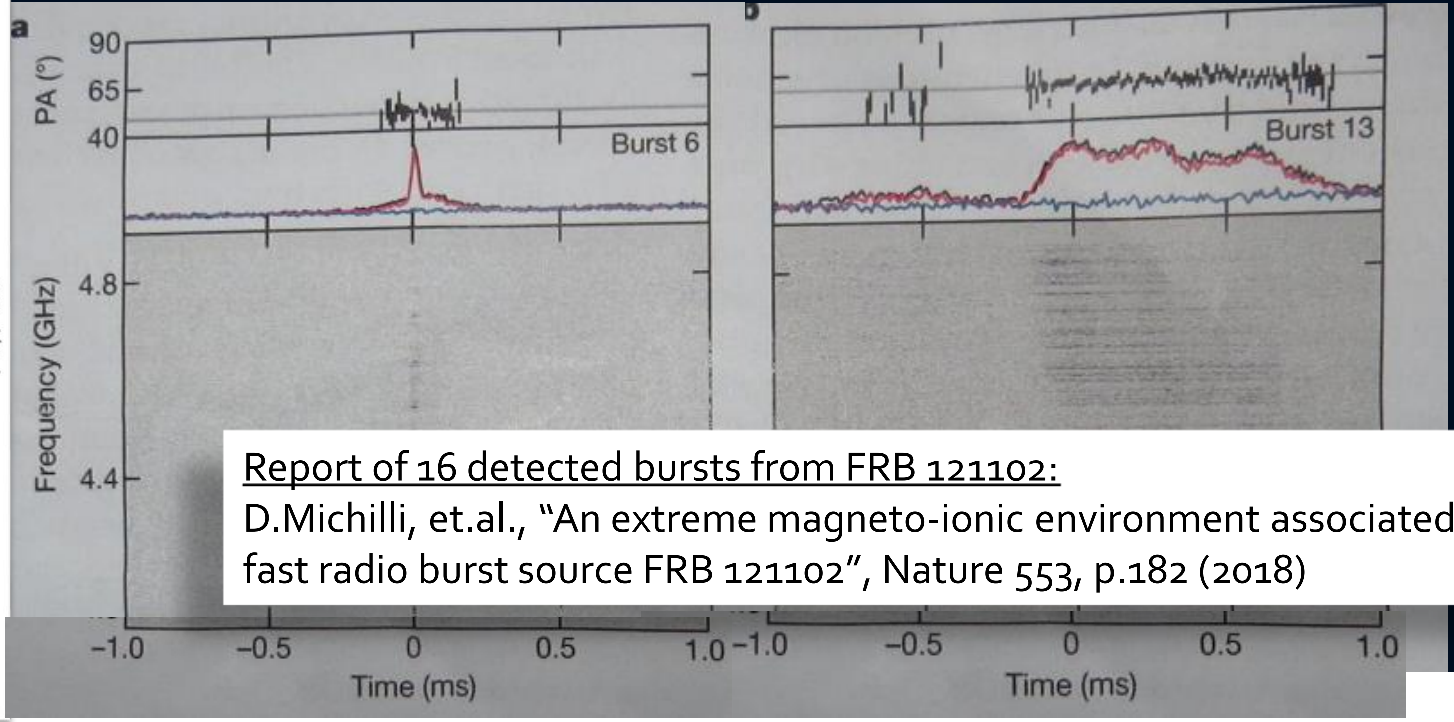

Report of 16 detected bursts from FRB 121102:

D.Michilli, et.al., “An extreme magneto-ionic environment associated with the fast radio burst source FRB 121102”, Nature 553, p.182 (2018)

M.Hanauske, et.al., “Twin Star Oscillations” (in preparation)

Hanauske, M., Yilmaz, Z.S., Mitropoulos,C., Rezzolla, L.,, and Stöcker, H., EPJ Web Conf. 171, 20004 (2018)

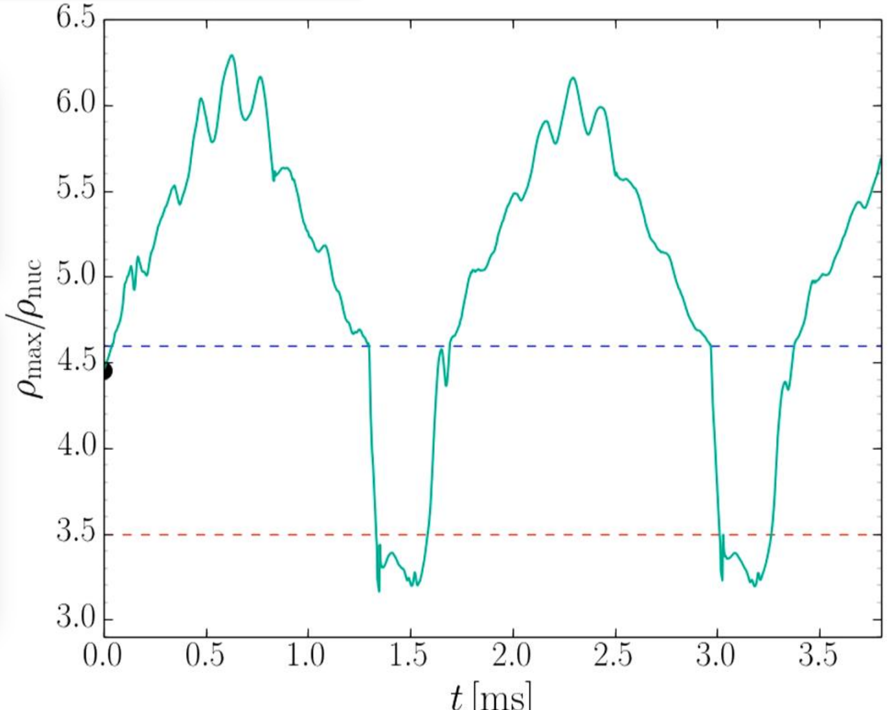

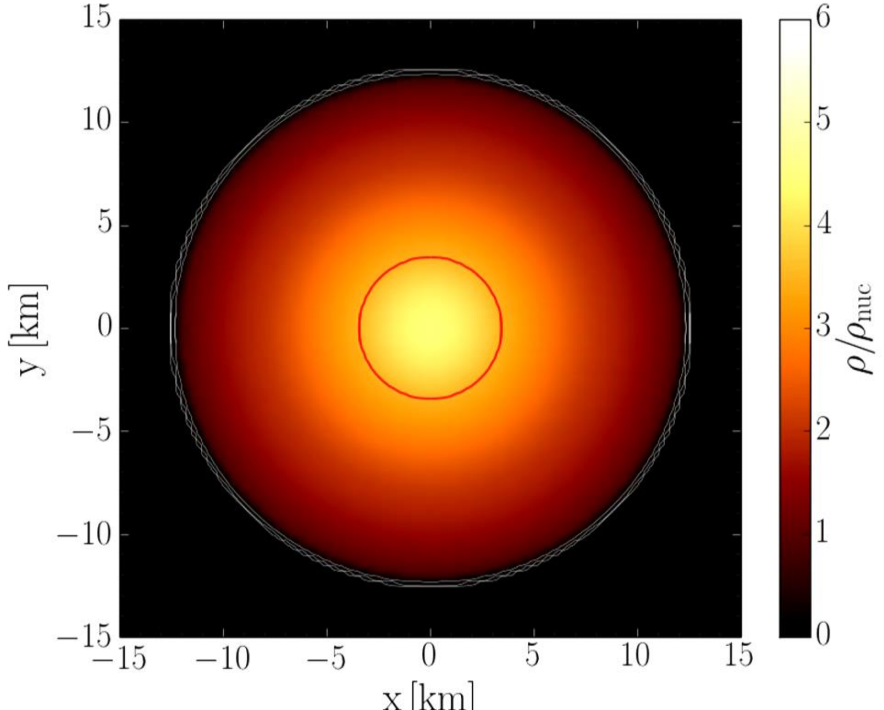

Neutron Star Mergers in the Context of a Twin Star Collapse

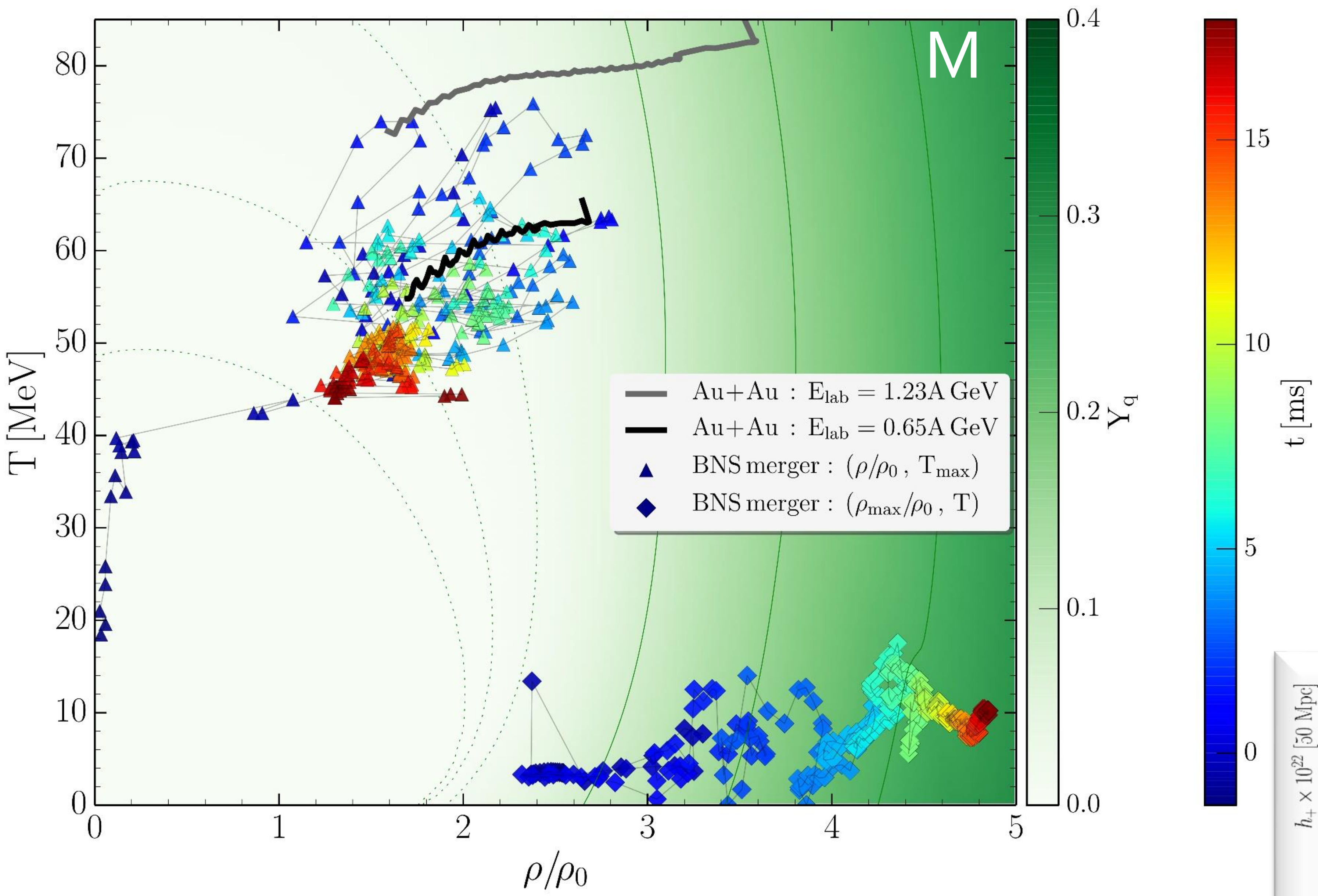

The astrophysical consequences of a rearrangement of a compact star due to the quark core formation, namely a twin star collapse or twin star oscillation, will be imprinted in the emitted GW-signal and would give an additional contribution to the dynamically emitted outflow of mass.

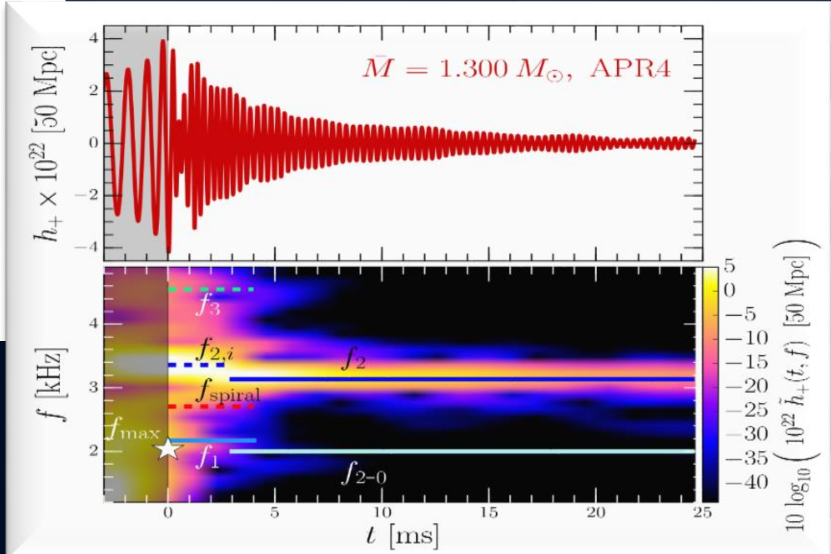

If the unstable twin star region is reached during the "post-transient" phase, the f2-frequency peak of the GW signal will change rapidly due to the sudden speed up of the differentially rotating HMNS.

Evolution of Tracer-particles tracking individual fluid elements in the equatorial plane of the HMNS at post-merger times

Rotational behavior of deconfined quark matter

Different rotational behaviour of the quark-gluon-plasma produced in non-central ultra-relativistic heavy ion collisions
L. Adamczyk et.al., "Global Lambda-hyperon polarization in nuclear collisions: evidence for the most vortical fluid", Nature 548, 2017

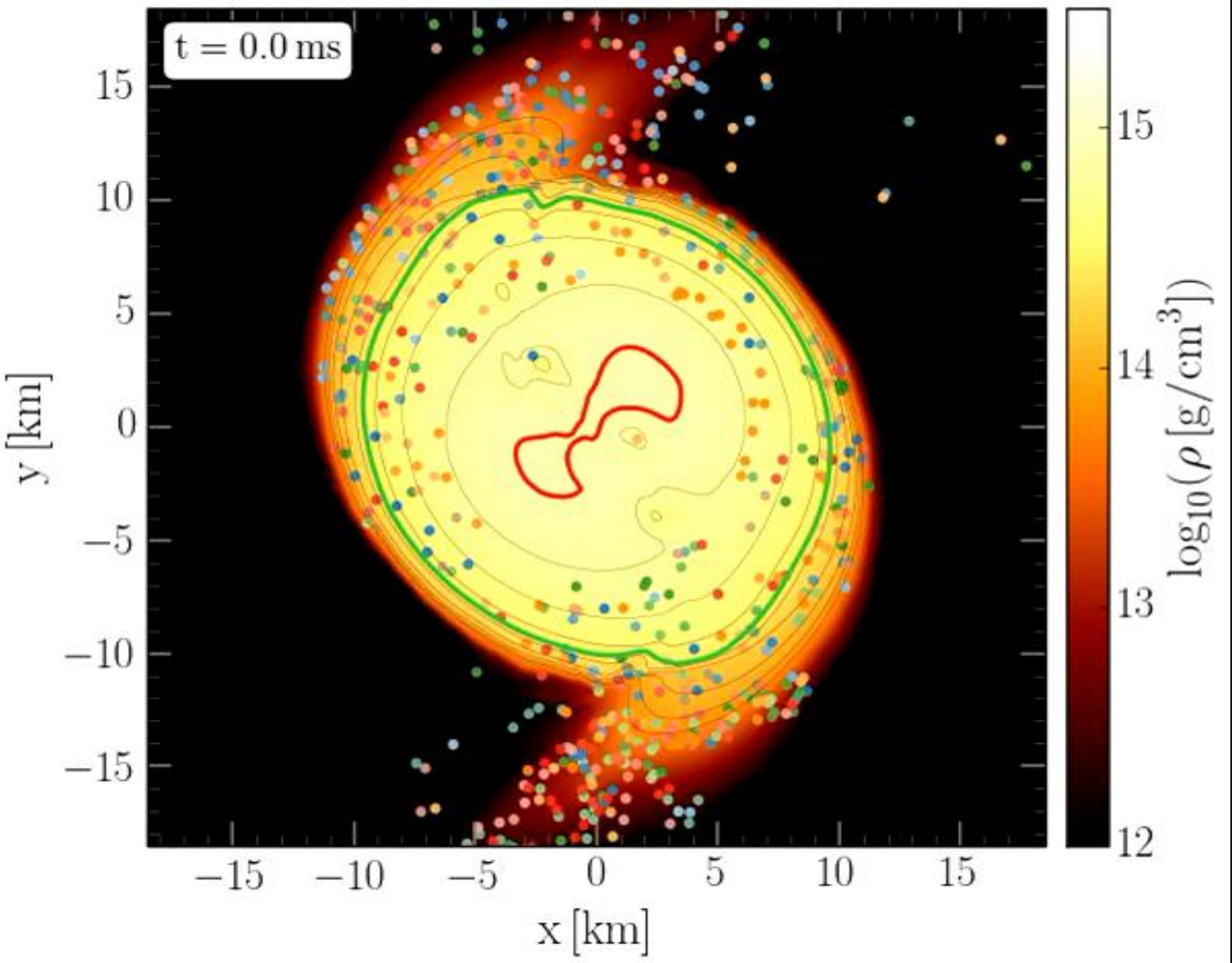

Summary and Discussions

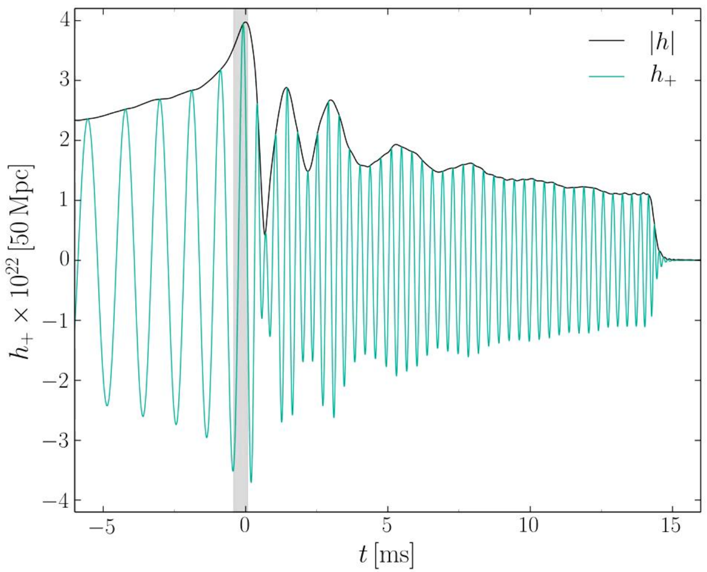

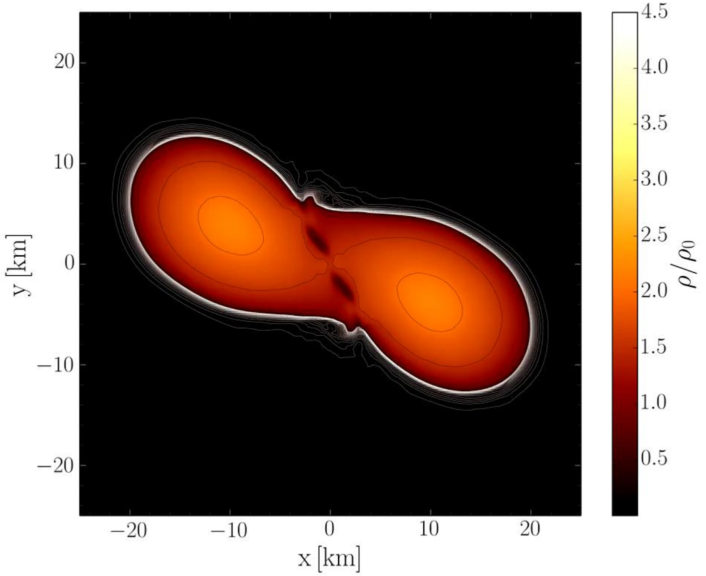

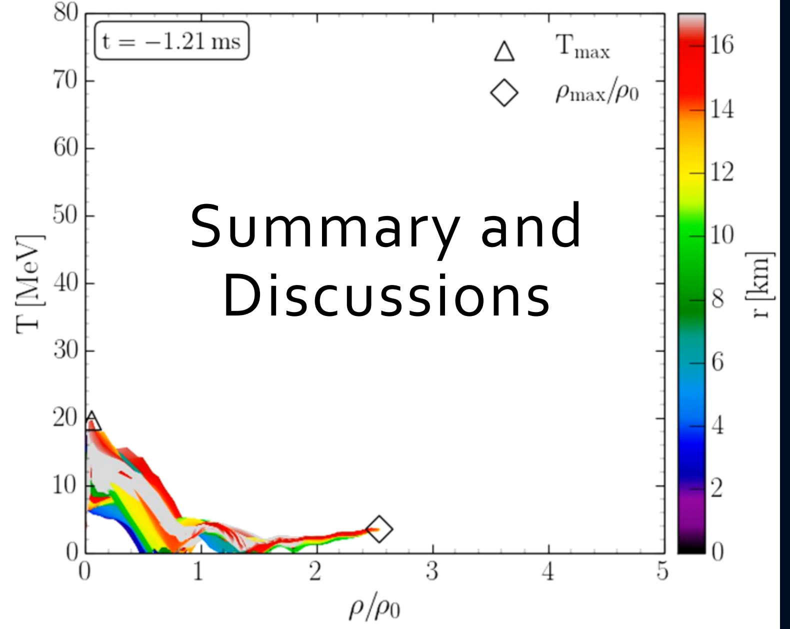

- In the post-merger phase of a binary neutron star merger, the density and temperature will reach extreme values and it is expected that a hadron-quark phase transition will be present in the interior region of the supramassive or hypermassive neutron star.
- Astrophysical observables of the hadron-quark phase transition:
  - If a twin star collapse would happen during the post-merger phase it will be imprinted in the GW-signal
  - If the unstable twin star region is reached during the "post-transient" phase, the f2-frequency peak of the GW signal will change rapidly due to the sudden speed up of the differentially rotating HMNS
  - Effects on the kilonova and neutrino emission?
  - Twin Star Collaps/Oszillations and the repeating fast radio burst (FRB 121102).

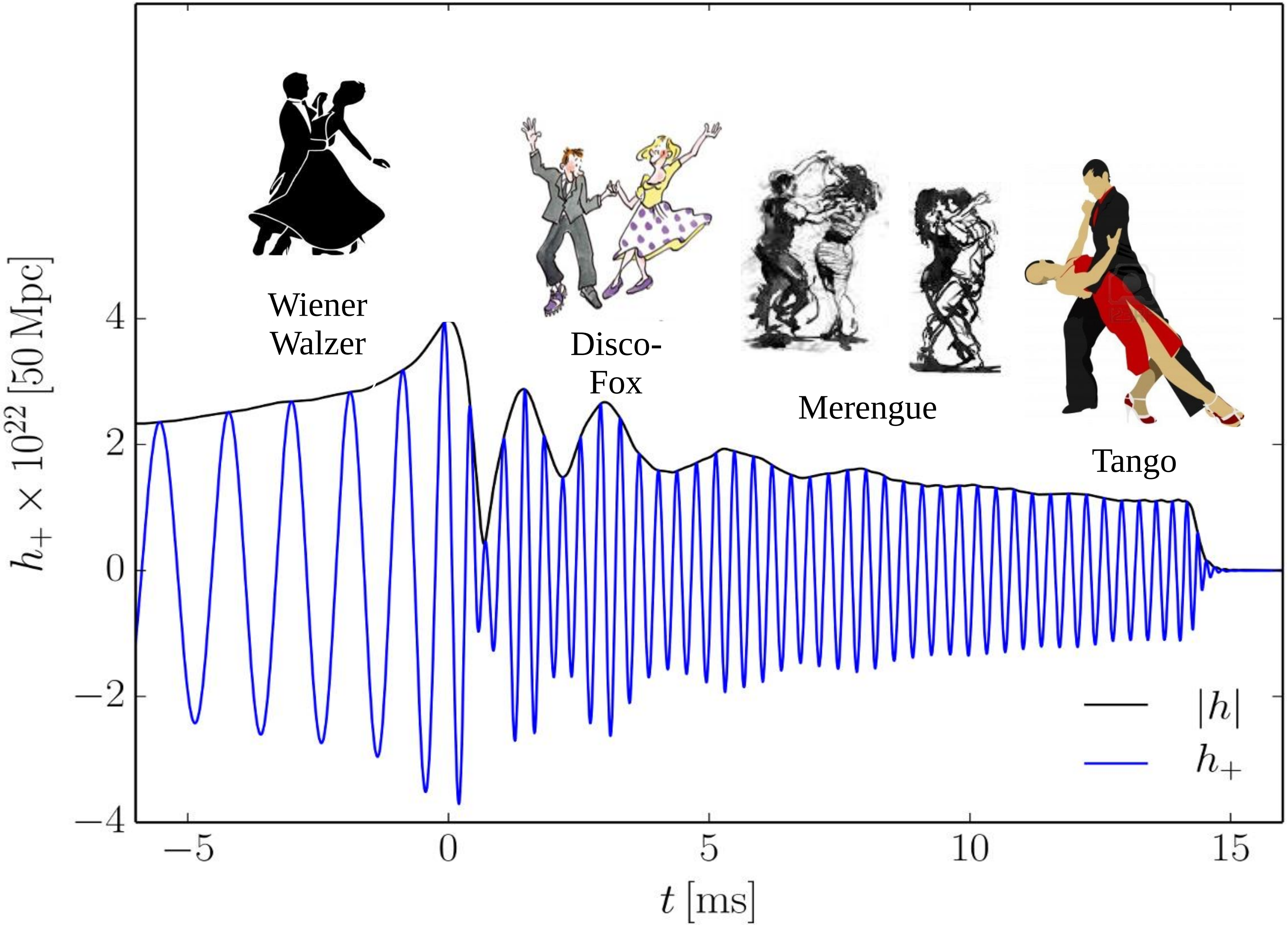
Wiener
Walzer
Disco-
Fox
Merengue
Tango
|h|
h+
h+ × 10^22 [50 Mpc]
t [ms]
−5
0
5
10
15
4
2
0
−2
−4

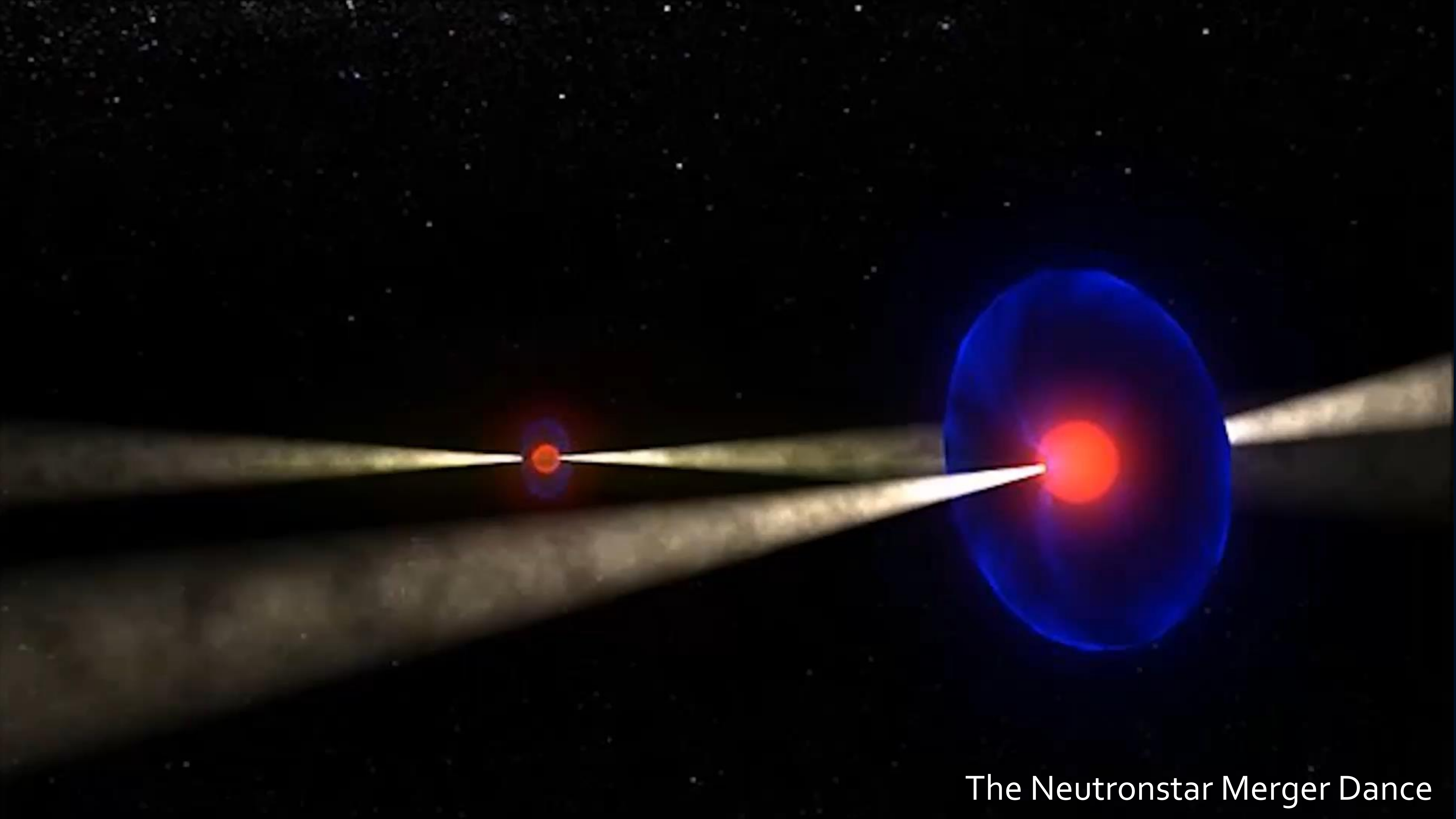

The Neutronstar Merger Dance

Additional Slides

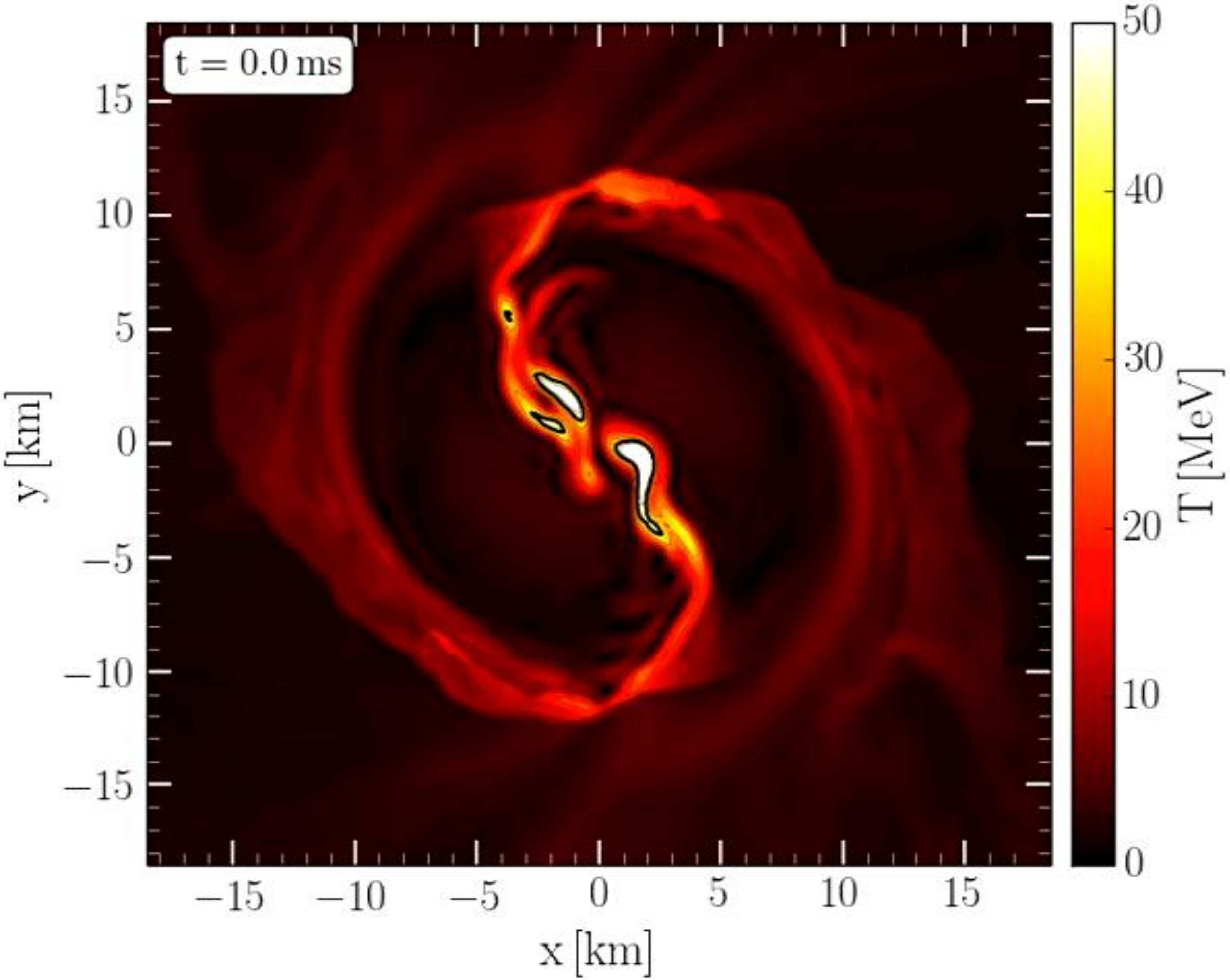

Evolution of the Temperature in the post merger phase

Hanauske, M., Takami, K., Bovard, L., Rezzolla, L., Font, J. A., Galeazzi, F., & Stöcker, H. (2017). Rotational properties of hypermassive neutron stars from binary mergers. Physical Review D, 96(4), 043004

Kastaun, W., Ciolfi, R., Endrizzi, A., & Giacomazzo, B. (2017). Structure of stable binary neutron star merger remnants: Role of initial spin. Physical Review D, 96(4), 043019

M. Hanauske, et.al., Connecting Relativistic Heavy Ion Collisions and Neutron Star Mergers by the Equation of State of Dense Hadron-and Quark Matter as signalled by Gravitational Waves, Journal of Physics: Conference Series, 878(1), p.012031 (2017)

The Maxwell Construction

If the surface tension between the hadron and quark phase is large, the mixed phase could completely disappear -> sharp boundary between hadronic and quark. The Hadron-quark phase transition is then described using a Maxwell construction.

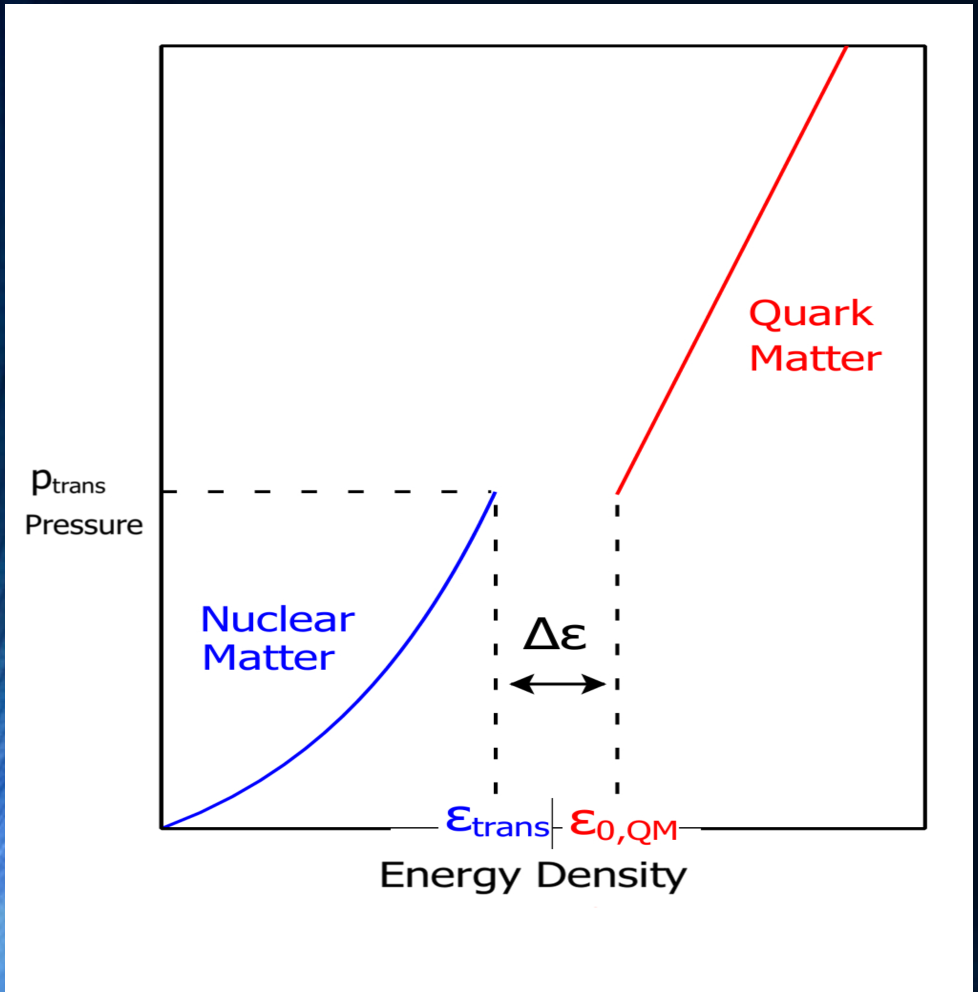

Pressure and baryon chemical potential stays constant, while the density and the charge chemical potential jump discontinuously during the phase transition.

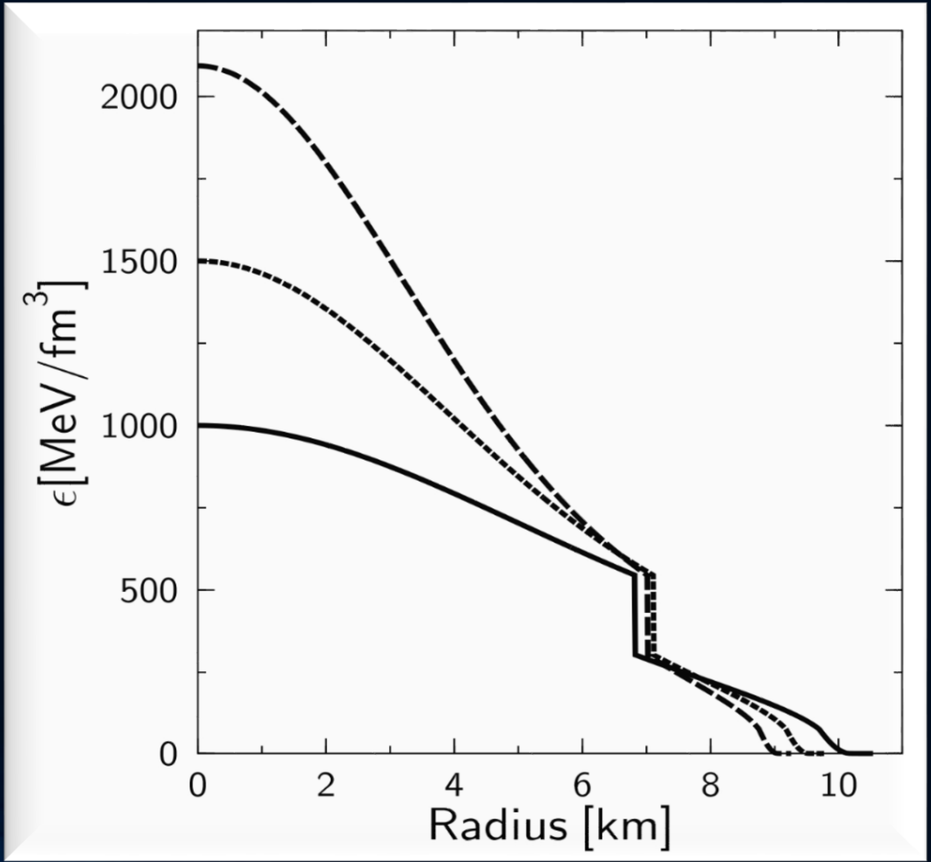

Image from M.G. Alford, S. Han, and M. Prakash, Phys. Rev. D 88, 083013 (2013)

Angular Velocity away from the equatorial plane

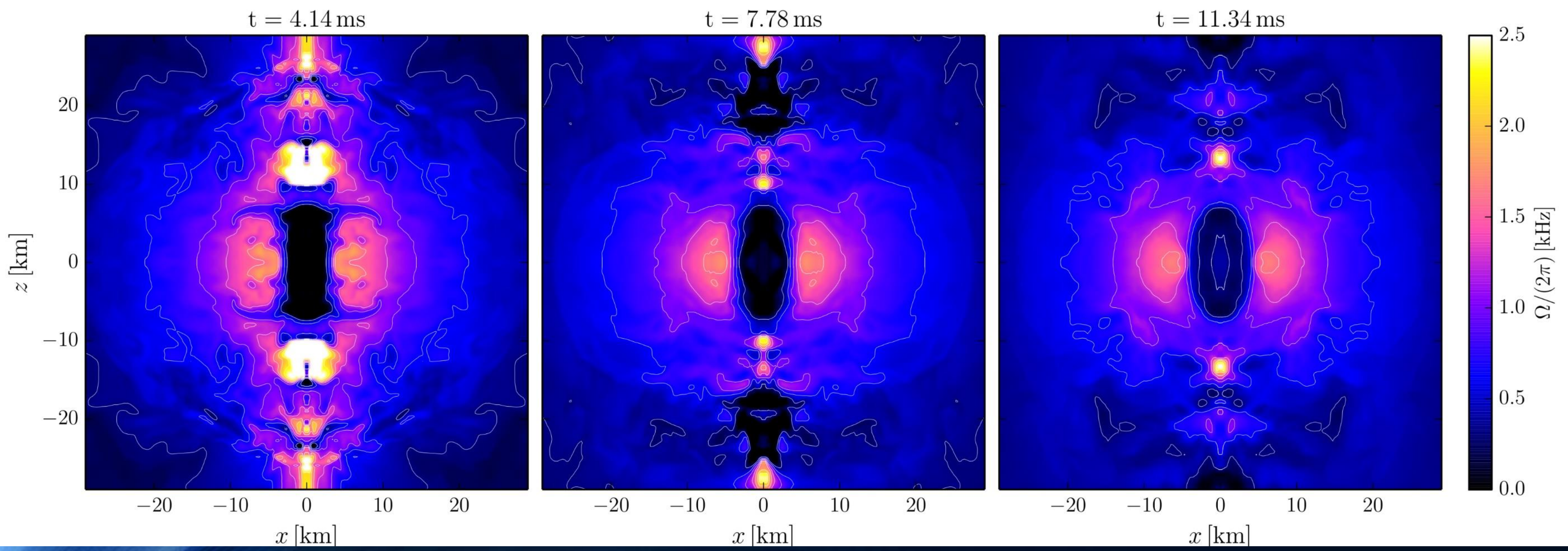

Neutron Stars, Hybrid Stars, Quark Stars and Black Holes

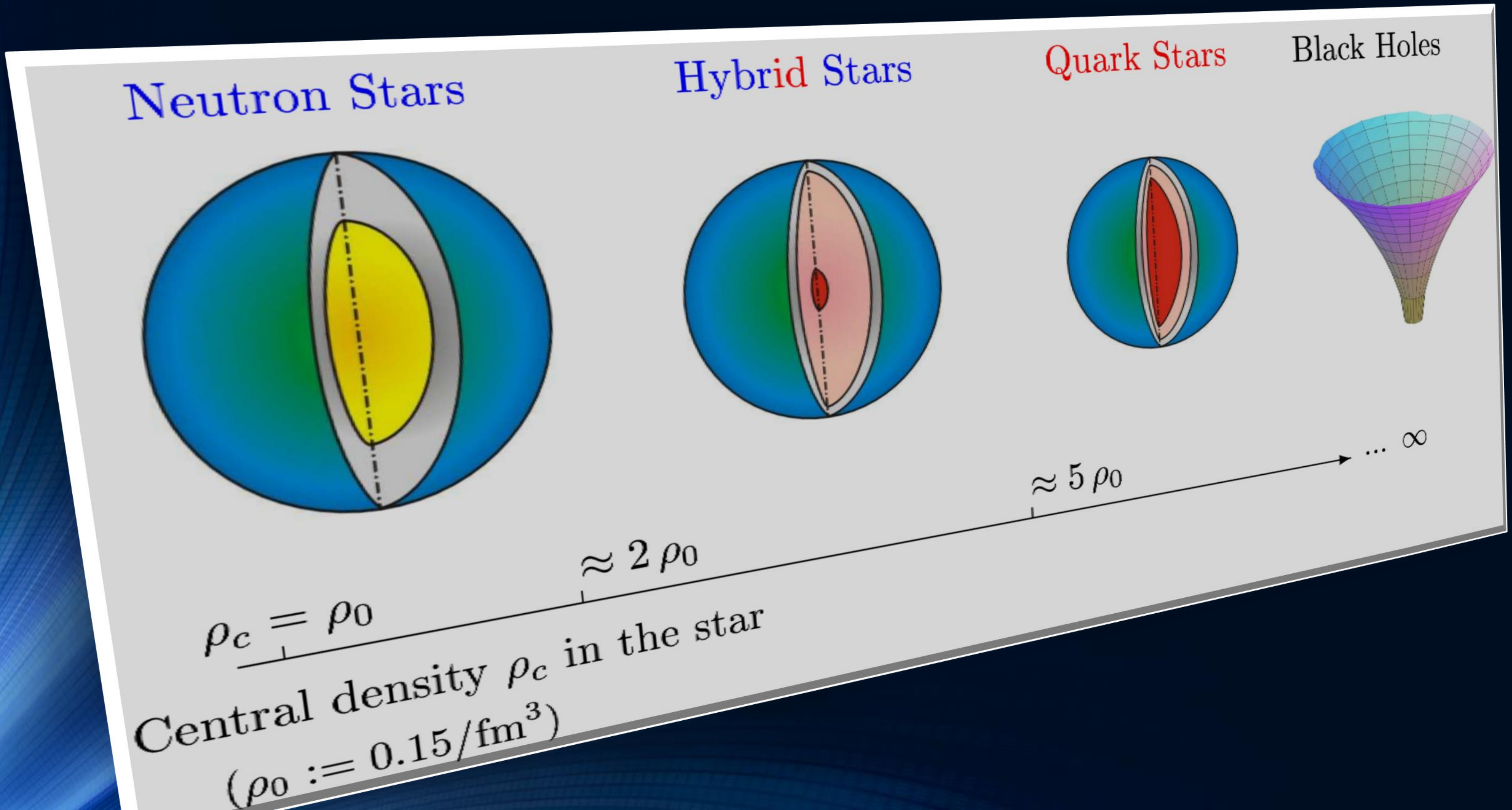

The Formation of the Event Horizon of the Black Hole and the Deconfinement of Elementary Matter

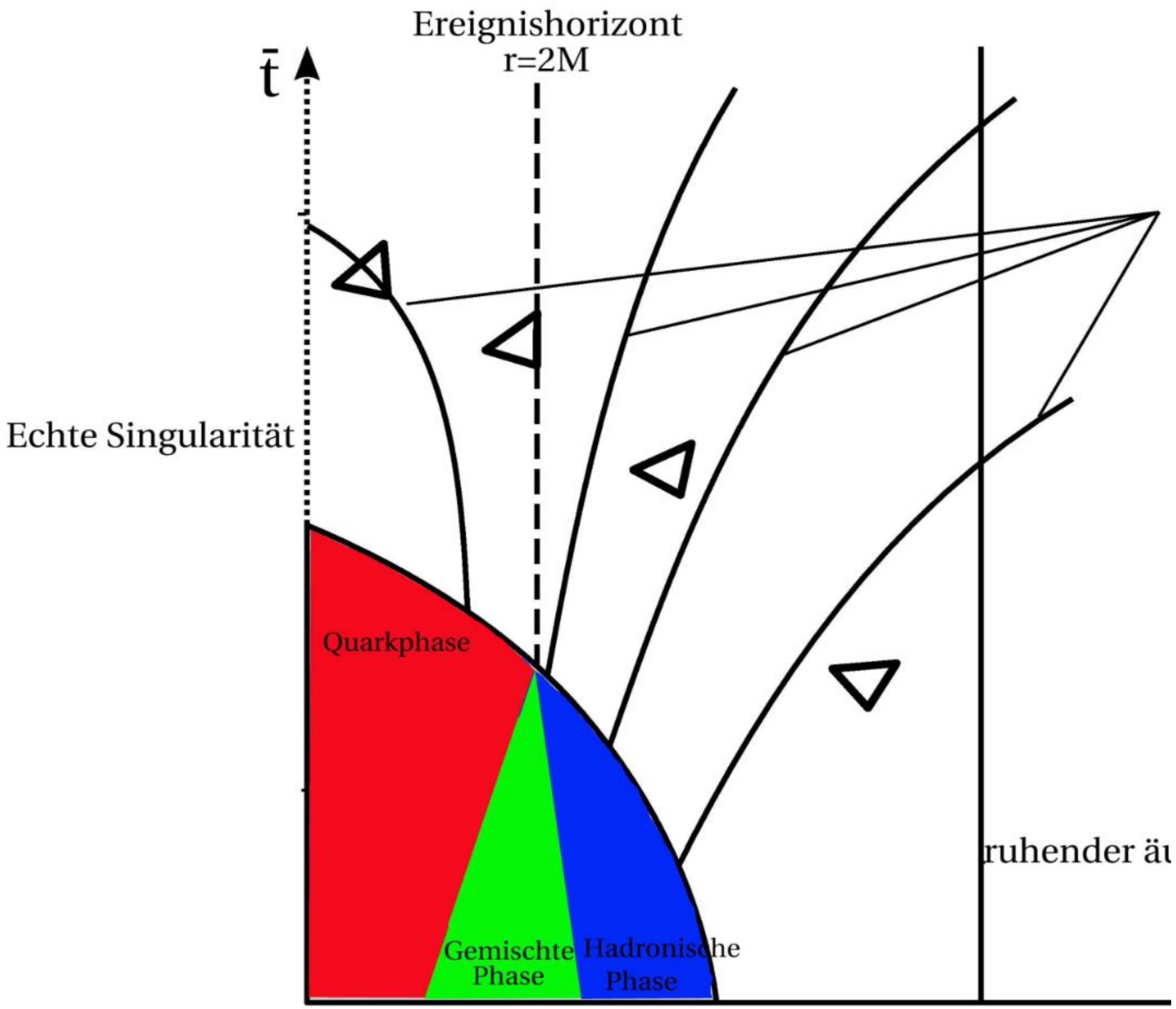

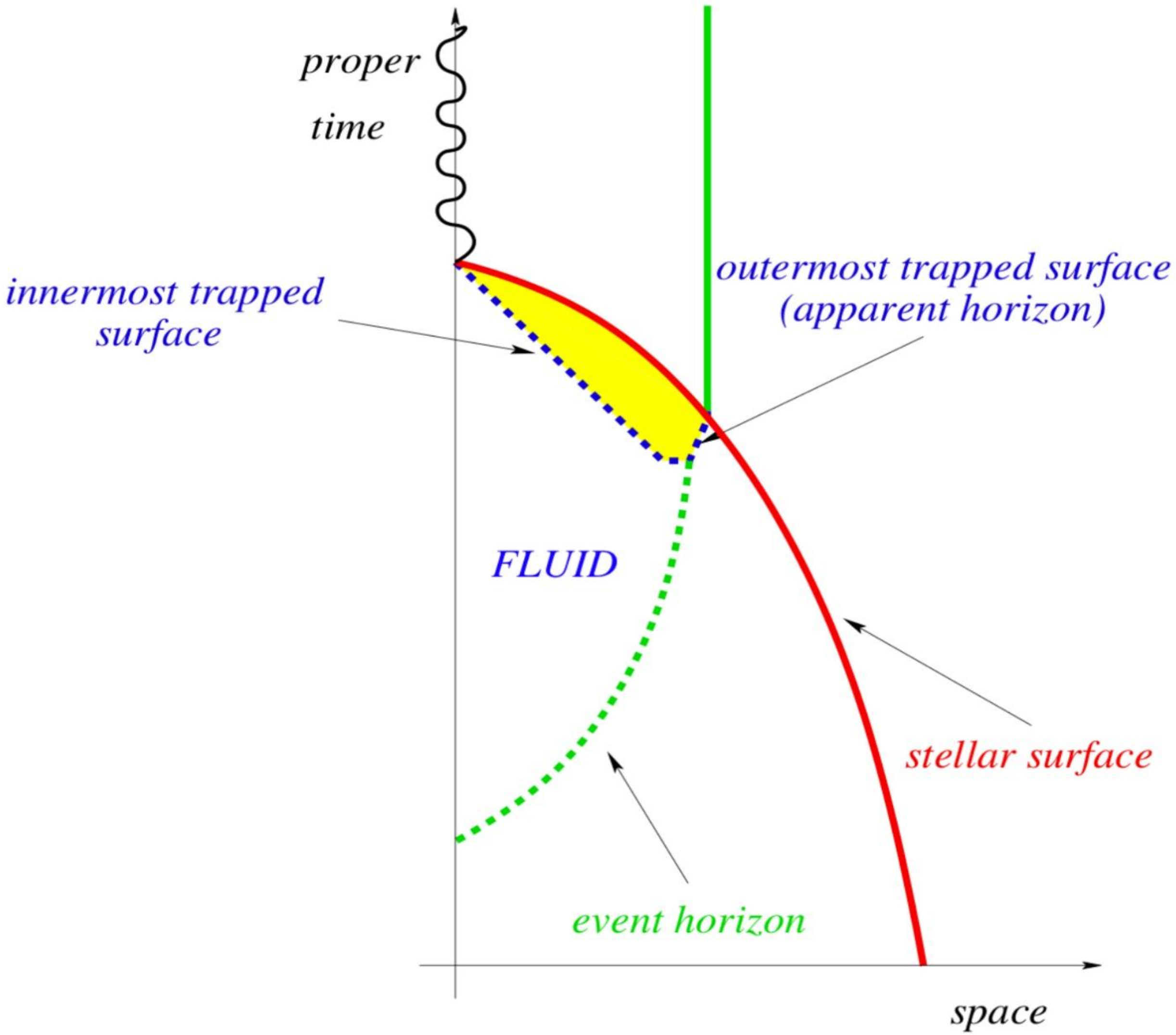

Numerical Setup

BSSNOK conformal traceless formulation of the ADM equations. 3+1 Valencia formulation and high resolution shock capturing methods for the hydrodynamic evolution. Full general relativity using the **Einstein-Toolkit** and the **WHISKY/WhiskyTHC code** for the general-relativistic hydrodynamic equations.

Grid Structure:

Adaptive mesh refinement (six ref. levels)

Grid resolution: (from 221 m to 7.1 km)

Outer Boundary: 759 km

Initial separation of stellar cores: 45 km

HMNS Evolution for different EoSs

High mass simulations (M=1.35 Msolar)

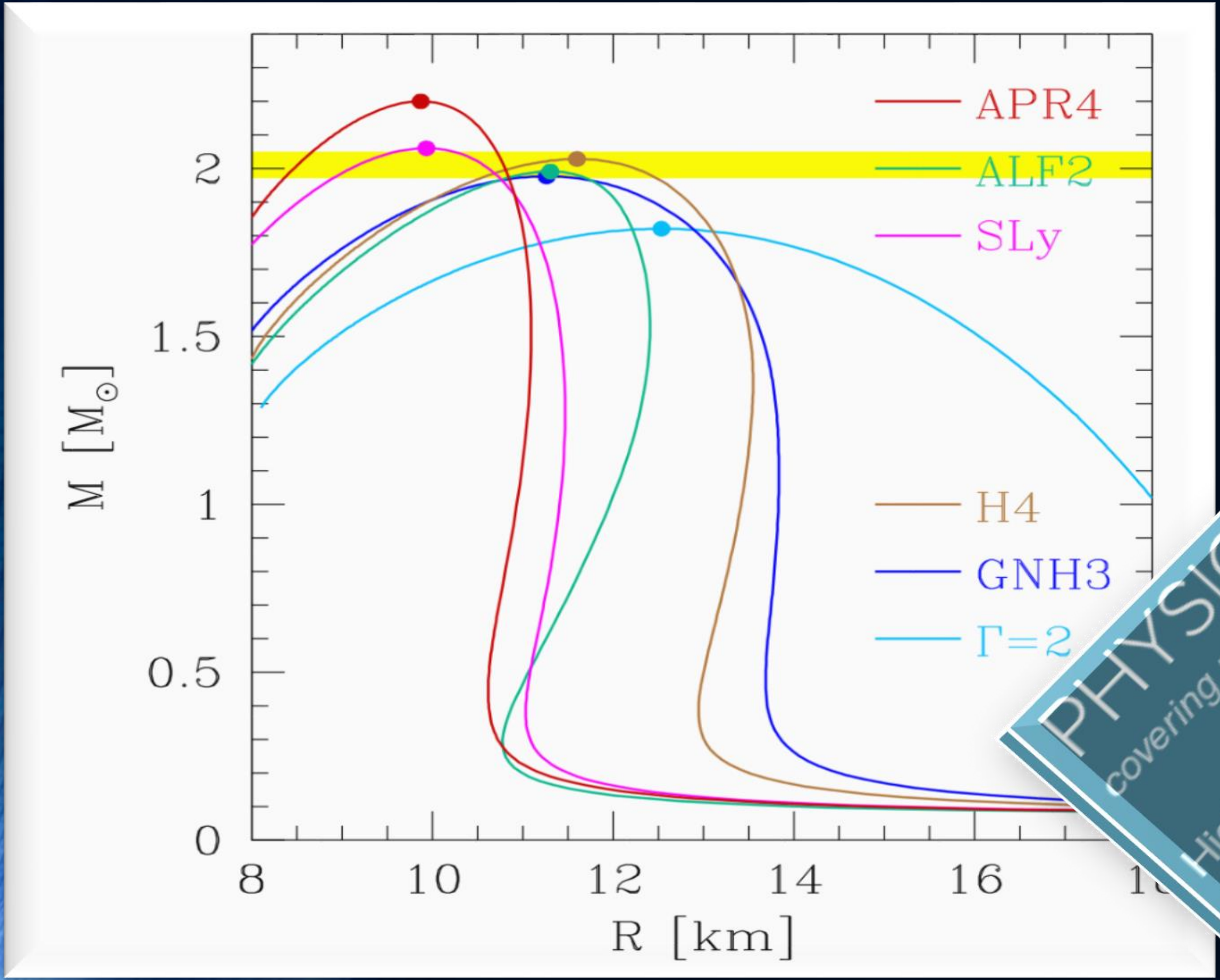

Mass-Radius relation for different EOSs

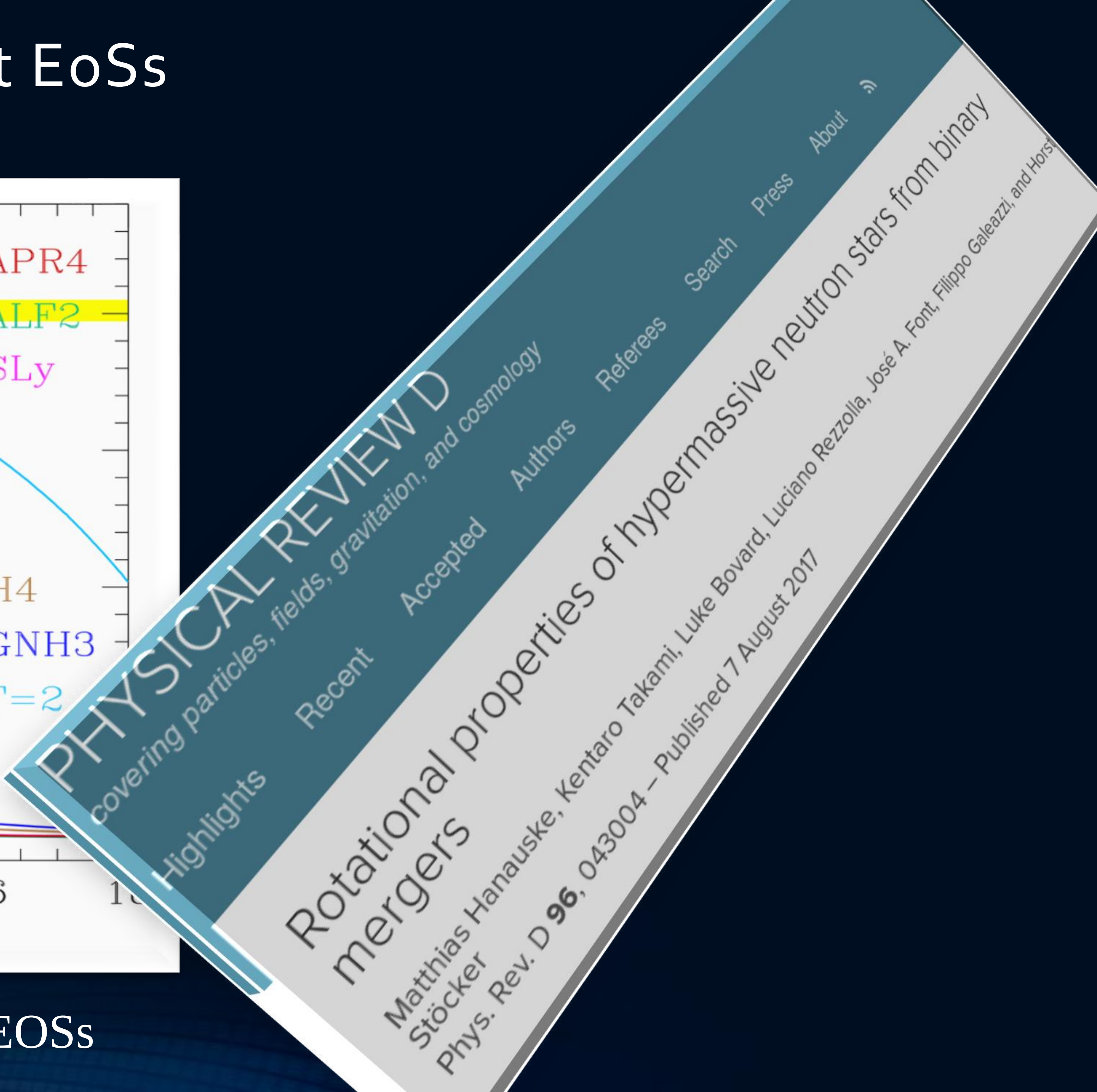

The Structure of Ω

$$\Omega(x,y,z,t) = \frac{u^\phi}{u^t} = \alpha\, v^\phi \;-\; \beta^\phi$$

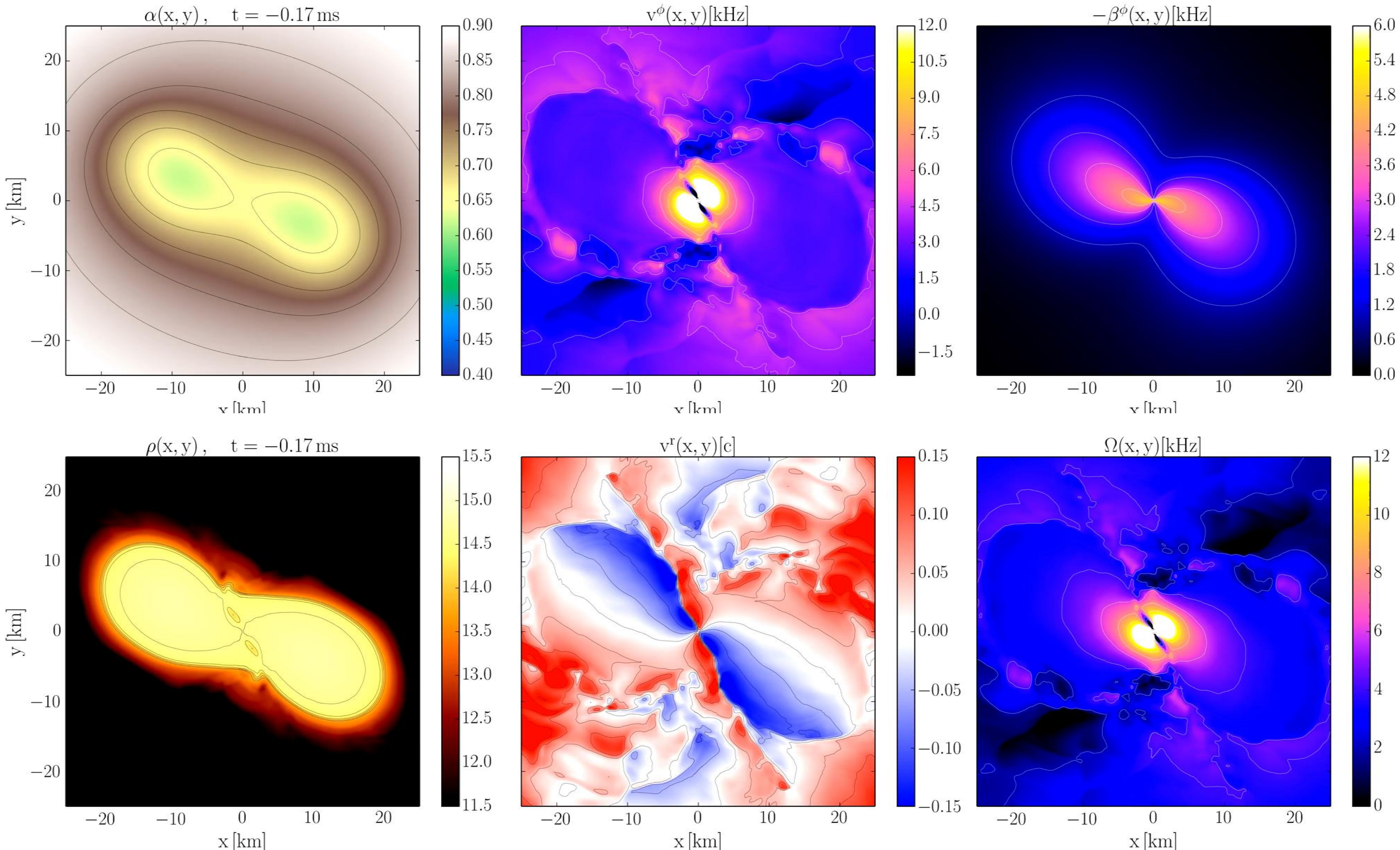

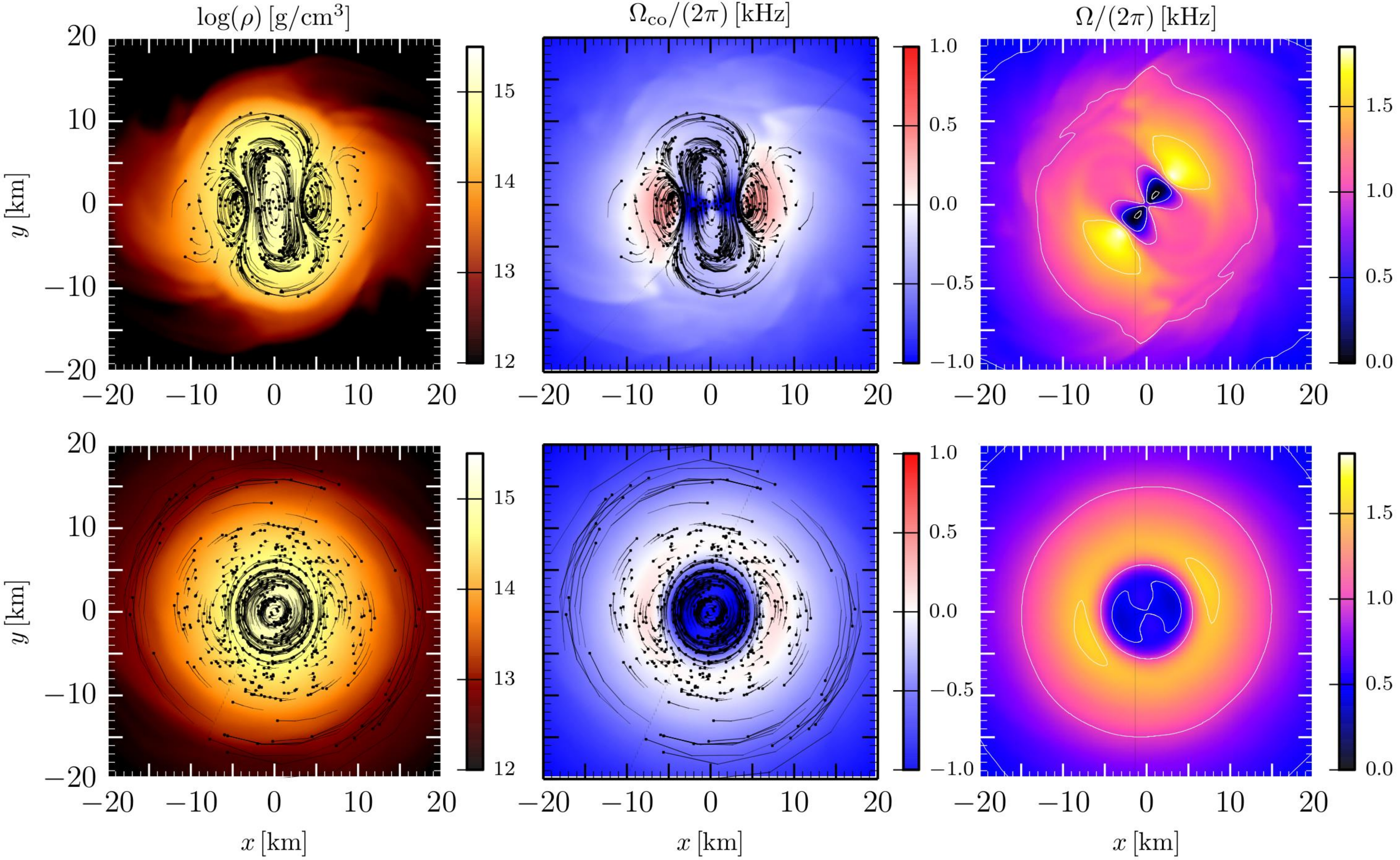

$\log(\rho)$ [g/cm^3]
$\Omega_{co}/(2\pi)$ [kHz]
$\Omega/(2\pi)$ [kHz]
y [km]
x [km]

Averaging Procedure for Ω

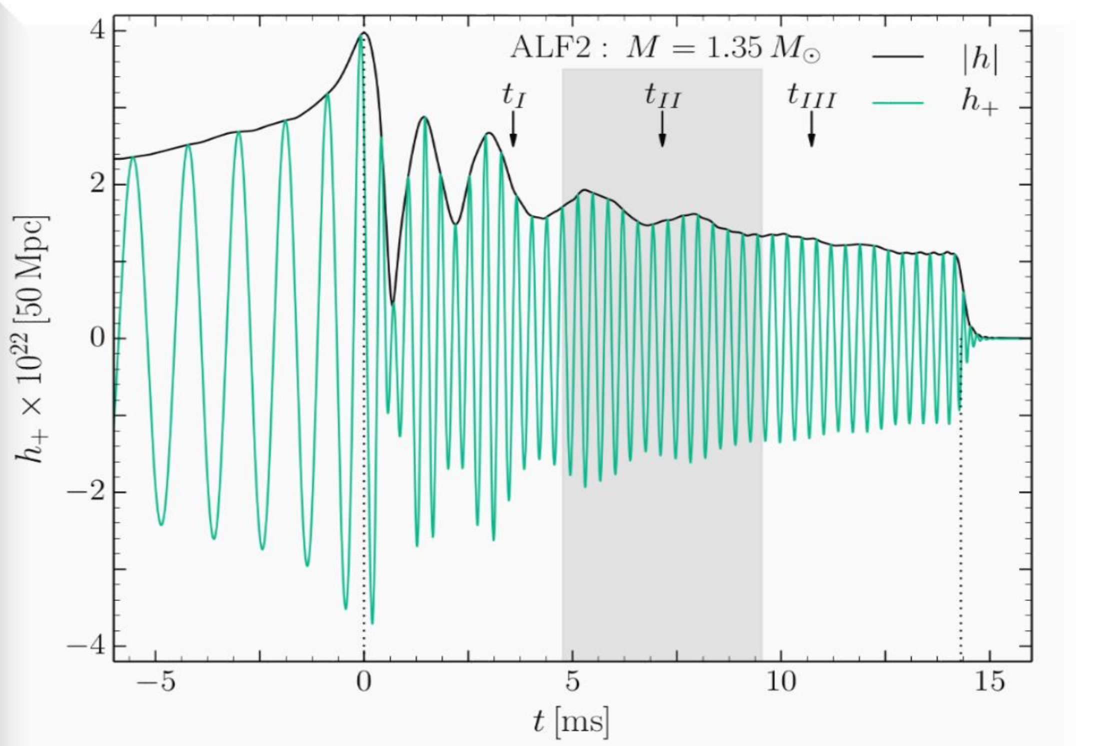

FIG. 2. Gravitational wave amplitude $|h|$ and h_+ at a distance of 50 Mpc for the ALF2-M135 model.

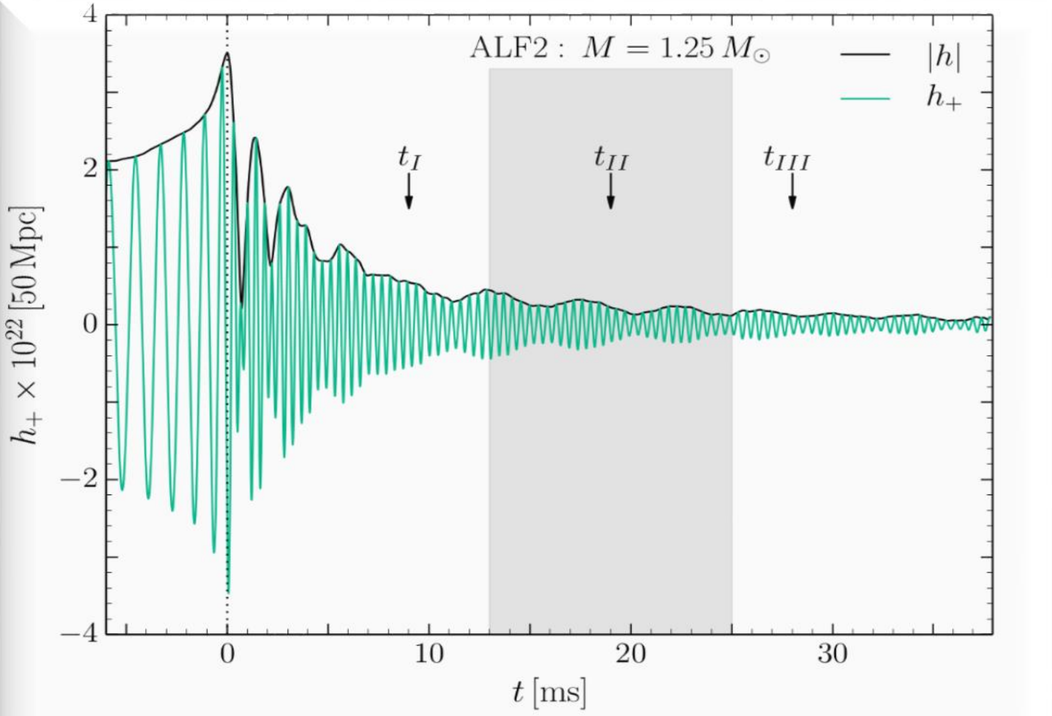

FIG. 10. Gravitational wave amplitude h_+ and $|h|$ at a distance of 50 Mpc for the ALF2-M125 model.

$$\bar{\Omega}(r, t_c) = \int_{t_c-\Delta t/2}^{t_c+\Delta t/2} \int_{-\pi}^{\pi} \Omega(r, \phi, t')\; d\phi\, dt'$$

In order to compare the structure of the rotation profiles between the different EOSs, a certain time averaging procedure has been used:

Dependence on the time averaging window

For all EOS the same time averaging window. From the left to right the data refer to time windows [6 ; 11]; [6 ; 13] and [6 ; 15] ms, respectively.

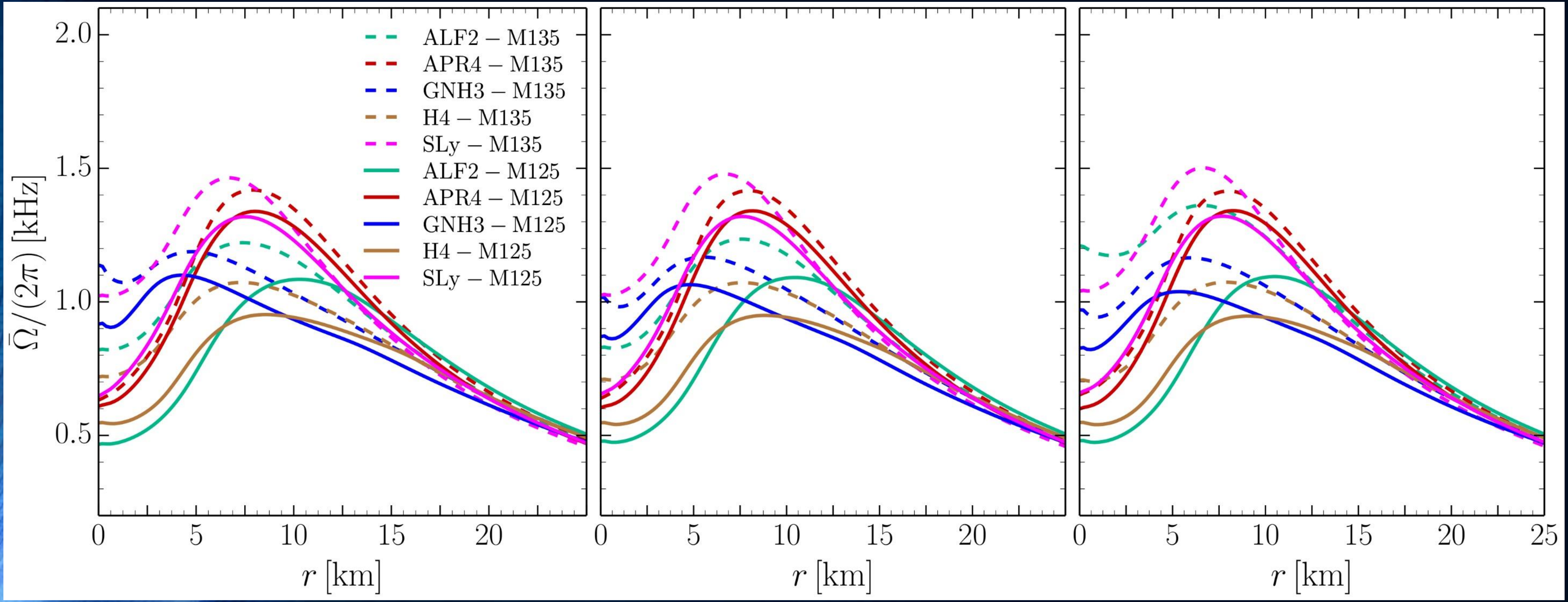

Dependence on the time averaging window

Averaged angular-velocity profiles when the avering windows is set to be 7 ms for all EOSs and masses, but where the initial averaging time is varied and set to be 5 (red line), 6 (blue line), 7 (green line), and 8 ms (black line), respectively. The four lines refer to averaging windows given by [5; 12], [6; 13], [7; 14], and [8; 15] ms, respectively; note that the top part of each panel refers to the low-mass binary, while the bottom one to the high-mass one.

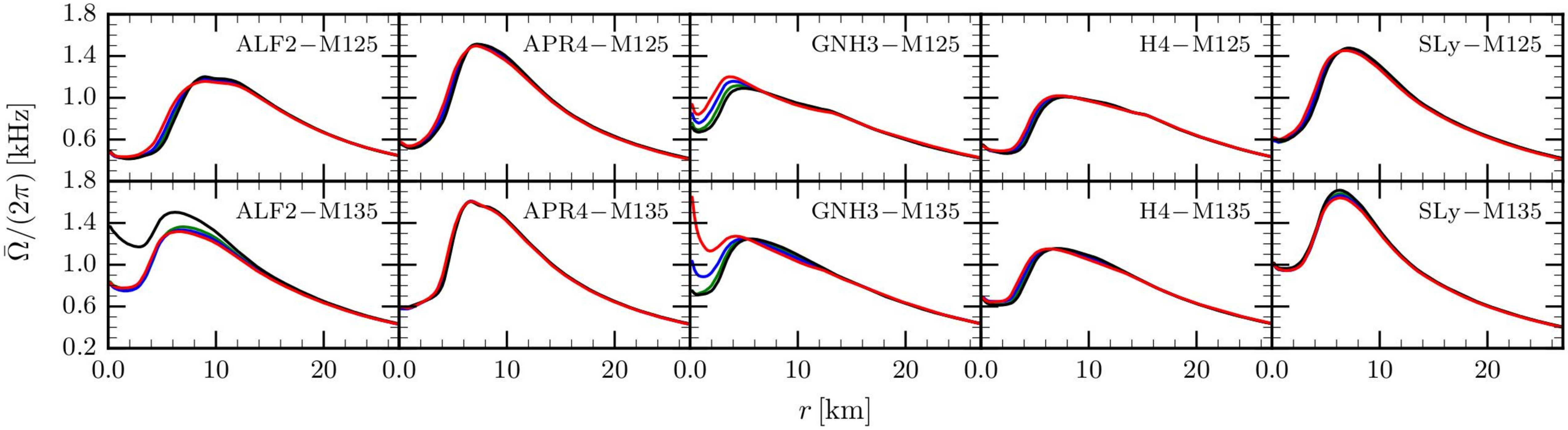

Ω*(t) [rad/s] and R*(t) for ALF2, M=1.35

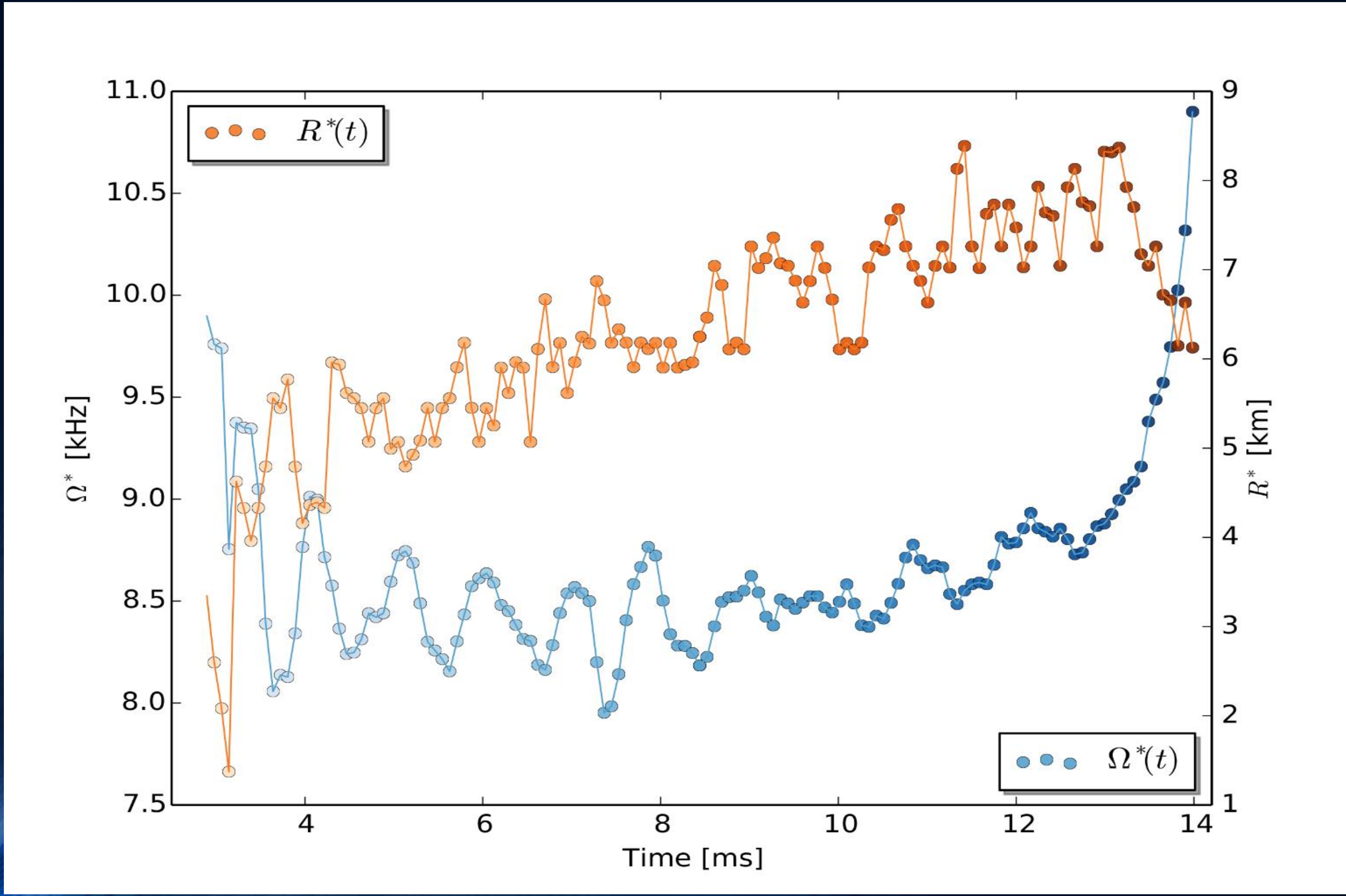

Gravitational Waves and the Maximum of the Rotation Profile

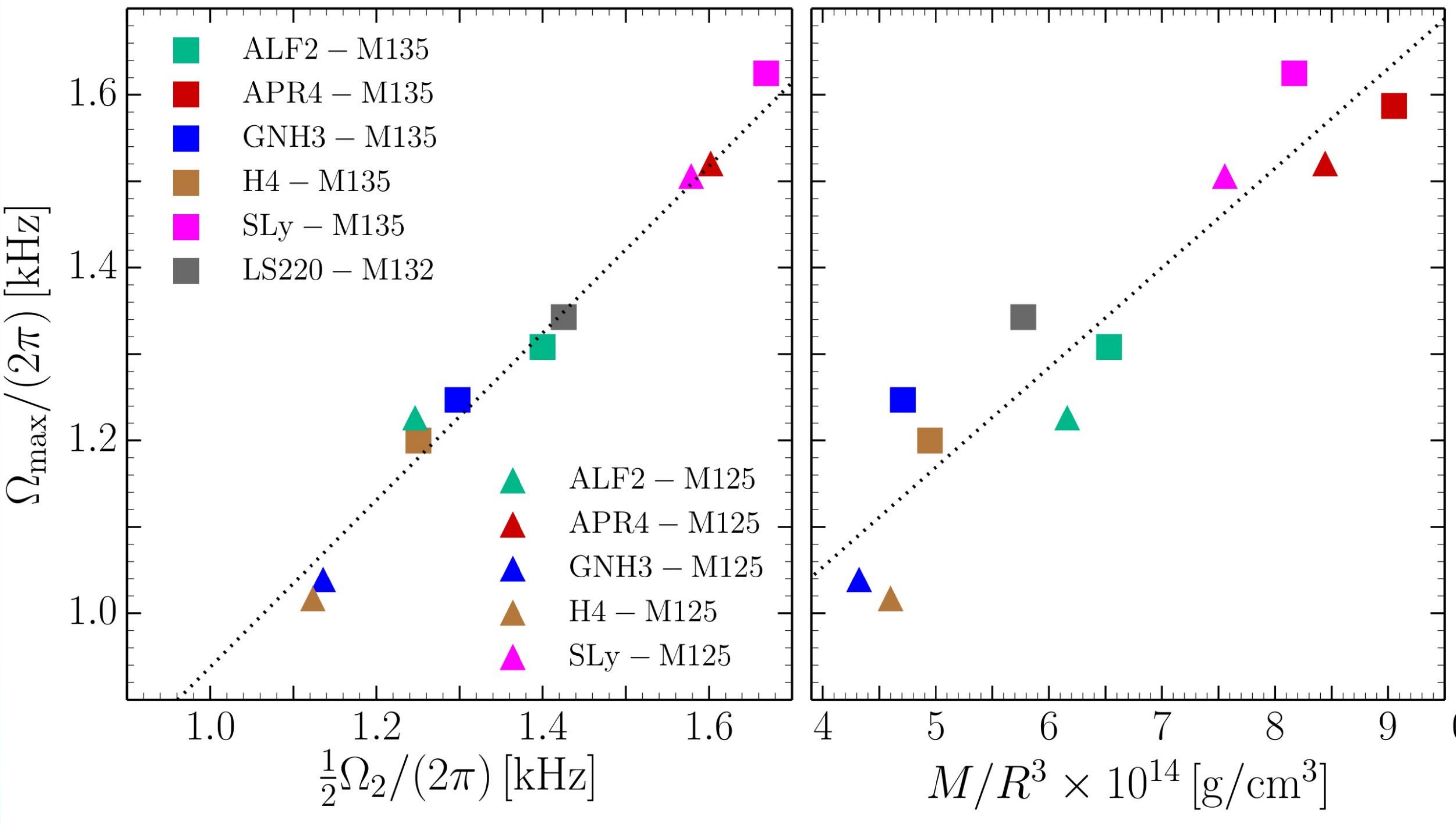

Merger Product from an eccentric colliding Neutron Star Binaries

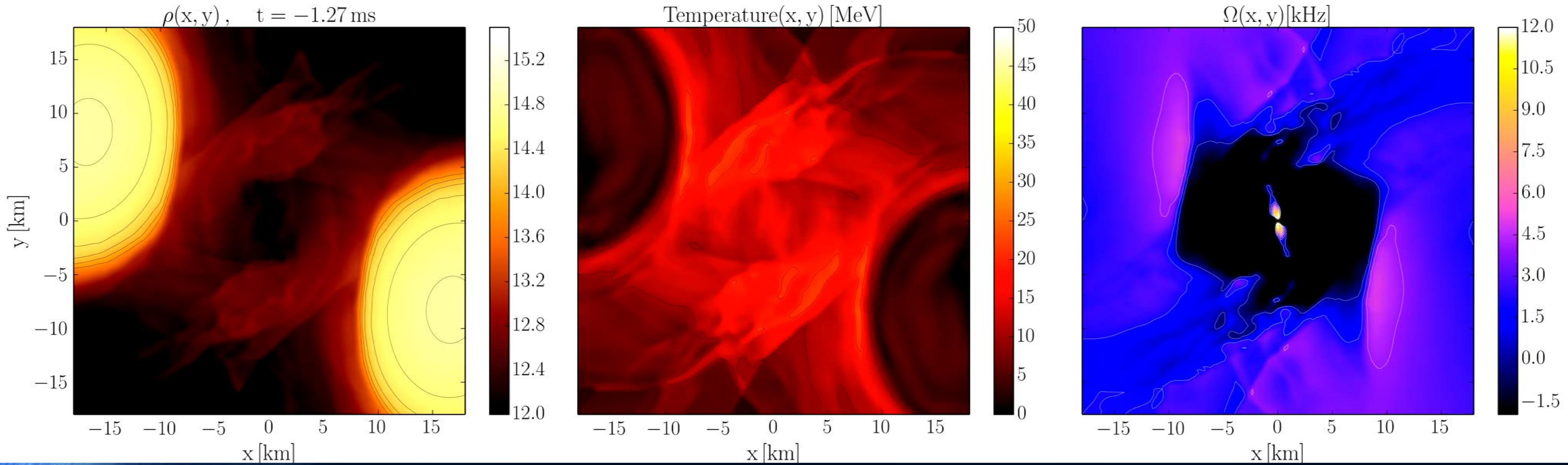

Summary

- On August 17, 2017, a long-awaited event has taken place: the Advanced LIGO and Virgo gravitational-wave detectors have recorded the signal from the inspiral and merger of a binary neutron-star system.
- The analysis of the gravitational wave data in combination with the independently detected gamma-ray burst and electromagnetic counterpart results in a neutron star merger scenario which is in good agreement with numerical simulations of binary neutron star mergers performed in full general relativity.
- During the late post-merger simulation, the value of central rest-mass density will reach extreme values and it is expected that a hadron-quark phase transition will be present in the interior region of the HMNS.
- Astrophysical observables of the hadron-quark phase transition may be detectable when advanced gravitational wave detectors reach design sensitivity or with next-generation detectors.

Time dependence of the Rotation Profile

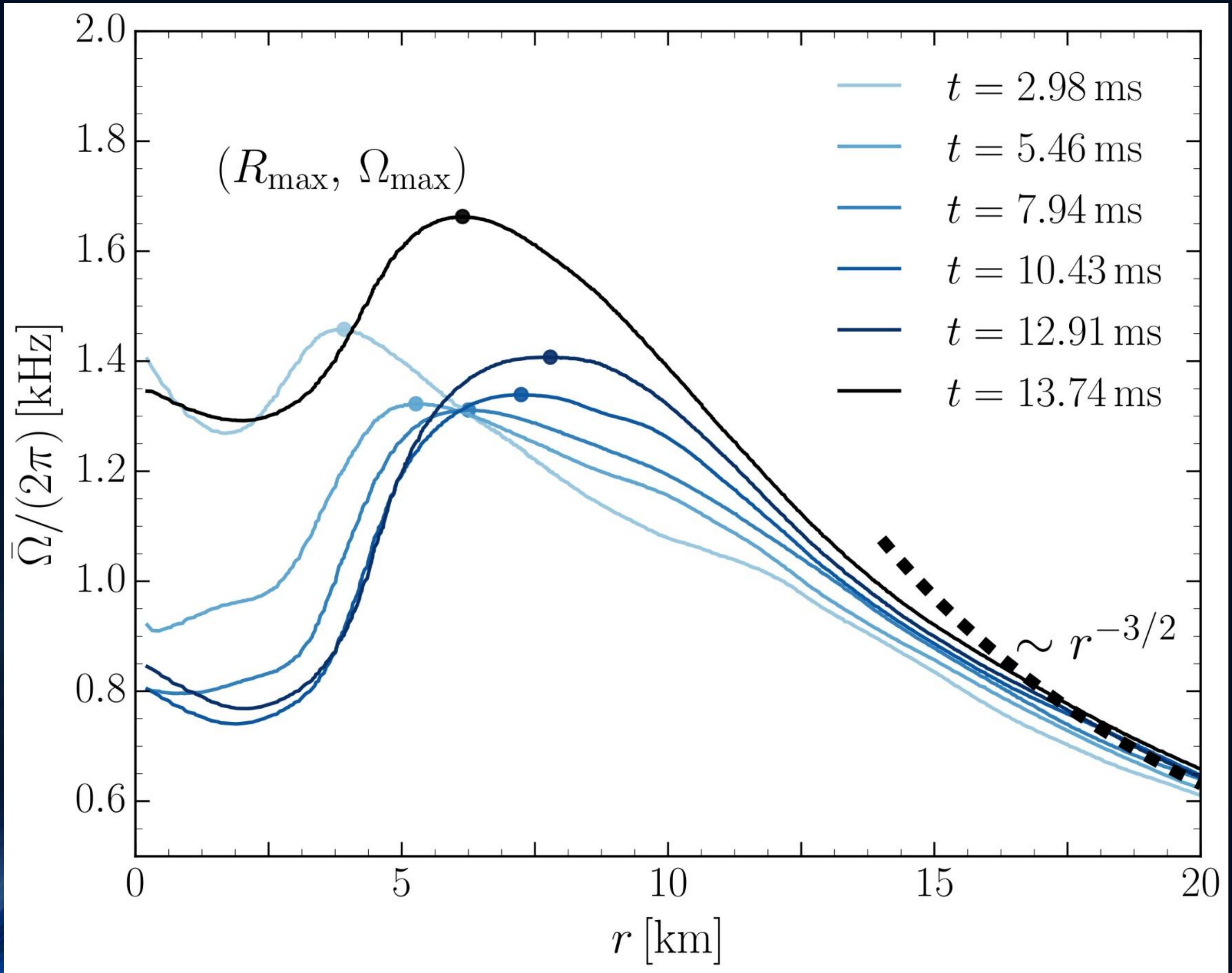

Averaged fluid angular velocity on the equatorial plane for the ALF2-M135 binary as averaged at different times and with intervals of length t = 1 ms.

Gauge Conditions

On each spatial hypersurface, four additional degrees of freedom need to be specified: A slicing condition for the lapse function and a spatial shift condition for the shift vector need to be formulated to close the system. In an optimal gauge condition, singularities should be avoided and numerical calculations should be less time consuming.

Bona-Massó family of slicing conditions: $\partial_t \alpha - \beta^k \partial_k \alpha = -f(\alpha)\, \alpha^2 (K - K_0)$

"1+log" slicing condition: $f = 2/\alpha$ where $f(\alpha) > 0$ and $K_0 := K(t = 0)$

"Gamma-Driver" shift condition:

$$\partial_t \beta^i - \beta^j \partial_j \beta^i = \frac{3}{4} B^i,$$

$$\partial_t B^i - \beta^j \partial_j B^i = \partial_t \tilde{\Gamma}^i - \beta^j \partial_j \tilde{\Gamma}^i - \eta B^i$$

The Gibbs Construction

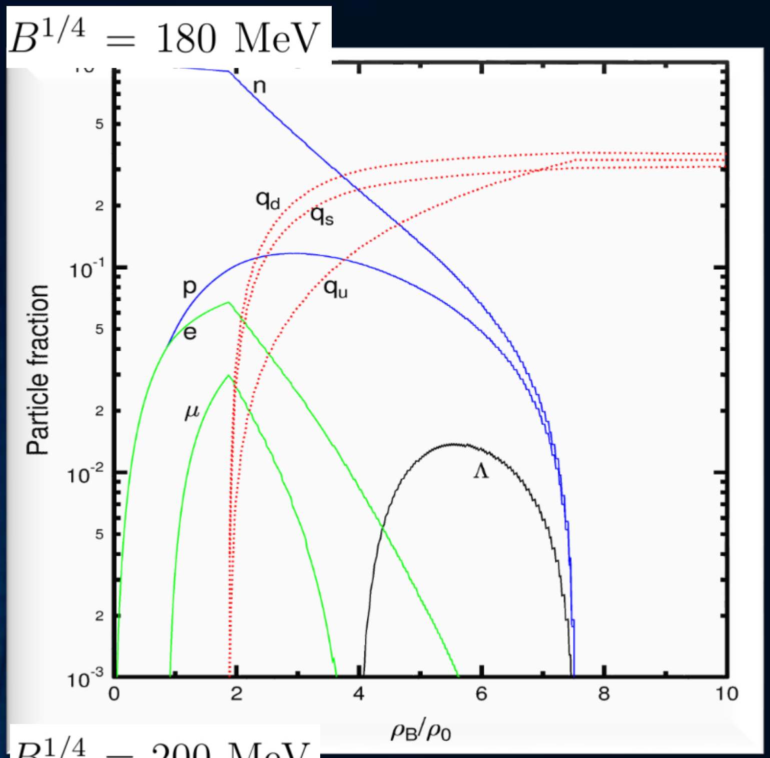

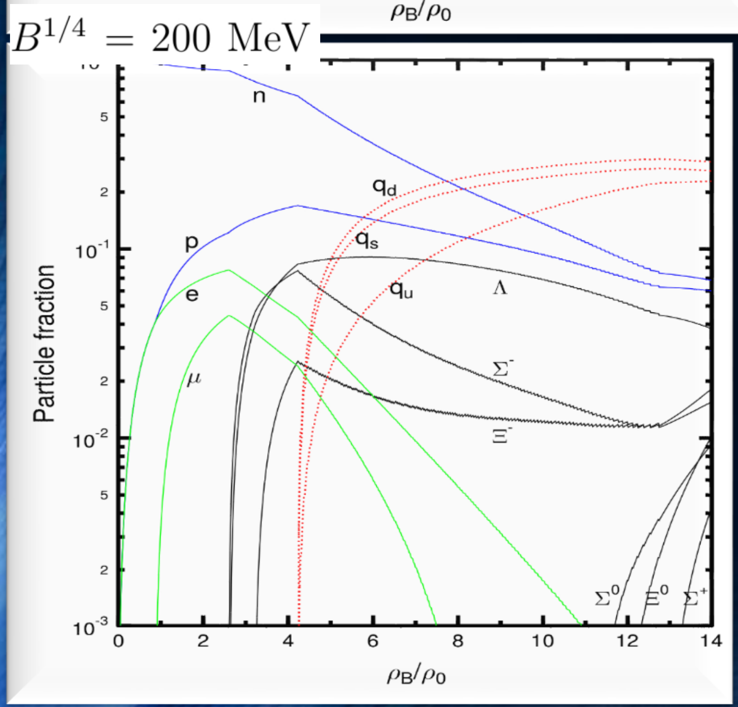

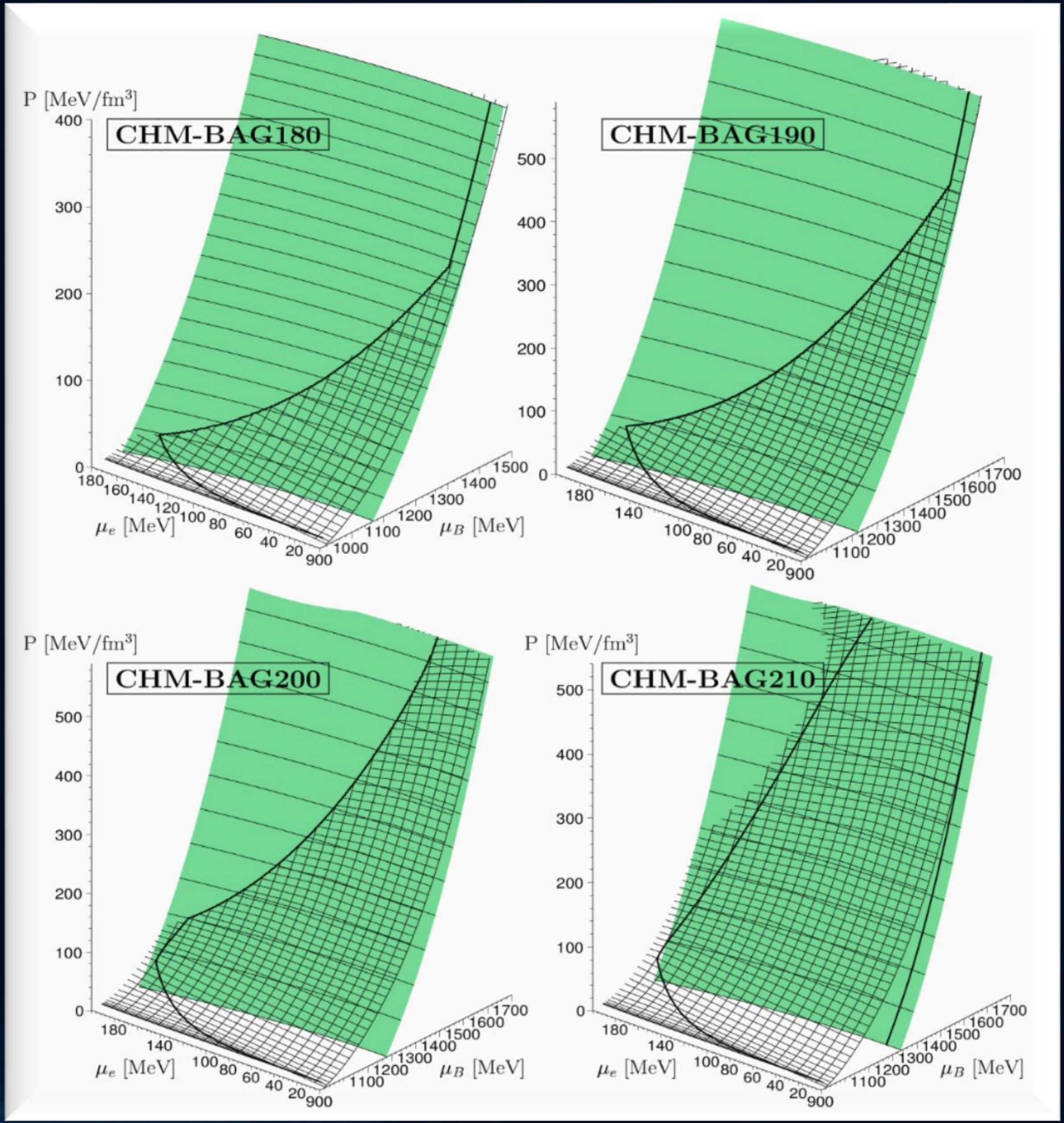

Spectral Properties of GWs

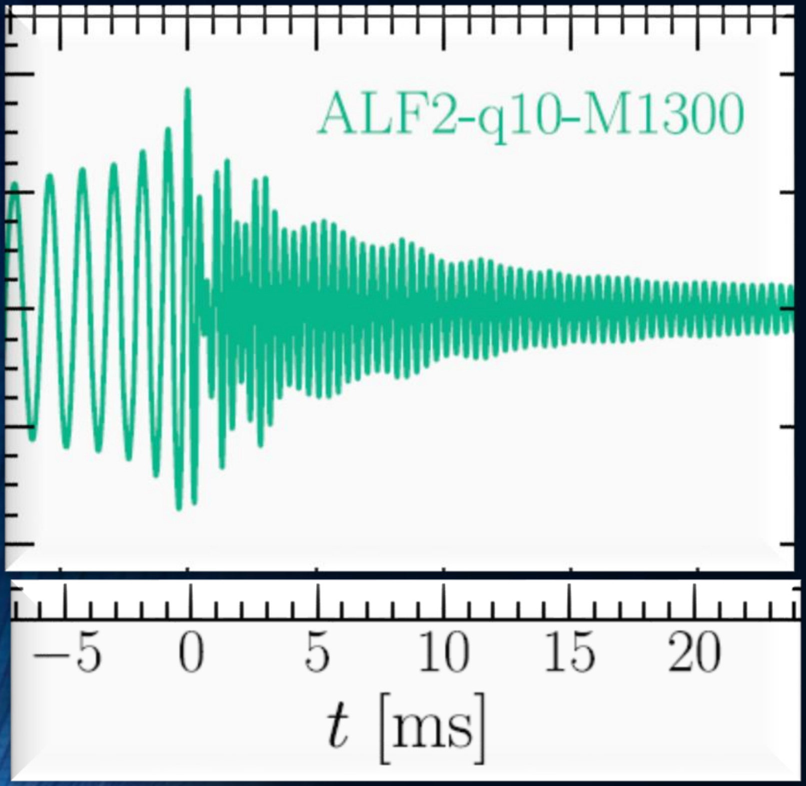

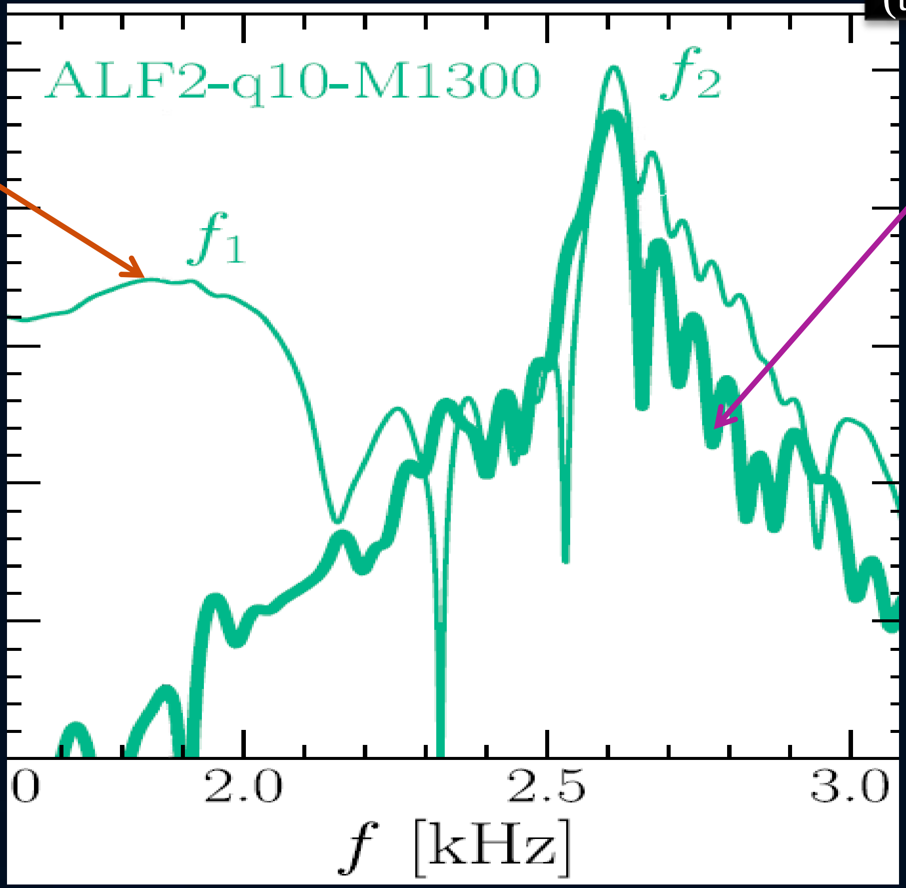

Two characteristic GW frequency peaks (f_1 and f_2);

the origin of f_1 comes from t<3 ms. By measuring M, f_1 and f_2 one can set high constraints on the EoS.

“Spectral properties of the post-merger gravitational-wave signal from binary neutron stars”,
Kentaro Takami, Luciano Rezzolla, and Luca Baiotti, PHYSICAL REVIEW D 91, 064001 (2015)

Universal Behavior of f_1 and f_{max}

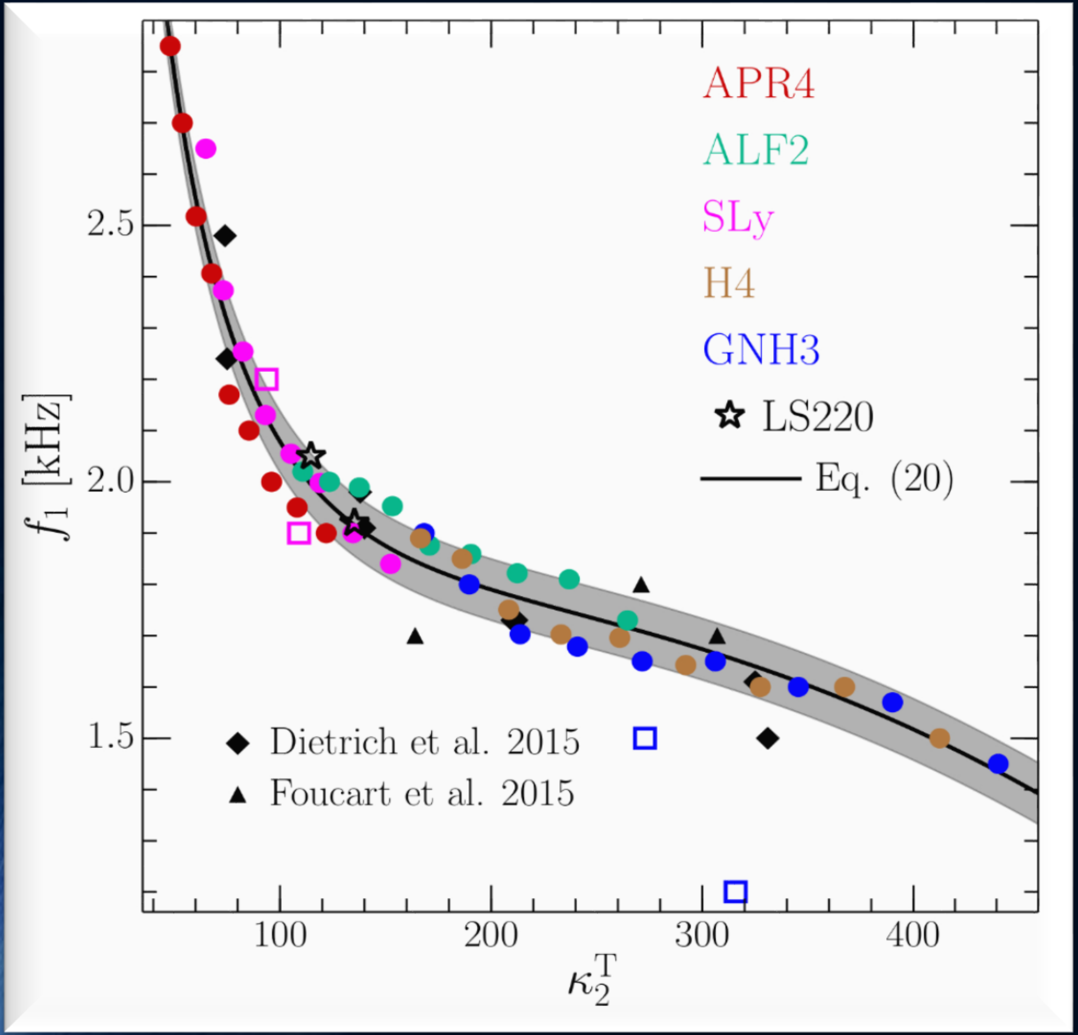

Values of the low-frequency peaks f_1 shown as a function of the tidal deformability parameter κ^T_2.

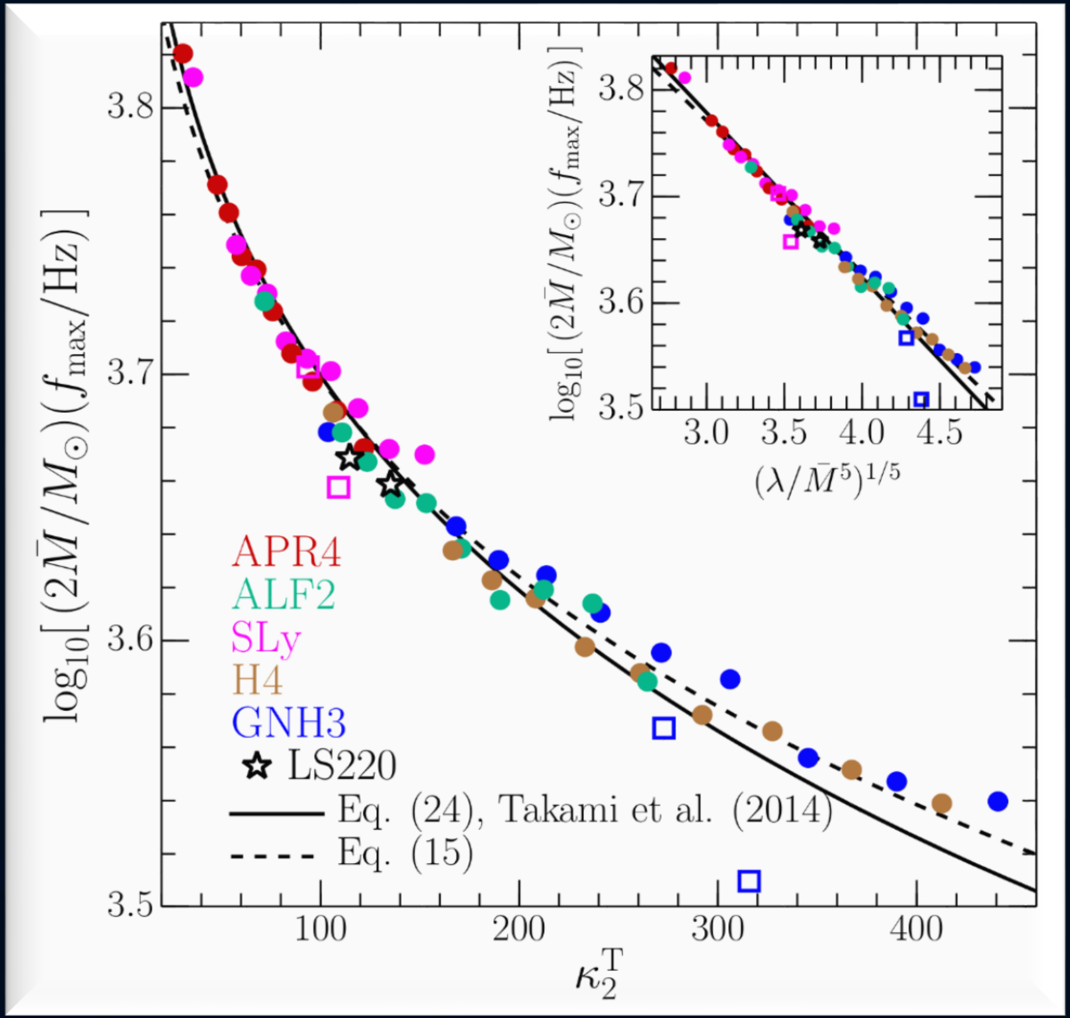

Mass-weighted frequencies at amplitude maximum f_{max} shown as a function of the tidal deformability parameter κ^T_2.

Universal behavior of the f_2-peak

Values of the high-frequency peaks f_2
Shown as a function of the tidal deformability parameter κ^T_2.

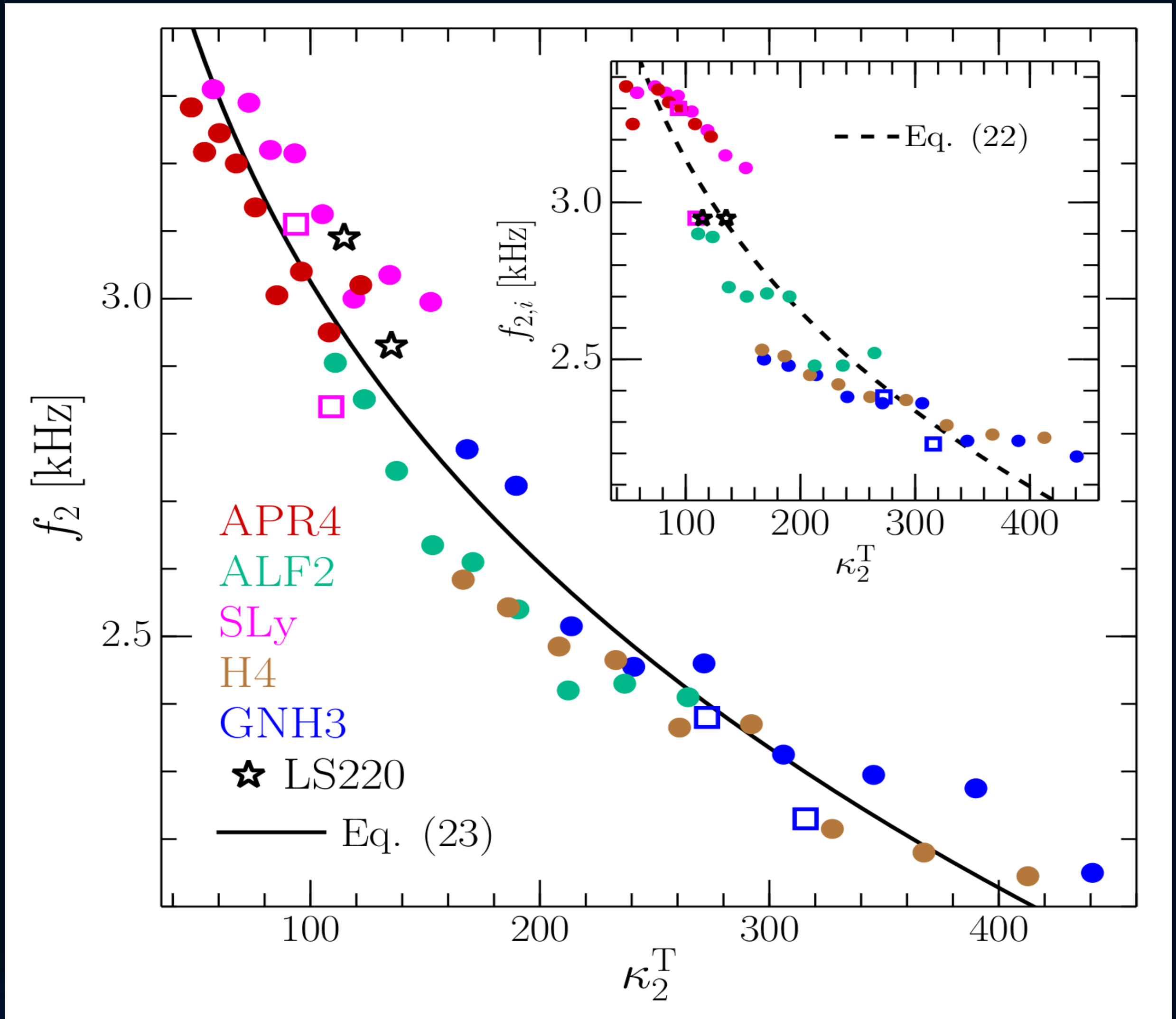

Gravitational Waves ➡ Equation of State

The detection of GWs from merging neutron star binaries can be used to determine the high density regime of the EOS. With the knowledge of f_1, f_2 and the total mass the system, the GW signal can set tight constraints on the EOS.

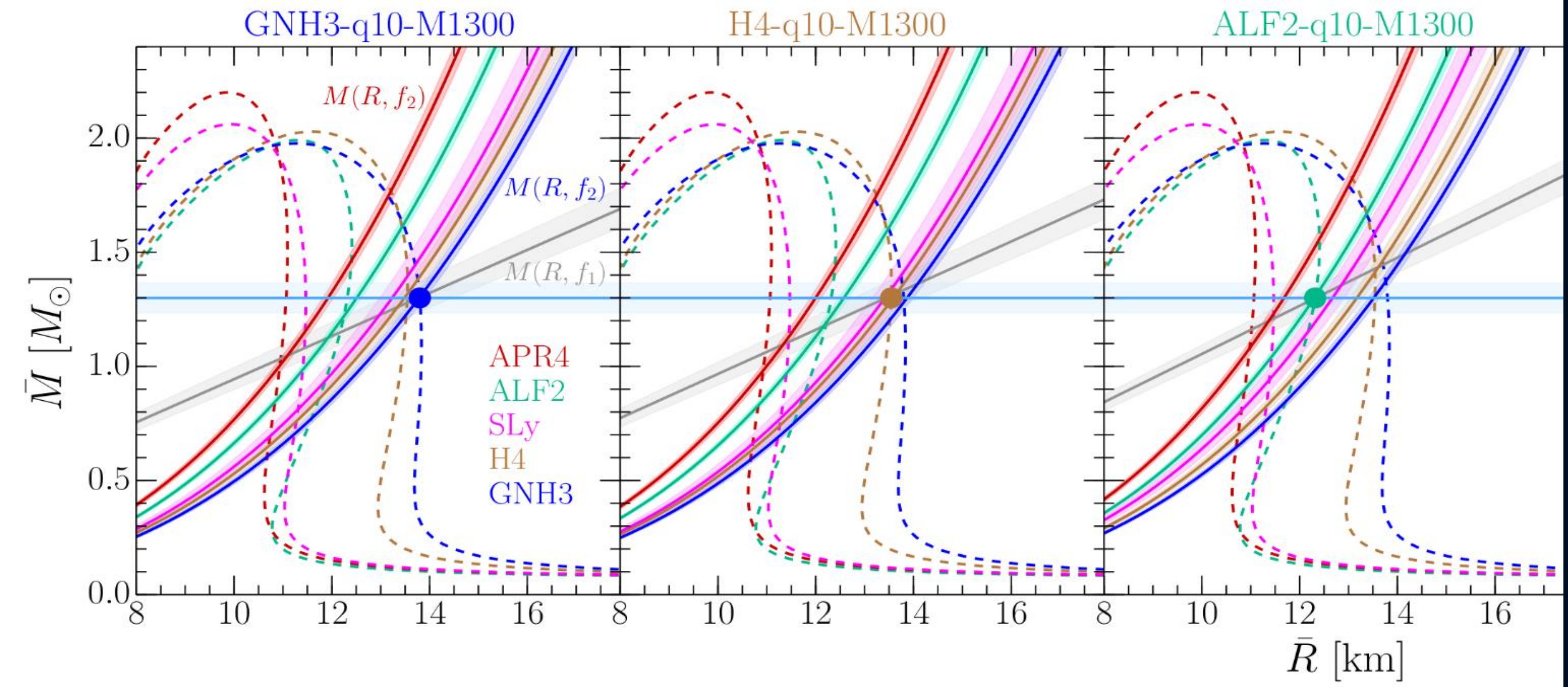

L.Rezzolla and K.Takami, arXiv:1604.00246
K.Takami, L.Rezzolla, and L.Baiotti, Physical Review D 91, 064001 (also PRL 113, 091104)

Computersimulation of a Neutron Star Merger in full General Relativity

Credits: Cosima Breu, David Radice and Luciano Rezzolla

Density

8.5 14

lg(rho) [g/cm^3]

Temperature

0 50

T [MeV]

The late inspiral, merger phase and postmerger phase

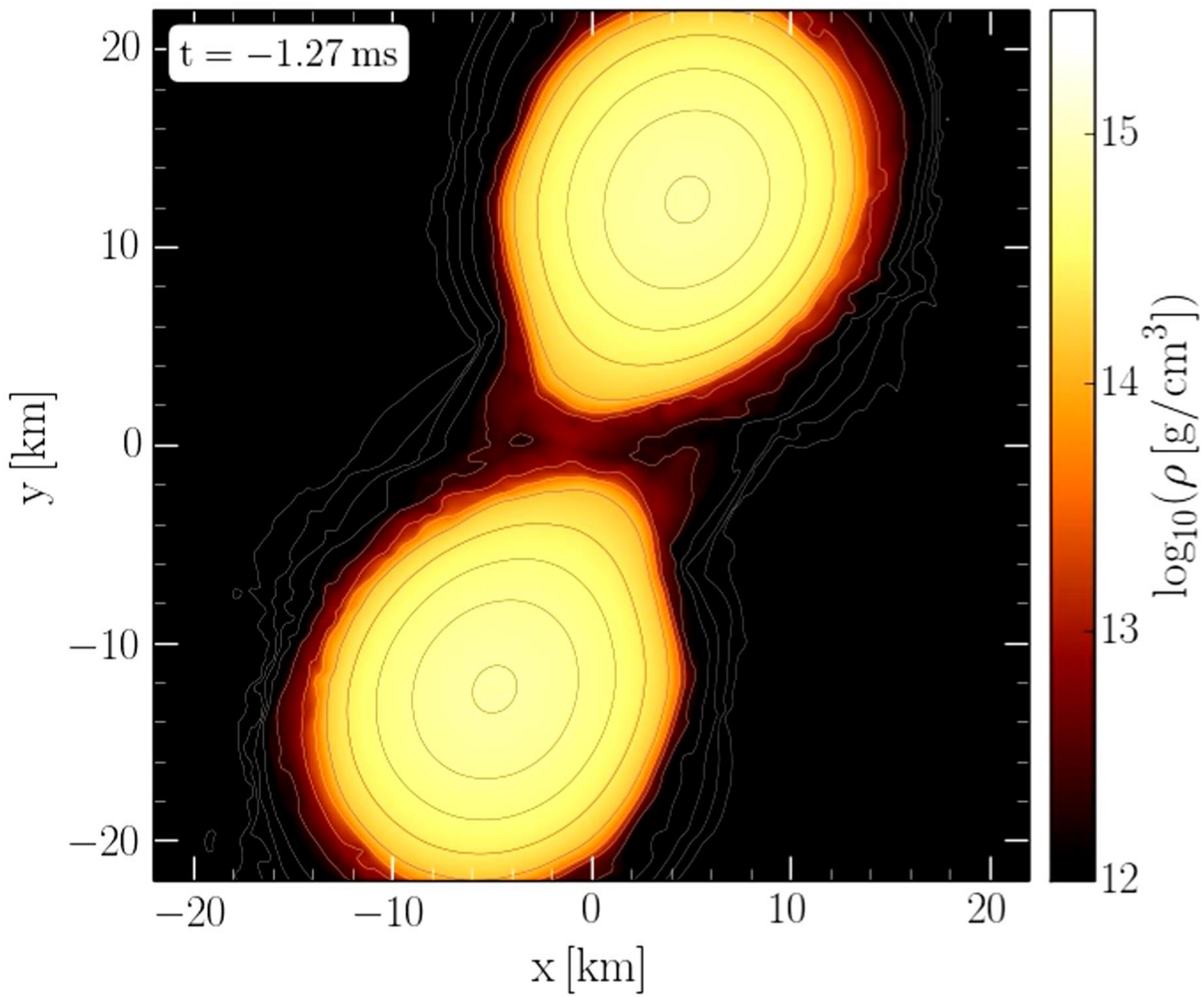

Rest mass density on the equatorial plane

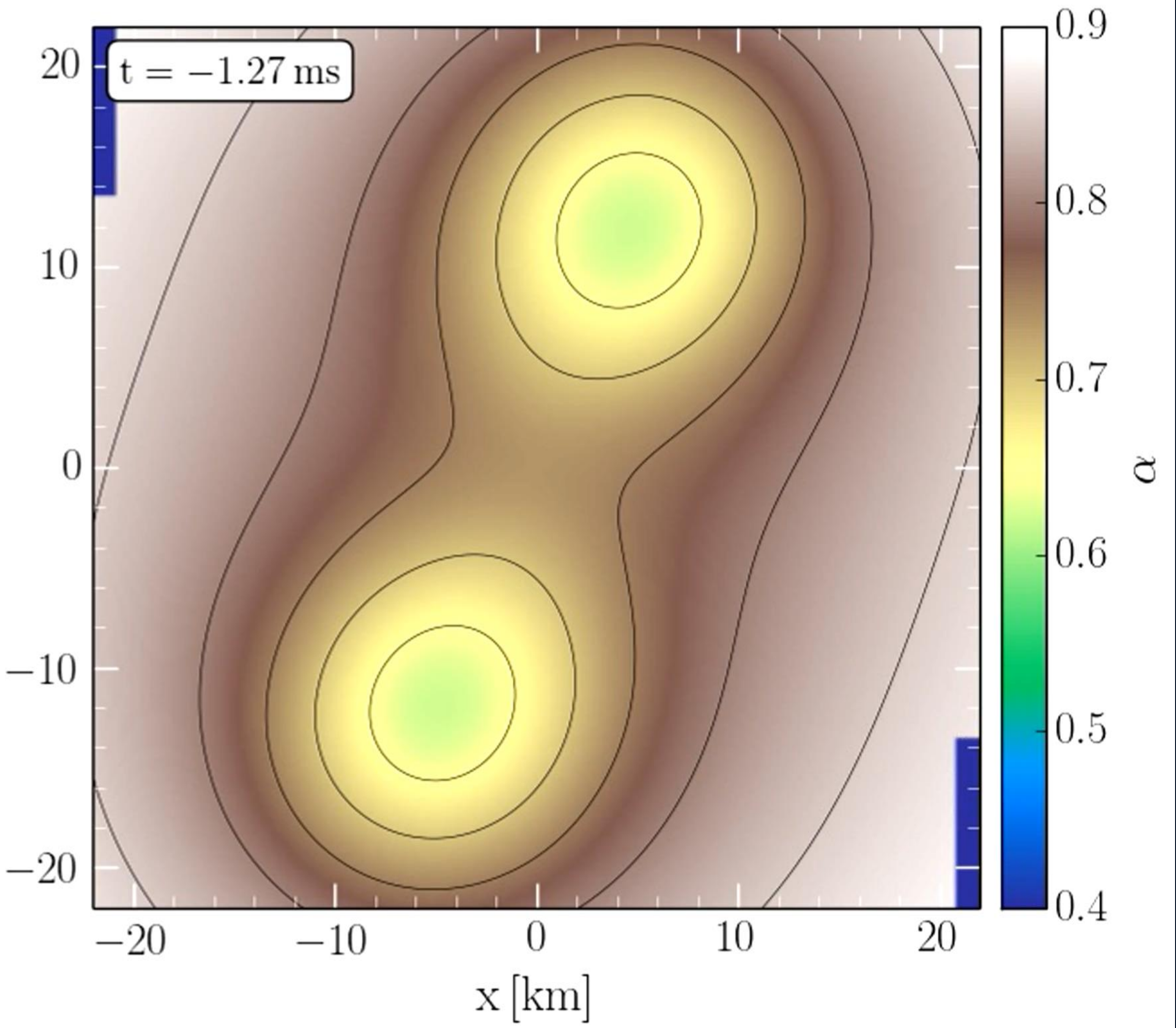

Lapse function on the equatorial plane

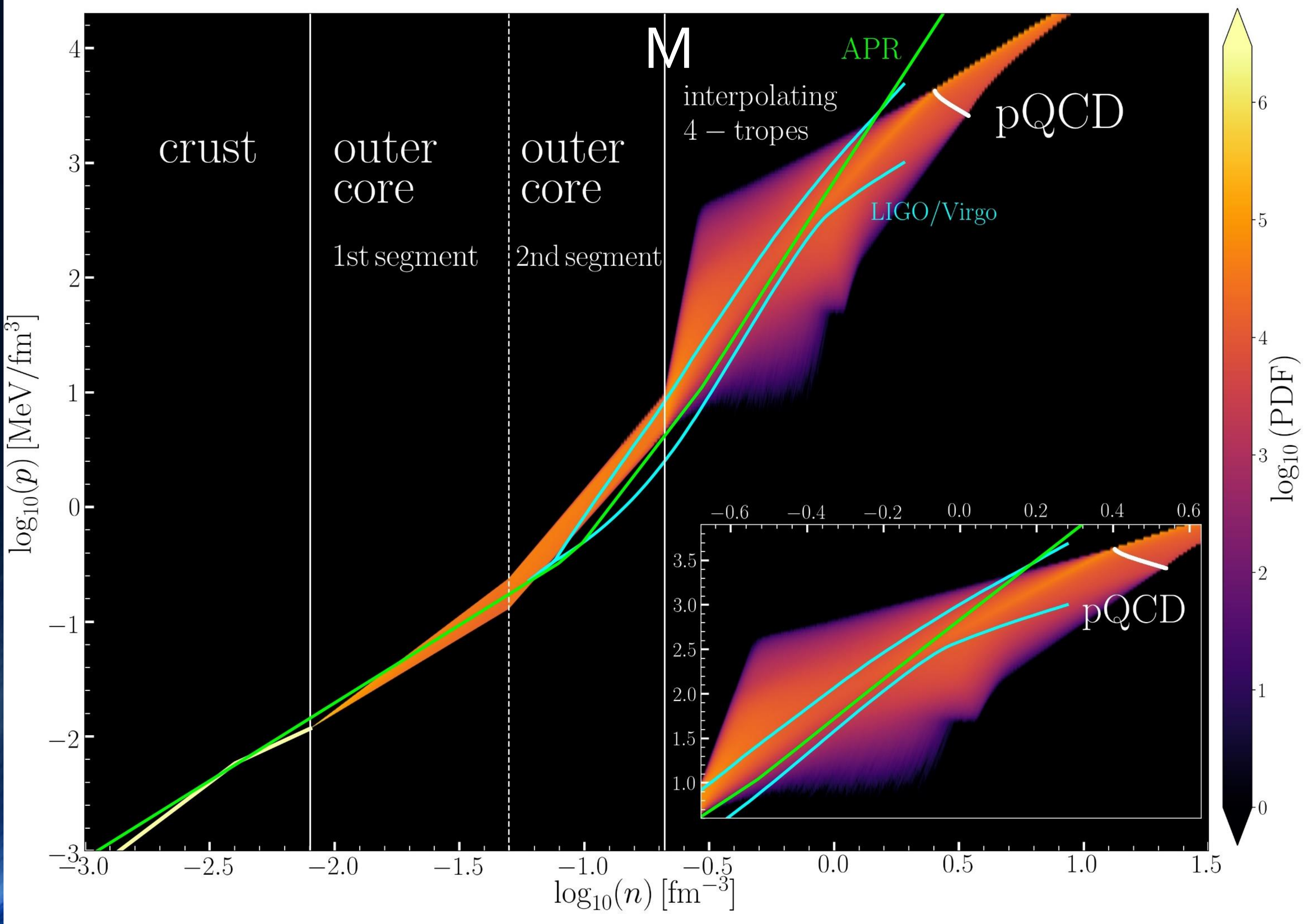

M
crust
outer
core
1st segment
outer
core
2nd segment
interpolating
4 − tropes
APR
pQCD
LIGO/Virgo
pQCD
$\log_{10}(p)$ [MeV/fm^3]
$\log_{10}(n)$ [fm^{-3}]
$\log_{10}$(PDF)

EOSs

Several different EOSs : ALF2, APR4, GNH3, H4 and Sly, approximated by piecewise polytopes. Thermal ideal fluid component (Γ=2) added to the nuclear-physics EOSs.

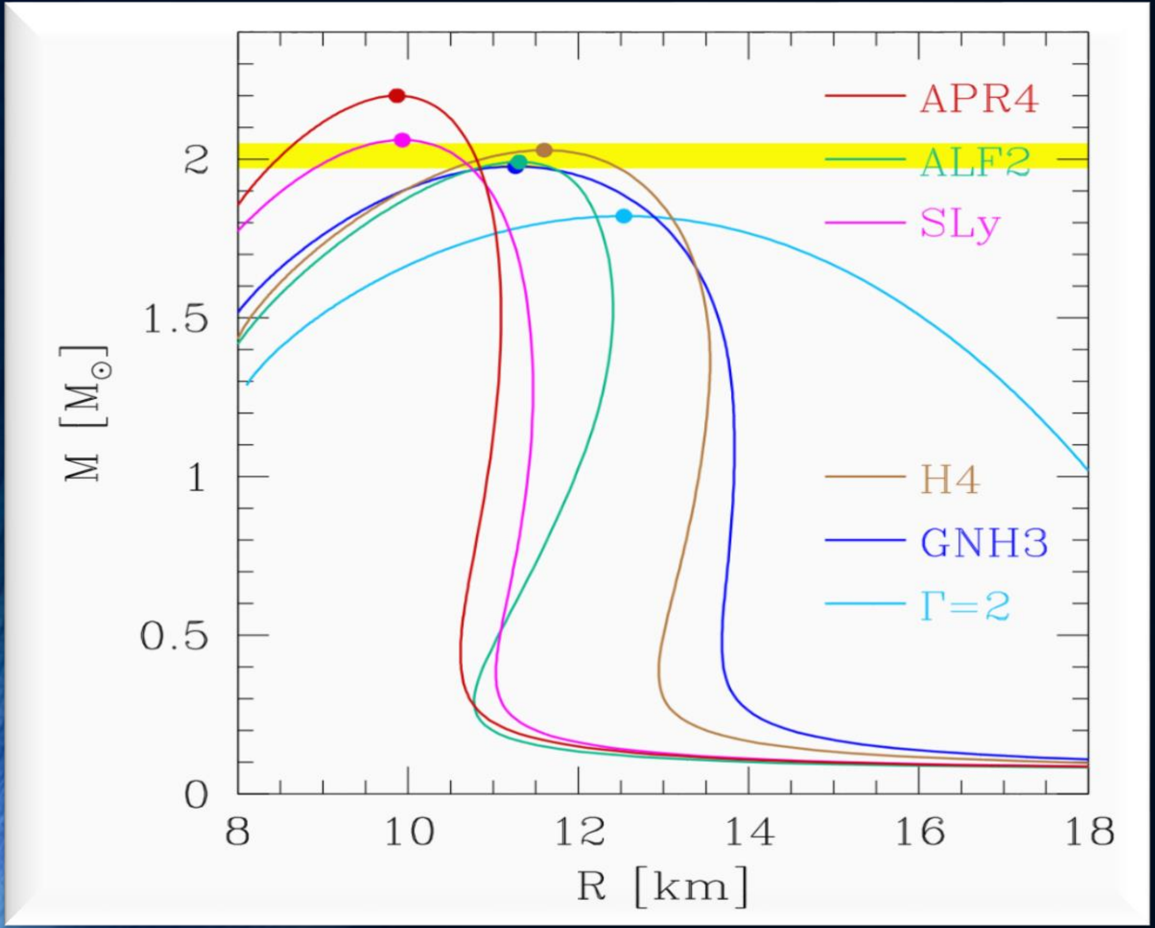

composed of a "cold" nuclear-physics part and of a "thermal" ideal-fluid component[1] [56]

$$p = p_{\mathrm{c}} + p_{\mathrm{th}}\,, \qquad \epsilon = \epsilon_{\mathrm{c}} + \epsilon_{\mathrm{th}}\,, \tag{6}$$

where p and ϵ are the pressure and specific internal energy,

The "cold" nuclear-physics contribution to each EOS is obtained after expressing the pressure and specific internal energy ϵ_{c} in the rest-mass density range $\rho_{i-1} \leq \rho < \rho_i$ as (for details see [36, 64–66])

$$p_{\mathrm{c}} = K_i \rho^{\Gamma_i}\,, \qquad \epsilon_{\mathrm{c}} = \epsilon_i + K_i \frac{\rho^{\Gamma_i - 1}}{\Gamma_i - 1}\,. \tag{7}$$

($\Gamma_1 = 4.070$ and $\Gamma_2 = 2.411$). Finally, the "thermal" part of the EOS is given by

$$p_{\mathrm{th}} = \rho \epsilon_{\mathrm{th}} (\Gamma_{\mathrm{th}} - 1)\,, \qquad \epsilon_{\mathrm{th}} = \epsilon - \epsilon_{\mathrm{c}}\,. \tag{8}$$

where the last equality in (8) is really a definition, since ϵ refers to the computed value of the specific internal energy. In all of the simulations reported hereafter we use $\Gamma_{\mathrm{th}} = 2.0$

Additionally LS220-EOS used: Density and Temperature dependent EOS-table (Lattimer-Swesty)

HMNS Evolution for different EoSs

Low mass simulations (M=1.25 Msolar)

Central value of the lapse function α_c (upper panel) and maximum of the rest mass density ρ_{max} in units of ρ_0 (lower panel) versus time for the high mass simulations.

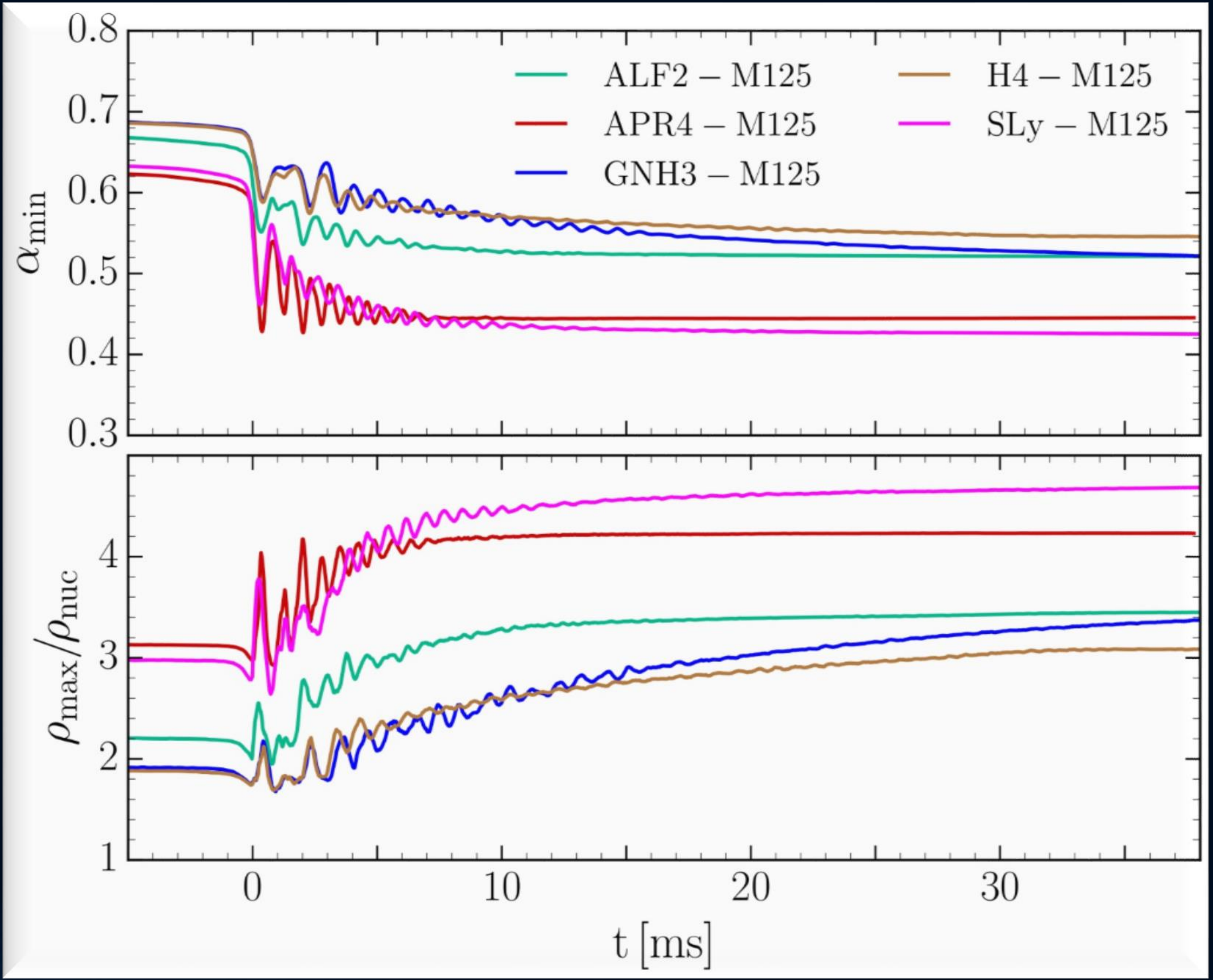

Hanauske, et.al. PRD, 96(4), 043004 (2017)

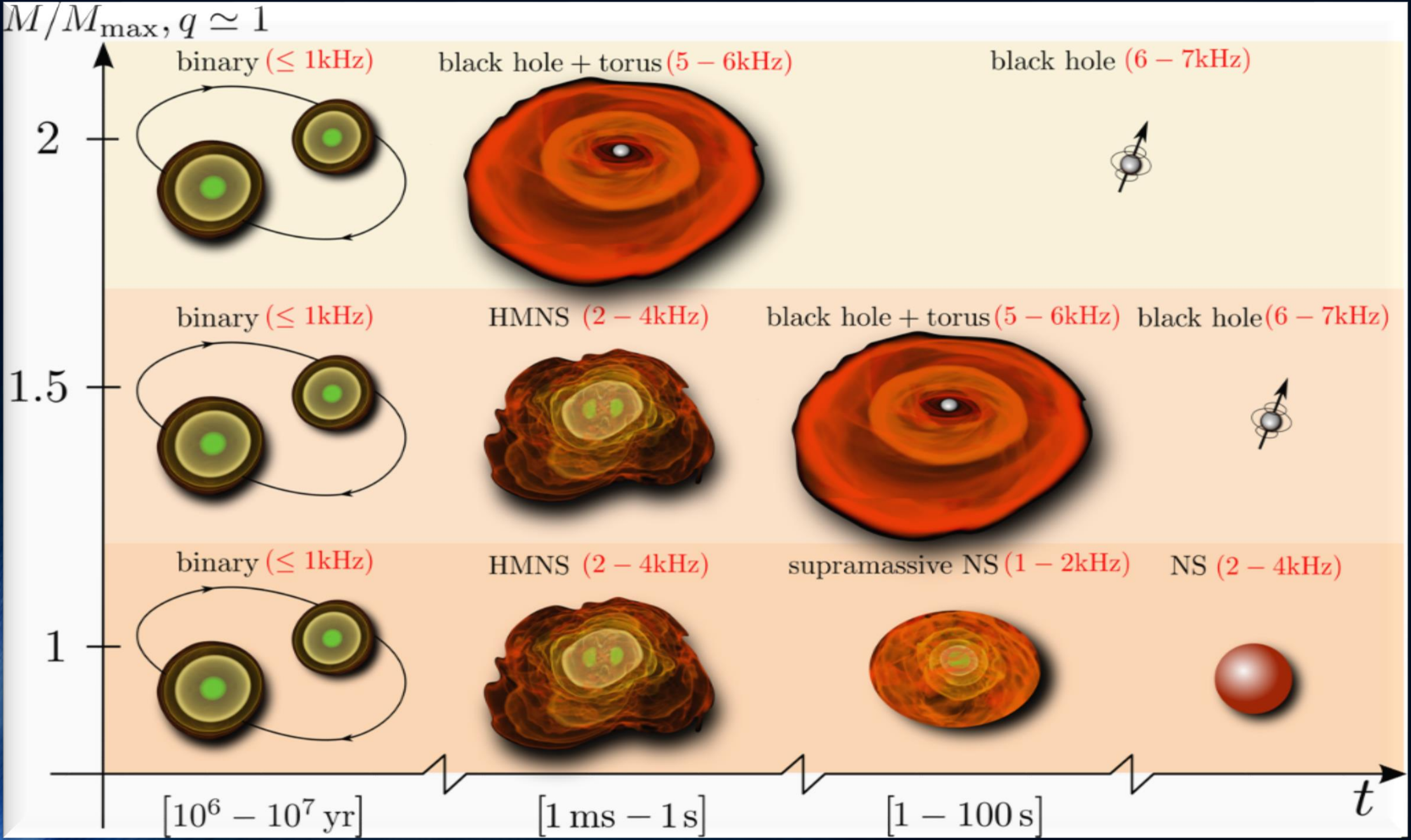
$M/M_{\rm max}, q \simeq 1$
binary ($\leq$ 1kHz)
black hole + torus (5 – 6kHz)
black hole (6 – 7kHz)
2
binary ($\leq$ 1kHz)
HMNS (2 – 4kHz)
black hole + torus (5 – 6kHz)
black hole (6 – 7kHz)
1.5
binary ($\leq$ 1kHz)
HMNS (2 – 4kHz)
supramassive NS (1 – 2kHz)
NS (2 – 4kHz)
1
$[10^6 - 10^7\,{\rm yr}]$
$[1\,{\rm ms} - 1\,{\rm s}]$
$[1 - 100\,{\rm s}]$
t

Density Temperature

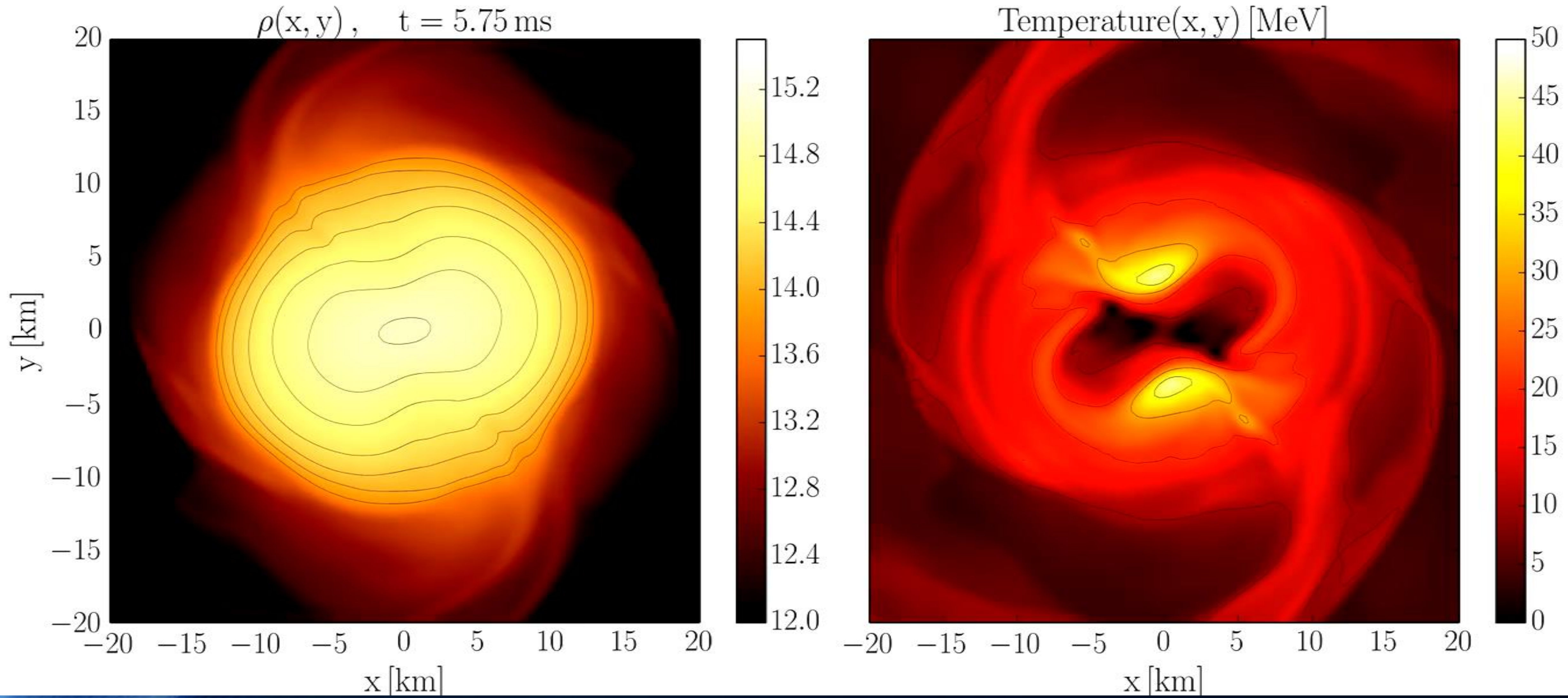

EOS: LS200 , Mass: 1.32 M_{solar}, simulation with Pi-symmetry